A Cable-Driven Pelvic Robot: Human Gait Adaptation and Rehabilitation Studies

Vineet Vashista

Submitted in partial fulfillment of the
requirements for the degree of
Doctor of Philosophy
in the Graduate School of Arts and Sciences

COLUMBIA UNIVERSITY

2015

Abstract

A Cable-Driven Pelvic Robot: Human Gait Adaptation and Rehabilitation Studies

Vineet Vashista

Walking is a state of continuous imbalance that requires a complex control strategy and cyclic activation of leg muscles to achieve successful interlimb coordination. Neuromusculoskeletal impairments, such as stroke, cerebral palsy, and spinal cord injury, affect one's ability to voluntarily contract muscles to normal amplitudes. This change in muscle activation pattern reduces the joint level torque generation and as a result impairs the ability to walk normally. Technological advances over the last two decades have resulted in the development of rigid link robotic exoskeletons that aim to improve gait deficits. These devices reduce repetitive and manual labor of therapists while providing objective measurement of the therapy during the gait rehabilitation. Despite the development of these robotic devices, no consensus has emerged about the superiority of robot-aided gait rehabilitation over the traditional methods. This may be because of the inherent complexity of the human musculoskeletal system and the constraints that rigid linked systems impose on the human movement.

In this work, we present a cable-driven Active Tethered Pelvic Assist Device (A-TPAD) for gait rehabilitation that can apply a controlled external wrench to the human pelvis in any direction and at any point of the gait cycle for a specified duration. The A-TPAD does not add undesirable inertia on the user and does not constrain the user's motion during training. The A-TPAD provides a technological platform to scientifically study human adaptation in gait due to externally applied forces and moments on the pelvis. Human studies with the A-TPAD can motivate new gait rehabilitation paradigms which can potentially be used to correct gait deficits in human walking.

The human nervous system is capable of modifying the motor commands in response to alterations in the movement conditions. Several studies have demonstrated the flexibility of human locomotion despite motor impairments and have shown the potential of using such paradigms for gait rehabilitation. In this work, we present a number of human experiments using the cable-driven A-TPAD to propose novel force interventions that induce adaptation in human gait kinematics and kinetics. In particular, stance phase gait interventions have been developed for gait rehabilitation

of hemiparetic patients. In these interventions, the external force vector was applied to the pelvis to target weight bearing during walking and to promote longer stance durations. A single-session force training experiment with hemiparetic stroke patients was also conducted as a part of this work. It is shown that hemiparetic stroke patients improved the ground reaction force symmetry, forward propulsion effort, and stance phase symmetry during walking.

In this work, the A-TPAD is also used to develop an intervention to apply external gait synchronized forces on the pelvis to reduce the user's effort during walking. The external forces were directed in the sagittal plane to assist the trailing leg during the forward propulsion and vertical deceleration of the pelvis during the gait cycle. A pilot experiment with five healthy subjects was conducted. This study provides a novel approach to study the role of external forces in altering the walking effort, such understanding is important while designing assistive devices for individuals who spend higher than normal effort during walking.

Contents

List of Figures

List of Tables

Acknowledgment

I wish to express my deep sense of thanks and most sincere gratitude to my mentor and adviser Dr. Sunil K. Agrawal. His passion for research and excitement in regard to teaching have been very inspiring for me. Without his timely advice, meticulous scrutiny, and scientific approach this dissertation would not have been possible.

I would like to thank my committee members Dr. Richard Longman, Dr. Joel Stein, Dr. Andy Gordon, and Dr. Matei Ciocarlie for reviewing my work and giving me constructive feedback. I am also sincerely grateful to Dr. Darcy Reisman for her invaluable advice during the starting phase of this work.

I would like to thank all the members of the Robotics and Rehabilitation Laboratory with whom I have interacted through the course of my graduate study. I am deeply grateful for their inputs in various forms to help me polish my skills and better understand my research especially Dr. Damiano Zanotto, Dr. Ying Mao, Paul Stegall, Joon Park, Xin Jin, Jiyeon Kang, Emily Boggs, Moiz Khan, and Dario Martelli. I thankfully acknowledge the help of undergraduate and master students who helped me with fabricating hardware and conducting experiments. I would also like to thank Lauri Bishop and Isis Martinez for their advice and help in conducting experiments with stroke patients.

I would also like to thank the current and former staff of the Mechanical Engineering department for their kind support. I particularly thank Sandra Morris and Rebecca Chambers for their assistance on my academics, Rakhi Hossain for getting countless orders through, and Robert Stark and Mohammed Haroun for assistance in fabrication of many mechanical components for my research.

Most importantly, I am always indebted to my family: grandmother Santosh Kumari, father Ram N. Vashista, mother Suman Lata, aunt Lalita Gaur, and sisters Ritu and Preeti Vashista.

They have been a constant source of love, patience, support, and encouragement through the past few years. None of this would have been possible without the love and patience of my family.

Finally, I appreciate the financial support of the research discussed in this dissertation from the National Institutes of Health grant number HD38582 and the National Science Foundation IIS-1339666.

Part I

Introduction

Chapter 1

Introduction

In the United States alone, each year about 795,000 people suffer from a new or recurrent stroke, up to 20,000 people experience spinal cord injury (SCI), and about 764,000 children and adults manifest symptoms of cerebral palsy (CP) [29–31]. The individuals who survive the acute phase of these impairments are left with significant disabilities at the lower and upper limb levels. These conditions affect an individual's quality of life and independence by limiting the ability to perform activities of daily living (ADL).

The main focus of this work is to develop a cable-driven robot for gait rehabilitation of individuals with neural impairments. In this chapter, we first present the traditional gait rehabilitation methodologies used by the research and clinical communities for treatment of these conditions. Recently developed robotic devices for gait rehabilitation have also been presented, briefly outlining their benefits and challenges compared to traditional gait rehabilitation. The chapter concludes by introducing cable-driven devices and their usefulness for human rehabilitation applications, thereby motivating the novelty of this current work.

1.1 Human Walking

Walking is the main mode of locomotion among legged animals. Humans accomplish walking through successful inter-limb coordination and cyclic activation of leg muscles. Human walking is a mechanically-complex task that involves a state of continuous imbalance, where each step is taken to regain the body's balance [32–34]. In particular, sufficient foot clearance is required when

one leg is in swing phase to prevent stumbling. At the end of the swing phase, the swinging leg must be positioned ahead of body. This is accomplished through bearing weight on the leg in contact with ground (stance phase). At the end of a leg's stance phase, sufficient push-off force is needed to initiate the swing phase of that leg as well as to propel the body forward. Thus, a complex control strategy is indeed required during walking. In healthy individuals, a continuous gait pattern is characterized by repetitive movements of the lower limbs, which is smooth, regular, and has spatio-temporal symmetry. On even terrains, these lower limb movements generate symmetrical Ground Reaction Forces (GRF). The ease with which healthy individuals accomplish these patterns evidently masks the underlying complex nature of the neuro-musculoskeletal system.

Notably, neural impairments, such as stroke, cerebral palsy (CP), and spinal cord injury (SCI), damage the central nervous system (CNS) pathways in an individual. These damages limit one's ability to voluntarily contract muscles to normal amplitudes [35–38]. Additionally, muscle spasticity and inappropriately timed muscle activities are reported in individuals with these impairments. These abnormalities result in unstable and asymmetrical walking pattern, reduced limbs' excursion, and slow walking speed. For example, stroke survivors with hemiparesis demonstrate decreased hip and knee flexion-extension range of motion and shorter stance phase durations on the affected side. This leads to slow walking speed and asymmetric gait pattern [35–37]. Gait asymmetry is further associated with higher energy consumption, loss of balance, and increased risk of falling [39–43]. As a result of either complete or incomplete damage to nerves or the spinal cord, SCI patients demonstrate hyper-extension or knee buckling during the stance phase, inadequate limb clearance during the swing phase, sensory deficits, and loss of balance [30, 38]. Cerebral palsy, a group of permanent movement disorders, appears in early childhood and affects the muscle activation pattern, muscle strength, muscle spasticity/stiffness, and balance during walking [31, 37].

Consequently, improvements in gait of these patients is the main goal of any gait rehabilitation paradigm.

1.2 Manual-assisted Gait Rehabilitation

Patients with neurological impairments demonstrate reduced muscle activation levels, which result in reduced joint torques during walking. Thus, methods have been developed in the gait rehabili-

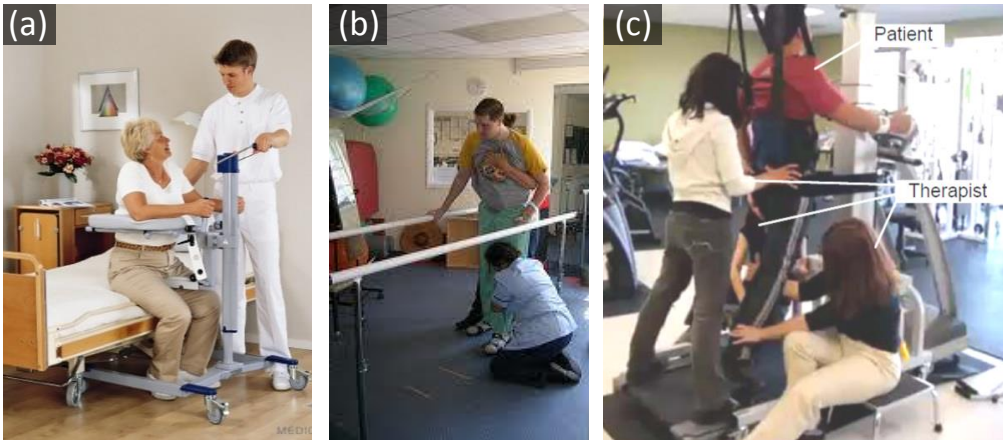

Figure 1.1: Manual-assisted gait training involve therapists to use (a) walker [1], (b) parallel bars, or (c) body-weight harness to support patients [2]. These procedures further involve manual manipulation of patient's legs during training.

tation community to reduce the amount of joint torques required during walking.

Currently, in most gait rehabilitation facilities, manual-assisted training is being used. These procedures require two or three therapists to manually assist a patient using a walker or parallel bars while walking, as shown in Fig. 1.1(a, b). These devices provide external support to patients and allow the therapists to manually execute the lower limb movements as well as help in the forward propulsion of a patient's body. Treadmill walking with a patient's weight partly supported by a body weight support system is also a widely adopted strategy [38,44], as shown in Fig. 1.1(c). These harnesses can provide body weight support ranging from 100% of body weight (BW), for patients who can not support their weight, to 0% BW as a safety device to prevent accidental falling during walking. As the manual-assisted gait rehabilitation procedures are highly labor intensive, the therapist's fatigue can sometimes affect the training assessment measures. In addition, lack of skilled therapists make these rehabilitation procedures very expensive, adding an immense pressure on the health care system.

1.3 Robot-aided Gait Rehabilitation

Technological advances over the last two decades have resulted in the development of robotic devices designed to help patients to improve their gait deficits. Robotic exoskeletons have been developed that use actuators to provide assistance at the lower-limb joints while walking, as shown in Fig.

1.2 and 1.3. These are programmable devices that can potentially interact with patients, similar to how physiatrists do during rehabilitation, while keeping the manual labor of therapists to a minimum. In addition, sensors on the machine can make objective measurements to guide the physical therapy. These robots can be used for pure functional assistance as well as to develop strategies that employ active-user involvement to facilitate learning among subjects [3, 4, 45].

1.3.1 Categories

In the robotic community, different exoskeleton designs have been proposed, as shown in Fig. 1.2, that are used for treadmill based gait training. An active leg exoskeleton (ALEX) [3, 6, 7] uses an assist-as-needed (AAN) control strategy, where the amount of external assistance is based on how closely a subject follows a target foot trajectory. Studies have been conducted with AAN control strategy to show improved training effects. As shown in Fig. 1.2(a, d, and e), three versions of this device have been developed. The latest ALEX III has 12 actively controlled degrees-of-freedom (DOFs) - 4 for the pelvis, and 4 for each leg. Another treadmill based exoskeleton using AAN rehabilitation strategy is called LOPES [4] (Fig. 1.2(b)). It uses a bowden cable-driven series elastic actuator to implement an impedance controller during walking. It actively controls 2 pelvic translational, 2 hip rotational, and 1 knee rotational DOFs, and has a passive pelvic vertical translation DOF. Lokomat [45] (Fig. 1.2(c)) is the only commercially available exoskeleton that has been used widely in various rehabilitation facilities. The Lokomat actively controls hip and knee joints flexion-extension motion, passively allows pelvic vertical motion, and restricts pelvic rotation, pelvic obliquity, and pelvic transverse plane motion. Pelvic assist manipulator (PAM) [8] (Fig. 1.2(f)) is another treadmill based robot that can actively control 5 pelvic DOFs using pneumatic actuators. It was developed to support and control pelvic motion, and to work alongside other lower limb devices.

Figure 1.3 shows robotic devices that are developed for over-ground walking. These robotic devices, such as WalkTrainer [9], KineAssist [10], and NaTUre-Gaits [11], use a mobile frame structure to support the actuators and links that are used to actuate human limb movements. In various research facilities, following similar design principles, portable robotic exoskeletons have been developed for human performance enhancement during walking and running, such as BLEEX, MIT exoskeleton, and HAL [46–48].

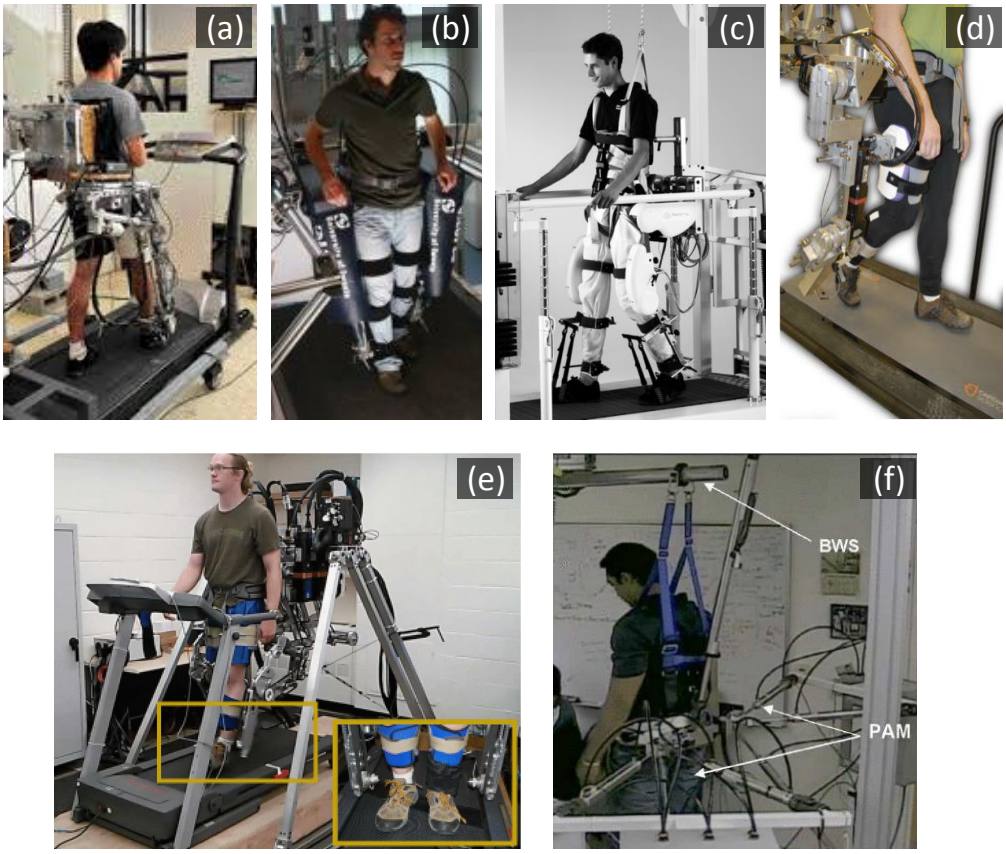

Figure 1.2: Treadmill based robotic exoskeletons: (a) ALEX I [3], (b) LOPES [4], (c) Lokomat [5], (d) ALEX II [6], (e) ALEX III [7], and (f) PAM [8].

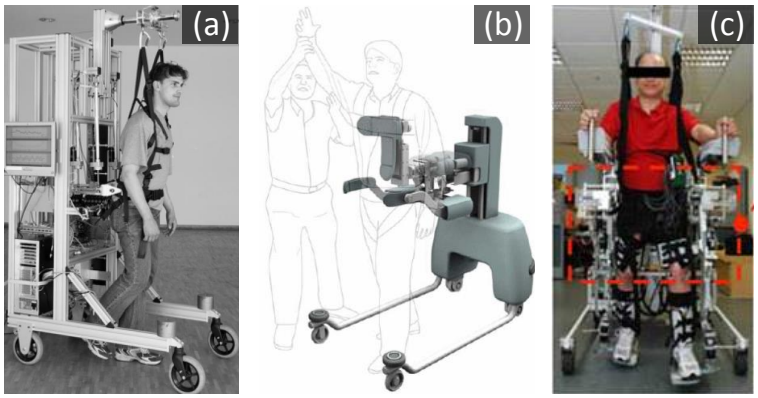

Figure 1.3: Robotic devices for over-ground assistance: (a) WalkTrainer [9], (b) Kine Assist [10], and (c) NaTUre-Gaits [11].

1.3.2 Challenges

Despite the variety of robotic gait rehabilitation devices that have been developed and the studies performed with these devices, no consensus has emerged about the superiority of robot-aided gait rehabilitation over the traditional physical therapy [49–52]. One critical limitation of these devices is the use of rigid links to mimic the human lower limb kinematics. Due to the complex human musculoskeletal structure, various simplifications are made in the design process, which induce mobility constraints in the form of human-robot joint misalignment. In addition, since actuating all lower limb DOFs increases the cost and design complexity, rigid link robotic devices provide actuation only at a subset of these DOFs. For example, in most robotic exoskeletons the pelvic motion is typically constrained by the design of the robot. Thus, undesirable external kinematic constraints are added on the human motion.

In addition, due to the moving inertia of the rigid links, these devices have their own dynamics. As these links are connected to human legs, they affect the human walking dynamics. It has been reported in [53] that a robot, which adds around 6 kg mass on the human pelvis or 2 kg mass on the ankle, can affect a subject's gait significantly. Undesirable results on the instability of the gait due to added inertia at pelvis have also been reported in [54]. Noting these challenges, some preliminary studies have been proposed recently to reduce the robot inertia effects on the human walking. In [55], the interaction forces/torques between the robot and human leg were used to close a feedback loop on the joint actuators. Separately in [56], the robot transparency during cyclic walking was improved by using adaptive frequency oscillators and kernel-based nonlinear filters. These strategies are still in their preliminary stages and have only been tested with a small group of subjects.

Considering the potential benefits an automated robotic system can bring to the rehabilitation process, there is a need to overcome these challenges and to develop novel gait rehabilitation strategies. In the following section, we briefly describe the benefits and challenges of using a cable-driven robotic technology in the context of human-related applications.

Figure 1.4: Cable-driven systems with industrial applications: (a) NIST Robocrane [12], (b) Sky-CAM [13], and (c) Large Adaptive Reflector (LAR) - multi-tethered aerostat system [14].

1.4 Cable-driven Robotic Systems

A cable-driven robotic system uses cables instead of rigid links for actuation. Cables have very unique properties, such as low mass, flexibility in routing, and the ability to carry large tensile loads. However, unlike rigid links, cables can only operate in tension, i.e., they can only apply a pulling force on the end-effector. Thus, cable-driven systems are widely used in the construction industry as cranes. One of the earliest crane cable-driven industrial design is the NIST Robocrane [12], as shown in Fig. 1.4(a). The ability of a cable to be wound on a spool facilitates large workspace compared to a rigid link mechanism. This further facilitates placement of actuators/winches at the base of the structure away from the moving joints. The cable-driven systems can also achieve high payload speed and acceleration. One such application is the SkyCam [13], a cable suspended camera to broadcast live video feed of large sports events as shown in Fig. 1.4(b). Actuated cables have also been used for telescopes applications. One such application large adaptive reflector (LAR) is reported in [14], where an aerostat position-controlled using three cables is used to lift the receiver (Fig. 1.4(c)).

1.4.1 Human-related Applications

A cable-driven system, using low mass cables and few rigid components, offers advantages such as avoiding the issue of human-robot joint misalignment and reduced external inertial dynamics during human related applications. Further, the inherent flexibility of cables makes a cable-driven system safer in case of a collision with human. Thus, cables have been used to control an end-effector to provide haptic interface to humans. Common applications are simulated sports training [15]

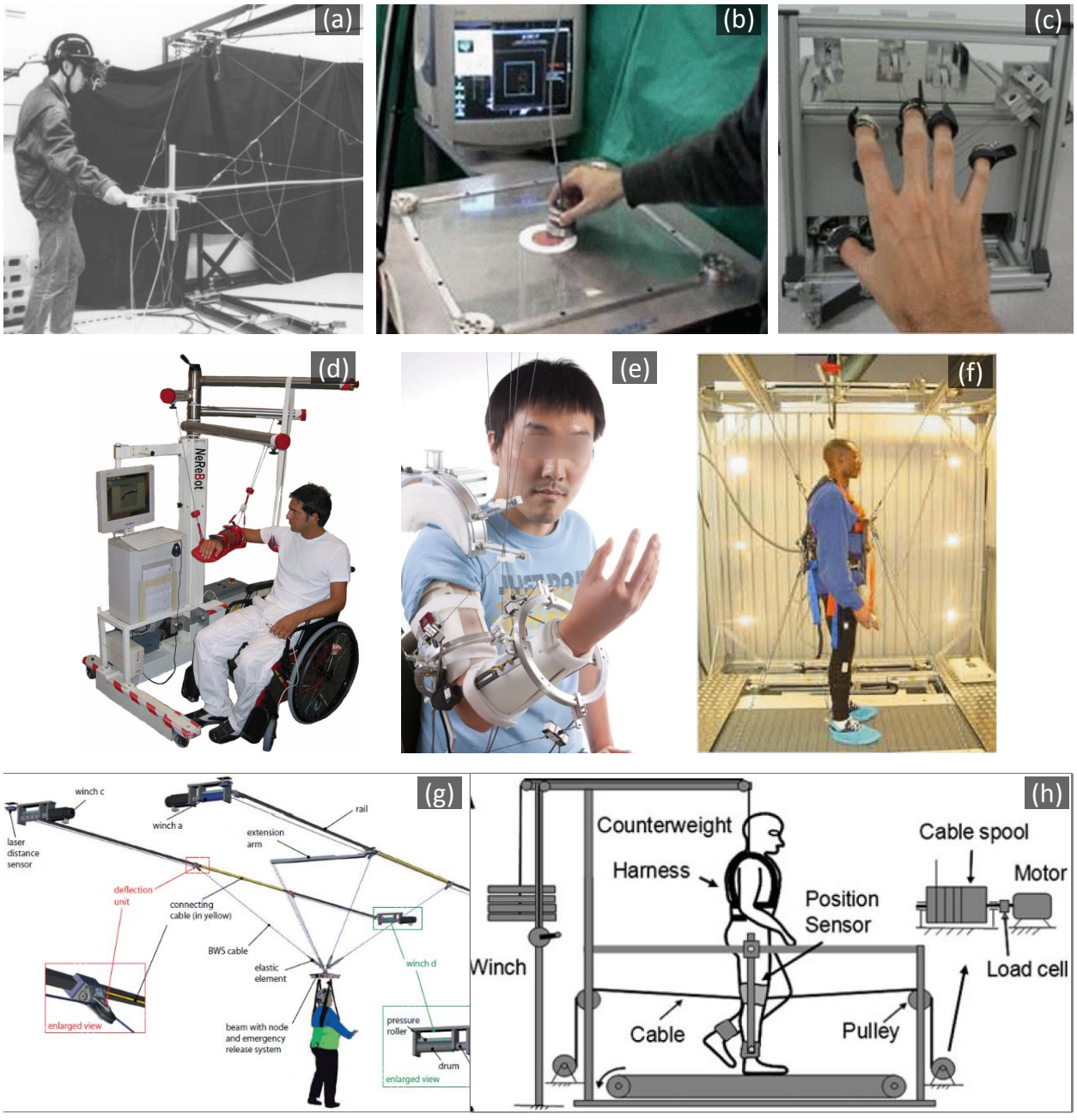

Figure 1.5: Cable-driven systems for human related applications: (a) Sport simulator [15], (b) Feriba3 [16], (c) HandCARE [17], (d) NeReBot [18], (e) CAREX [19], (f) STRING-MAN [20], (g) FLOAT [21], and (h) A cable system to apply resistive and assistive forces on leg [22].

(Fig. 1.5(a)), and Feriba3 - a haptic display for hand training [16] (Fig. 1.5(b)). Cable systems have further been extended to control the human fingers and arm movements. HandCARE [17] (Fig. 1.5(c)) and NeReBot [18] (Fig. 1.5(d)) are cable-driven systems developed for training hand movements after stroke. CAREX, [19] (Fig. 1.5(e)), a cable-driven arm exoskeleton has been developed for neural rehabilitation. It is a 5 DOFs system which actively controls shoulder flexion-extension, adduction-abduction, and internal-external rotations, and elbow flexion-extension and forearm pronation-supination.

Unlike upper-limb rehabilitative cable-driven systems, very few cable robots have been reported in the literature for gait rehabilitation. STRING-MAN (Fig. 1.5(f)), a full body wire-robot to provide body support during walking was described in [20]. In the available documents on this device only conceptual human interface has been described without actual human experiments. Apart from this work, a number of crane type cable-driven systems have been used in gait rehabilitation to provide body weight support during walking. Such architectures utilize the user's weight to keep the cables taut and overcome the shortcoming of cables as a unilateral actuation source. The Zero-G [57], NaviGAITor [58], and FLOAT [21] (Fig. 1.5(g)) are some of the active multi-directional body weight support systems. Some simple cable architectures have also been used in literature to apply uni-directional forces on an individual. For example, in [22], a cable-driven system has been used to apply resistive and assistive forces to the legs during walking to study walking adaptation in spinal cord injury (SCI) patients, as shown in (Fig. 1.5(h)). Thus, a cable-driven system using low mass cables and few rigid components can offer advantages over existing robotic exoskeletons during gait rehabilitation.

In the current work, we present a novel cable-driven pelvic robot, Active Tethered Pelvic Assist Device (A-TPAD), for gait rehabilitation that can apply a controlled external wrench to the human pelvis in any direction and at any point of the gait cycle for a specified duration. The A-TPAD does not constrain human motion and does not add undesirable mass/inertia on the human. The design provides flexibility to achieve different cable configurations and to use different number of motors. The A-TPAD controller uses a real-time motion capture system and an online optimization scheme to keep positive cable tension during the human motion.

1.5 Overview of the Dissertation

The first goal of this work is to develop a cable-driven robot that can be used to apply controlled external forces in desired directions to the human pelvis during walking. The second goal of this work is to scientifically study human locomotor adaptation when the human walking dynamics is modified through externally applied forces using the cable robot. Overall, the main focus of this work is to use the understanding of force adaptation during human walking to develop novel gait rehabilitation paradigms for neurologically impaired patients.

These aims are accomplished as a part of this dissertation and are discussed in the subsequent chapters. Chapter 2 describes a passive cable system that was developed to conduct preliminary studies to investigate the force adaptation in human walking when external forces were applied to the pelvis. Based on this preliminary work, an active version of the cable-driven robot, Active Tethered Pelvic Assist Device (A-TPAD), was developed. The design, modeling, and control methodologies developed as part of the A-TPAD are described in chapter 3. Chapter 4 presents healthy subject experiments, where novel stance phase interventions for gait rehabilitation were developed using A-TPAD. A single-session experiment with hemiparetic stroke patients is described in Chapter 5. In Chapter 6 a healthy subject experiment is presented, where A-TPAD was used to apply external forces on the pelvis to reduce the walking effort. The conclusions drawn from this dissertation are discussed in Chapter 7 with potential future directions.

In the following chapters, some terminologies related to human motion analysis have been used. A brief introduction of commonly used ideas are put together at the end of this dissertation in the form of appendices for the reader's reference. In particular,

Appendix A: Gait Cycle and Events

Appendix B: Lower Limb Frame Assignments

Appendix C: Surface EMG activity

Part II

Tethered Pelvic Assist Device (TPAD)

Chapter 2

Pelvic Interventions during Walking

Rigid link robotic exoskeletons help to reduce therapists' repetitive manual labor and provide objective measurement of therapy during gait rehabilitation. However, the inherent human musculoskeletal complexities make it challenging for any rigid link design to actively control a lower limb joint without adding undesirable constraints. Studies with these devices have shown that current robotic exoskeletons primarily target lower-limb joint motion during walking and add external inertial and mobility constraints at the pelvic level. Since the pelvic motion plays an important role during walking, an external intervention at the pelvis alone can result in locomotor adaptation. Thus, for any gait rehabilitation paradigm, it is important to understand how the human gait adapts when external constraints are induced at the pelvic level. In this chapter, we present two experiments to investigate human walking adaptation with external forces applied to the pelvis using a passive cable system.

2.1 Pelvic Motion during Walking

The human pelvis acts as the supportive segment for the head, arms, and trunk (HAT), and a mobile link between the two lower-limbs [32]. During steady-state walking, the pelvis undergoes motion in all six directions (three translational and three angular). During each stride, pelvic translational motion displays one oscillation in the medial-lateral direction, two oscillations in the anterior-posterior direction, and two oscillations along the vertical axis. The pelvic center is used to generate the baseline patterns in Fig. 2.1 for a healthy subject walking on a treadmill at 3.8 *kmph*.

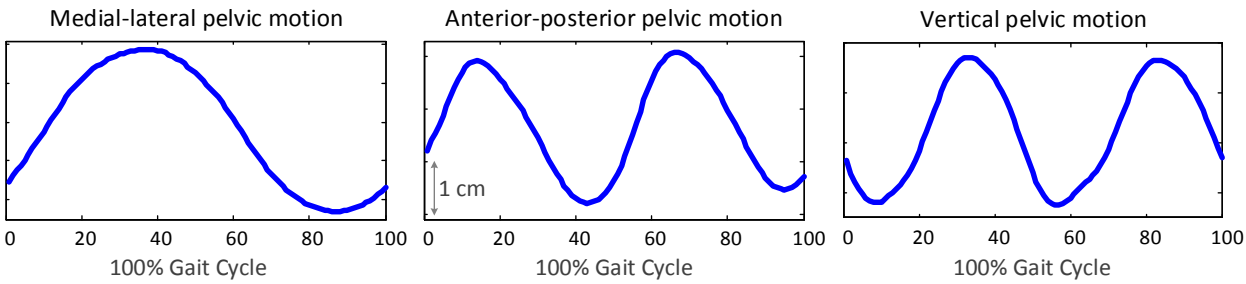

Figure 2.1: Pelvic motion of a representative healthy subject walking at 3.8 *kmph* on a treadmill in the medial-lateral, anterior-posterior, and vertical directions over a gait cycle. Here 0 and 100% represent right heel strike events.

The pelvic center was calculated as the centroid of a triangle formed by three pelvic anatomical locations (human anatomical locations and body frames are presented in Appendix B). Pelvic angular displacements are typically defined as the rotation about the local pelvic axes, described as: tilt (about the medio-lateral axis), obliquity (about the anterior-posterior axis), and rotation (about the vertical axis). The amplitude, frequency, and mean position of the pelvic translational and rotational oscillations during walking depend on the walking speed, step rate, and stride length parameters [9, 32, 59, 60]. Thus, any change in the gait parameters due to an externally applied intervention would require some kind of pelvic motion adaptation.

Due to the proximity of the pelvis segment to the body's center of mass (COM), pelvic motion plays a central role in maintaining balance during walking [61]. Vertical pelvic motion for example modulates the vertical displacement of the COM, which allows the exchange of gravitational potential and kinetic energy during walking [62]. Pelvic motion helps in transferring forces from the lower extremity to the trunk, and thus assists in the forward propulsion of the body [32]. In addition, pelvic medial-lateral movement assists in weight shift towards the stance leg, thereby bringing the COM projection above the stance foot to accomplish the swing initiation of the contra-lateral leg. Thus, any alteration in the pelvic motion due to added inertia or mobility constraints would also require adaptation of lower limb motion.

2.2 External Constraints on Pelvis: Walking Adaptation

The effects of adding external mass and inertia at the pelvic level have been investigated in the literature [53, 54, 63, 64]. Significant changes in the gait parameters as well as in the lower limb

muscle activation levels were reported in these studies. For example in [53], a mechanical setup was developed to determine a threshold of 6 kg for inertia addition at the pelvis above which gait parameters were observed to alter significantly. In [63, 64], weight bags were added on the pelvis and a body weight harness was used to alter the pelvic inertia during walking. Increase in the metabolic cost of walking was observed in direct proportion to the amount of added mass and weight on the pelvis. Higher muscle activation levels were also observed in the increased pelvic inertia condition.

In the gait rehabilitation community, studies have been conducted to investigate the effects of adding mobility constraints to the pelvis. In [6], one such experiment was conducted with an active leg exoskeleton (ALEX II) to study the effects of locking the anterior-posterior pelvic motion (pelvic lunge DOF). The study reported that locking just the pelvic lunge DOF negatively affects the learning and retention of a modified foot trajectory compared to when the pelvic lunge DOF was not locked. In a separate study [65], external mobility constraints were added to lock pelvic motion in the transverse plane. It was reported that fixing transverse plane pelvic motion alters the subject's lower-limb parameters while walking. The goals of these studies were to investigate the limitations of current robotic exoskeletons, and therefore to propose improvements in their design.

In the current chapter, we present two experiments that were conducted to investigate human walking adaptation when external forces were applied to the human pelvis. These studies explore the use of force interventions at the pelvis for applications in gait rehabilitation.

2.2.1 Tethered Pelvic Assist Device (TPAD)

To apply the external forces and moments during the swing and stance phases of walking, a passive system with springs in series with cables was developed. We called this the Tethered Pelvic Assist Device (TPAD). Figure 2.2(a) and (b) show two configurations used during the experiments. One end of each tether was attached to a hip brace, with the other end attached to an inertially fixed frame around the subject. Each elastic tether consists of a spring (4.04 N/mm stiffness) connected in series with a cable. The springs in the system allow modulation of the Cartesian stiffness in 3D space, thereby applying external forces to the pelvis. An initial tension of $90 - 100N$ was set in each tether while the subject stood still and straight on the treadmill. These values were chosen so that subjects could safely balance and walk on the treadmill at 2.5 mph (1.12 m/s) for an extended

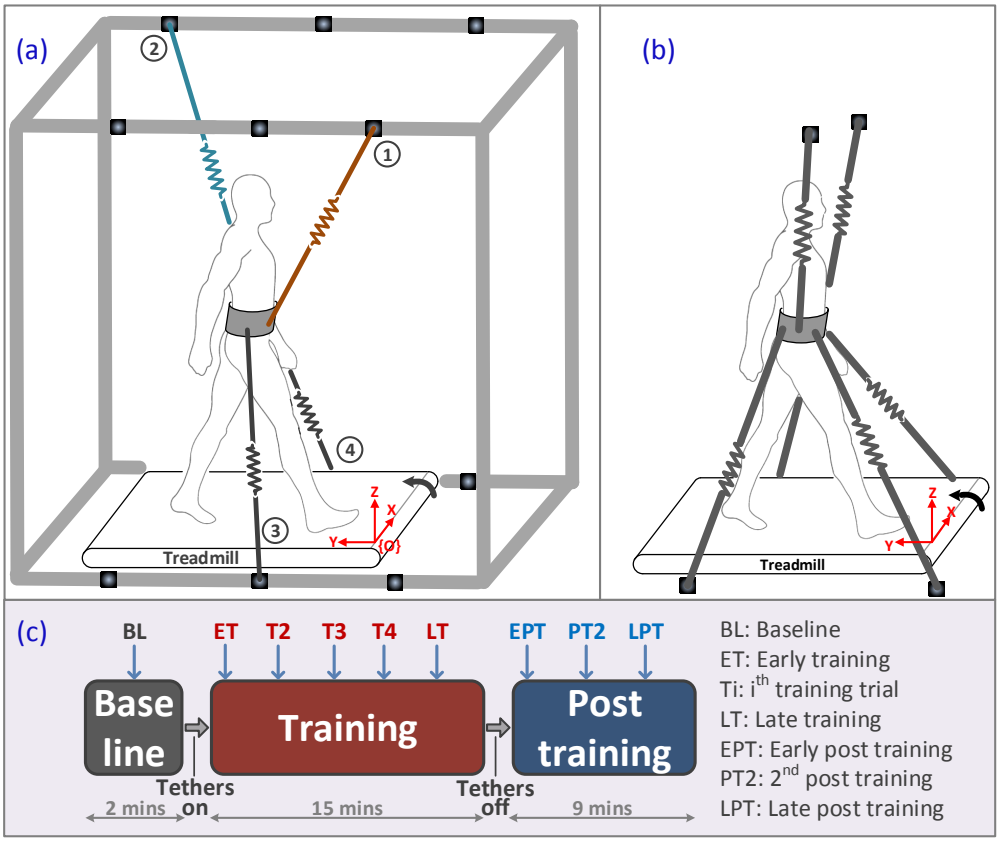

Figure 2.2: Experimental setup of TPAD for the (a) Experiment 1: asymmetric configuration [23], and (b) Experiment 2: symmetric configuration [24, 25]. (c) Experimental protocol for both experiments included baseline, training, and post training periods. Data collection time instances are shown by arrows for each period.

period of time. Load cells (MLP-200, Transducer Techniques, California), with a capacity of 200 *lbs* (889.6 *N*) were used to continuously measure the amount of tension in each tether. The tension data were logged in real time using a DAQ card (NI-PCI-6034E, National Instrument, Austin) and Labview software. A motion capture system (Vicon, Denver) was utilized to track reflective markers placed on the human body. Three force sensitive resistor (FSR) pressure pads were mounted on each shoe insole corresponding to the heel, ball, and toe positions, and were used to estimate foot pressure while walking. An Arduino Lillypad micro-controller was used to collect and store the pressure data on to a 2 *GB* SD card. Xbee® devices were used to monitor the pressure data wirelessly and send commands to the micro-controller.

2.2.2 Experimental Protocol

Eight healthy male subjects with age range 24-31 years (mean age: 27 *yrs* and SD: 2.33 *yrs*) and mean weight 76.12 *kg* (SD: 12.38 *kg*), all right handed, participated in the study. For each subject, the two experiments were conducted with a gap of at least one week in between. The study was approved by the University of Delaware Internal Review Board and involved Baseline, Training, and Post-training sessions, as shown in Fig. 2.2(c). All subjects walked at a constant speed of 2.5 *mph* during the experiment. Data collected during the two minutes of Baseline were treated as the reference data and labeled as BL. During the training session, each subject walked for fifteen minutes with tethers attached to the hip brace and the initial tension values adjusted in each tether. Data were recorded five times for one minute duration at the start, and the 3^{rd}, 6^{th}, 9^{th}, and 12^{th} minutes. These data collection instances were referred to as ET (early training), T2, T3, T4, and LT (late training) as shown in Fig. 2.2(c). During the post-training session, each subject walked for another nine minutes immediately after removing the tethers. Data were recorded three times for one minute duration at the start, and the 3^{rd}, and 6^{th} minutes. These data collection instances were referred to as EPT (early post training), PT2, and LPT (late post training).

2.2.3 Data Processing

For data analysis, the positions of the toe and heel markers with respect to the sacrum marker were used to determine the toe-off and heel strike gait events following the method illustrated in [66]. The time histories of all gait parameters were normalized in time to 100% of the gait cycle.

Marker data were processed to determine the relative joint angles. Pelvic center was calculated as the centroid of the triangle formed by three pelvis markers (right and left ASI and sacrum). Gait symmetry parameters such as the stance-swing ratio (SSR), stance period ratio (SPR), and double support ratio (DSR) were computed between the left and right legs. The tension data from each tether were used to calculate the resultant force and moment values at the sacrum marker location.

To study the adaptation in walking, baseline (BL) data were compared to early training (ET), late training (LT), early post training (EPT), and late post training (LPT) data. From the sample of one minute data, the first five gait cycles of each data set were averaged together to compare the performance. A significant difference between ET and LT in addition to between BL and LT and EPT implied adaptation. If a parameter changed significantly between BL and ET but not between BL and EPT or between ET and LT, then the changes were referred as reactive adaptation. Repeated measure ANOVA was performed to determine the statistical significance (defined as $p < 0.05$). Tukey's post-hoc honestly significant difference test was performed when a statistical significance was identified. Values plotted in the following section are given as means $\pm$ standard errors. An asterisk mark indicates a significant difference between the means of the two sessions.

2.3 Experiment 1

The TPAD was used to apply an asymmetric external force to the pelvis in the transverse plane of walking, as shown in Fig. 2.2(a). Walking on a treadmill involves rhythmic forward and backward anterior-posterior pelvic translation as well as clockwise (CW) and counter-clockwise (CCW) rotation in the transverse plane. Thus, in the presence of tethers while walking, subjects experienced an asymmetric pull on the pelvis. Particularly, tethers 1 and 2 provided a higher resistance to the anterior-posterior pelvic motion during the left leg swing phase and a CCW moment on the pelvis. We hypothesized that to continue walking on treadmill in the presence of these forces, subjects will develop an asymmetric walking pattern in response to the applied force intervention.

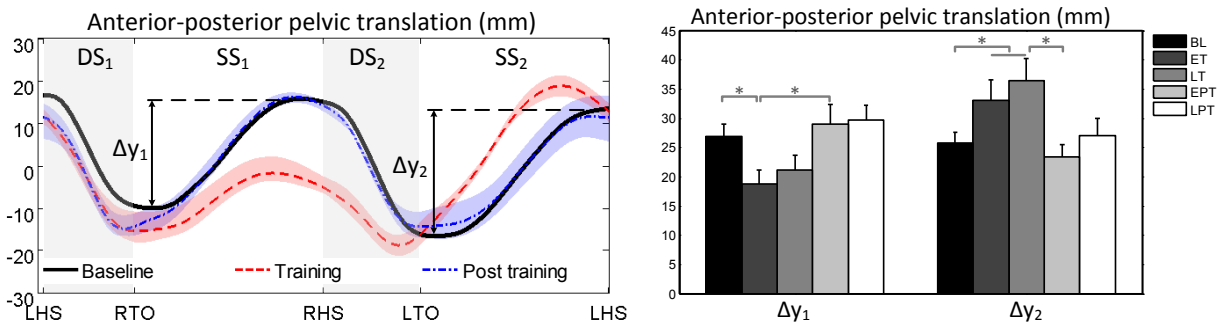

(a) (b)

Figure 2.3: (a) Pelvic translation along anterior-posterior direction for a representative subject with respect to its midpoint during a gait cycle. Single and double support phases for BL are indicated as SS and DS. (b) Pelvic translation during SS_2 phase, $\triangle y_2$, increased during training while pelvic translation during SS_1 phase, $\triangle y_1$, decreased during training for the group. '$*$' denotes significant difference ($p < 0.05$).

2.3.1 Results

Pelvic motion was described by the midpoint of the left and right anterior superior iliac spine markers (LASI and RASI). Figure 2.3(a) shows the pelvic anterior-posterior translation for a representative subject. To remove the offset caused by subject's movement on the treadmill between sessions, the pelvic translation data for each gait cycle were represented with respect to the midpoint value for each gait cycle. It was observed that the pelvis translates forward during the double support phases (DS) and backward during the single support phases SS. During the training period, the pelvic backward translation was comparatively larger during SS_2 than during SS_1. To quantify this difference over the group, net pelvic translation during each SS phase was calculated and represented as $\triangle y_1$ and $\triangle y_2$. It was observed that $\triangle y_2$ increased significantly from BL to ET and LT, while $\triangle y_1$ decreased significantly from BL to ET ($p < 0.05$) over the group, as seen in Fig. 2.3(b). The changes in the pelvic translation values during the SS phase were not significant in the post-training session.

Resultant force component values in the anterior-posterior direction, F_Y, for a representative subject, resolved at the midpoint between the LASI and RASI marker positions, are plotted in Fig. 2.4(a). A positive value of F_Y indicates that there was a net backward force on the pelvis, i.e., the pelvis was being pulled backward. F_Y values increased during the early part of the double support (DS) phases to a maximum and decreased during the early part of the single support (SS)

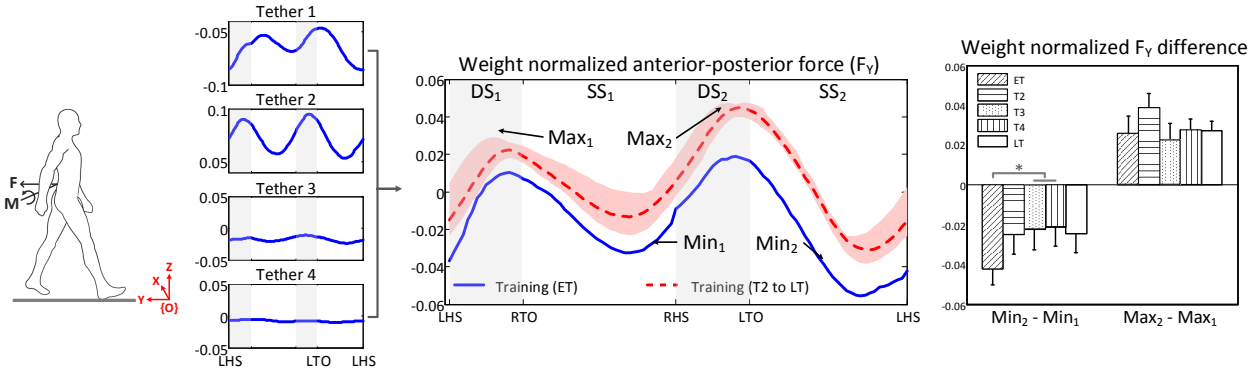

Figure 2.4: (a) Weight normalized resultant force along anterior-posterior direction on the pelvis of a representative subject. (b) Bar graph of the difference between the two peaks (Max) and valleys (Min) values for the group (six subjects).

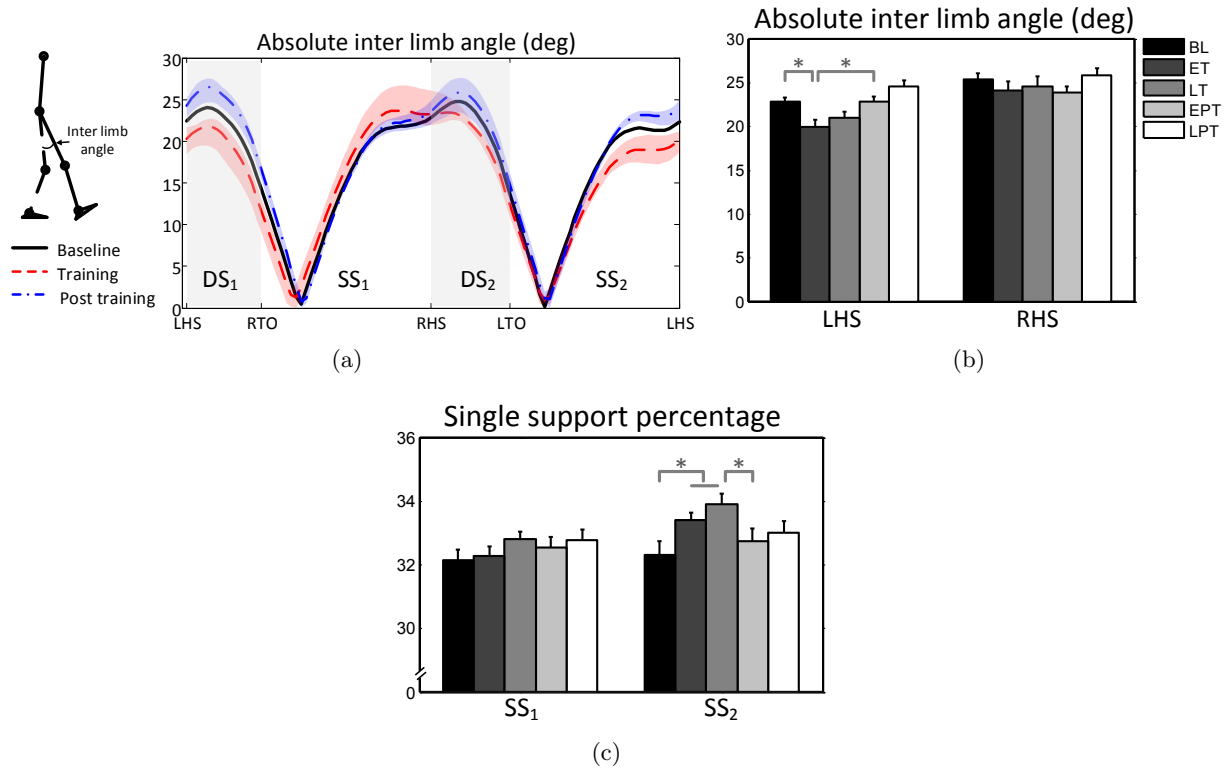

Figure 2.5: (a) Absolute values of inter-limb angle, defined as the angle between lines joining sacrum marker to two knee markers in the sagittal plane, are plotted for a representative subject. (b) During the training period, all subjects showed a reduction in the inter-limb angle at LHS. (c) The duration of SS_2 phase as a percentage of gait cycle increased during the training session for the group.

phases to reach a minimum. For the ET trial, the F_Y minimum values had a higher magnitude during the SS_2 phase, i.e., during the left swing phase. Notably, the difference between the F_Y minimum values during the two SS phases decreased with the progression of the training period. The difference between the F_Y minimum values during the SS phases and the difference between the F_Y maximum values during the DS phases are presented in Fig. 2.4(b) for the group. It was observed that the difference between the minimum values decreased significantly from ET to T3 and T4 ($p < 0.05$), while the changes in the difference between F_Y maximum values were not statistically significant over the training period.

Inter-limb angle was defined as the angle between two lines joining the sacrum marker to the two knee markers in the sagittal plane, as shown in Fig. 2.5(a). The absolute magnitude of the inter-limb angle for a representative subject is plotted in Fig. 2.5(a). The absolute magnitudes of the inter-limb angle at the left and right heel strikes for the group are presented in Fig. 2.5(b). Significant reduction was observed in the angle magnitudes at LHS from BL to ET ($p < 0.05$), while the changes in the angle magnitude were not statistically significant at RHS. No significant changes were reported in the sagittal plane hip, knee, and ankle joint angles during the experiment. Figure 2.5(c) presents the duration of the single support phases as a percentage of the gait cycle over the group. The SS_2 values increased significantly from BL to ET and LT ($p < 0.05$), though the differences between the baseline and post training values were not statistically significant. In addition, the changes in the SS_1 values were not significant over the experiment.

2.3.2 Discussion

In the current study, the application of an asymmetric force to the pelvis using the TPAD resulted in an asymmetric gait pattern. The chosen tether placement required higher effort from the subjects during the left leg swing phase compared to the right leg swing phase. This resulted in longer left leg swing phases, SS_2, which further induced asymmetric pelvic displacement in the anterior-posterior direction during a gait cycle. The difference between the inter-limb angle magnitudes between the left and right heel strikes also represented the asymmetric nature of the subjects' gait pattern.

By adopting the asymmetric gait pattern, subjects were able to distribute the applied external force symmetrically over a gait cycle. The results of the current experiment manifest the potential of developing force interventions at the pelvic level to improve the gait symmetry of a target patient

population.

2.4 Experiment 2

In this experiment, we studied walking adaptation in healthy subjects when an external downward force was applied to the pelvis during a gait cycle. The experiment setup is shown in Fig. 2.2(b). Four tethers were directed downward toward the floor, and two tethers were connected to the top of the frame to ensure subjects' safety while walking. The pelvis moves vertically upward during a single support phase, so a net downward pull was applied to the pelvis that modified the subject's apparent weight (without inertia alteration). We hypothesized that to walk with erect posture, subjects will need to work against the applied downward force. The spring in each tether will facilitate a balance between the vertical pelvic motion and downward force during walking. Thus, training for fifteen minutes will induce changes in gait kinetics. As the applied forces were symmetric for both legs, we hypothesized that the gait symmetry will be retained.

2.4.1 Results

The resultant force and moment at the sacrum marker location are shown in Fig. 2.6(a). Figure 2.6(b) shows the variation of the vertical force for a representative subject during the training. The force values were negative, F_Z down, during the single support phase, SS_1 and SS_2; and the force values were positive, F_Z up, during the double support phase, DS_1 and DS_2. An increase in the F_Z down values were reported as the training session progressed, and F_Z up values remained consistent throughout the training session. Figure 2.7(a) presents the group results for F_Z values. A significant increase was reported in the F_Z down values from ET to LT and from ET to T2 ($p < 0.05$). No significant changes were observed for F_Z up values.

Pelvic vertical motion was calculated from the pelvic center data. Highest and lowest positions during different sessions with respect to the static trial values are presented in Fig. 2.7(b) for the group. A significant decrease in the pelvic highest position was observed from BL to ET, from BL to LT, and from EPT to LT ($p < 0.05$). The differences between the baseline and post-training trials were not significant. Thus, these changes represented subjects' reactive adaptation to the force training. No significant changes were reported in the pelvic lowest position during the double

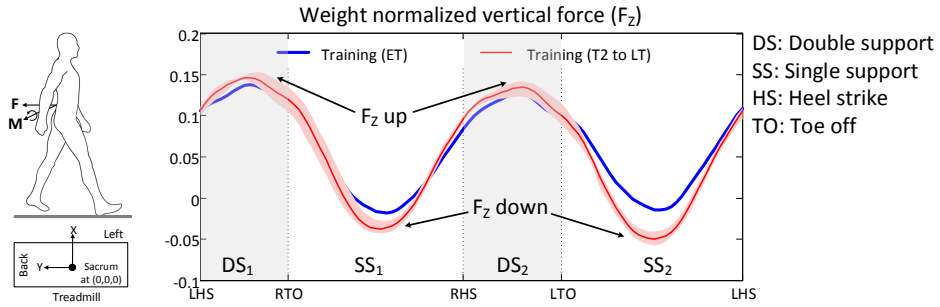

(a) (b)

Figure 2.6: (a) Resultant force and moment vector, (b) Weight normalized vertical component of the resultant force for a representative subject. Increase in F_Z down value can be observed as training progresses.

support phase (Fig. 2.7(b)).

The hip flexion values increased for both legs during the training session, and significant changes were reported between BL-ET, BL-LT, and EPT-LT ($p < 0.05$) as shown in Fig. 2.7(c). Similar to the pelvic position changes in the SS phase, the changes in the hip flexion values also represent subjects' reactive adaptation to the force training. Gait symmetry was investigated from the stance-swing ratio (SSR), stance period ratio (SPR), and double support ratio (DSR) values between the two legs over different trials. Each ratio was obtained by dividing the left leg parameter by the right leg parameter. The null hypothesis, indicating that gait symmetry was retained, was accepted for all three parameters (SSR: $p = 0.36$, SPR: $p = 0.67$ and DSR: $p = 0.83$).

An increase in the heel pressure values was observed during the training and post-training sessions. As seen in Fig. 2.7(d), the peak pressure values increased significantly between from BL to LT ($p < 0.05$) for both legs. An increase in the pressure values was expected during training because of the applied external downward force (F_Z down) on the pelvis. The peak pressure values also increased from ET to LT, though only significantly for the left heel. During the post training session, the peak pressure values remained higher compared to the baseline values, as shown in Fig. 2.7(d). The heel peak pressure values for both legs were significantly higher during LPT compared to BL ($p < 0.05$).

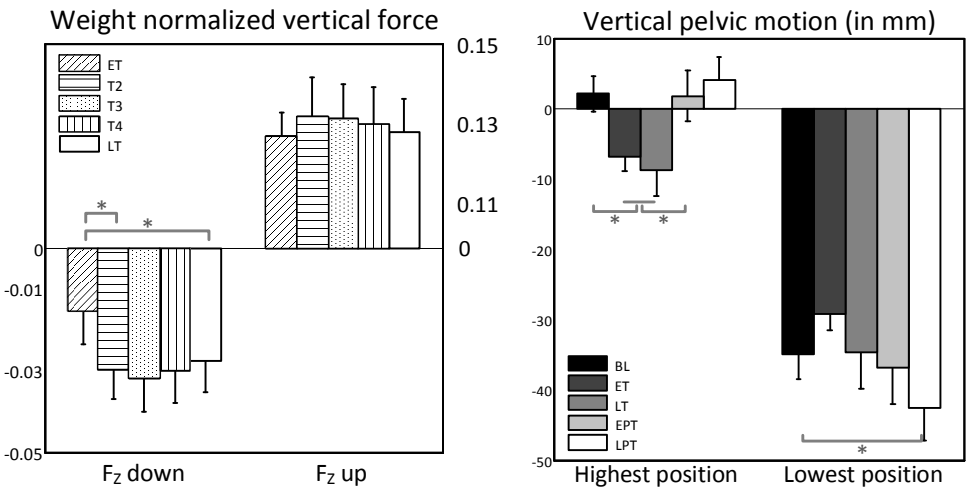

(a) Vertical force

(b) Vertical pelvic motion

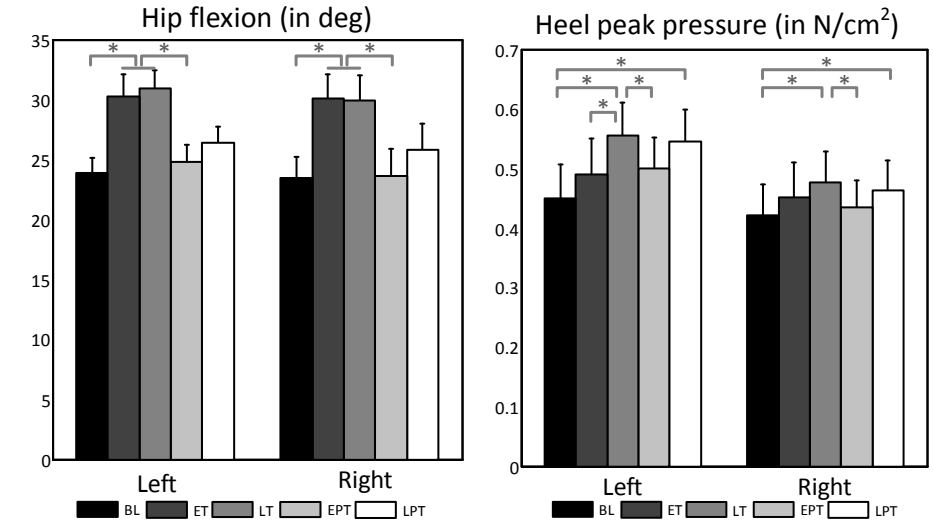

(c) Hip flexion

(d) Heel peak pressure

Figure 2.7: Bar graphs for the group. F_Z down value adapts during training while the variation in pelvic highest position was a reactive response to the applied force training. A reactive response was also noticed in hip flexion value during training. Heel peak pressure increased during training and showed aftereffects. '*' denotes significant difference ($p < 0.05$).

2.4.2 Discussion

In the results, it was observed that the net downward force (F_Z down) on the pelvis increased during the early part of training. At start of the training session, subjects were unaware of the nature of applied forces. As the training session progressed, they applied resistance against the pulling forces of the elastic tethers. Taking the advantage of setup's passivity, the subjects reached a configuration which they could sustain for the rest of the training session. In literature [67, 68], such adaptive human responses to the applied constraints are associated with the recalibration of motor commands, which cause aftereffects when the constraints are removed. In the current study, aftereffects were observed in the heel pressure values.

Results also showed that the presence of external forces on the pelvis reduced the pelvic range of motion. Particularly, subjects were unable to lift their pelvis to the normal height during the single support phases. This led them to increase the hip flexion during the swing phase. Such responses correspond to the feedback control strategies adopted by humans, which represent reactive adaptation to an applied intervention [67].

2.5 Conclusion

The importance of pelvic motion during walking has been explored in this chapter. Most existing robotic exoskeleton design either fails to allow all pelvic DOFs mobility or adds external mass/inertia at the pelvis, which alter the human walking dynamics. Since these constraints can not be efficiently accounted for while using these devices, undesirable changes in the gait parameters are observed.

In this regard, we showed feasibility of using cables and springs to apply pure force interventions on the pelvis. We demonstrated that the application of external forces to pelvis can result in both symmetric as well as asymmetric gait pattern adaptation. In experiment 1, the application of an asymmetric force to the pelvis resulted in asymmetric gait pattern. In experiment 2, healthy subjects showed adaptation in gait kinetics parameters in response to external downward force on the pelvis. The results of these studies suggest that controlled pelvic interventions have the potential to modify the gait parameters which can be used for gait rehabilitation applications.

However, the TPAD cannot control the magnitude and direction of the applied force once the

subject starts walking. Therefore, the following chapters describe an active cable-driven system to apply an external wrench (combined force and moment) to the human pelvis. Experiments using this device with healthy individuals as well as patients are also reported in the subsequent chapters.

Chapter 3

Active Tethered Pelvic Assist Device (A-TPAD)

In this chapter, the active version of the cable-driven robot developed in the Robotics and Rehabilitation (ROAR) laboratory at the Columbia University is presented. The mechanical setup, system modeling, and a brief description of the cable routing and cable configurations are presented. The control methodology and algorithms developed for the robot are also discussed in this chapter. The chapter concludes with an experiment conducted to validate the system's performance.

3.1 Active Tethered Pelvic Assist Device (A-TPAD)

The Active Tethered Pelvic Assist Device (A-TPAD) is a novel cable-driven robot. It was developed to apply an external wrench (combined force and moment) to the human pelvis, and control the magnitude, direction, duration, as well as synchronize the applied wrench to the gait events during walking. Figure 3.1 and 3.2 show the different components of the A-TPAD.

3.1.1 Mechanical design

An inertially fixed rigid frame was constructed from modular aluminium T-framing (8020 Inc., Columbia city, Illinois). Eight single phase AC servo motors were mounted on the frame using linear sliders, as shown in Fig. 3.3. Low-Stretch nylon-coated stainless steel wires with 540 N (120 lb) breaking strength were routed using pulleys within the workspace. This design provides

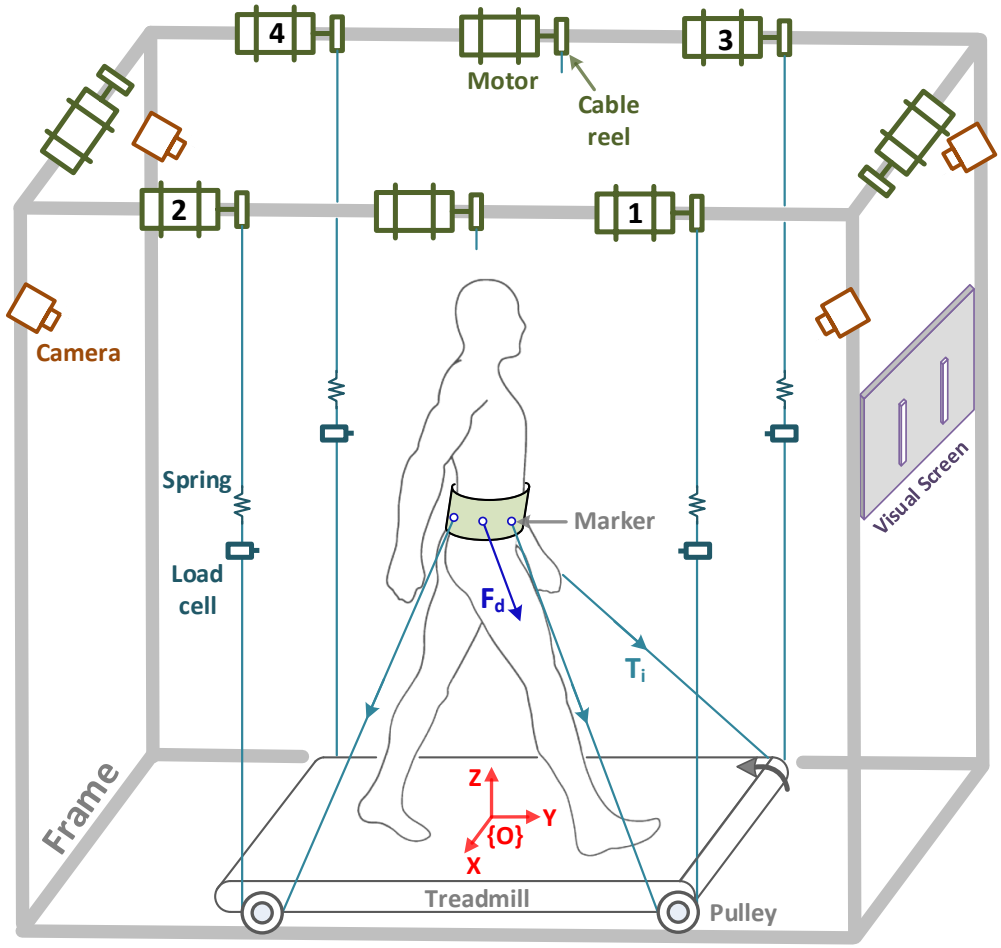

Figure 3.1: Schematic of the Active Tethered Pelvic Assist Device (A-TPAD) [26]. Eight motors are mounted on a rigid frame and cables are routed to the subject's pelvis using pulleys. Load cells are used to measure the cable tensions and a spring is placed in series between the motor and load cell. A ten-camera motion capture system is used to track the cable attachment points and human motion. A global coordinate system, $\{\mathbf{O}\} : XYZ$, is set at the center of the treadmill to facilitate analysis.

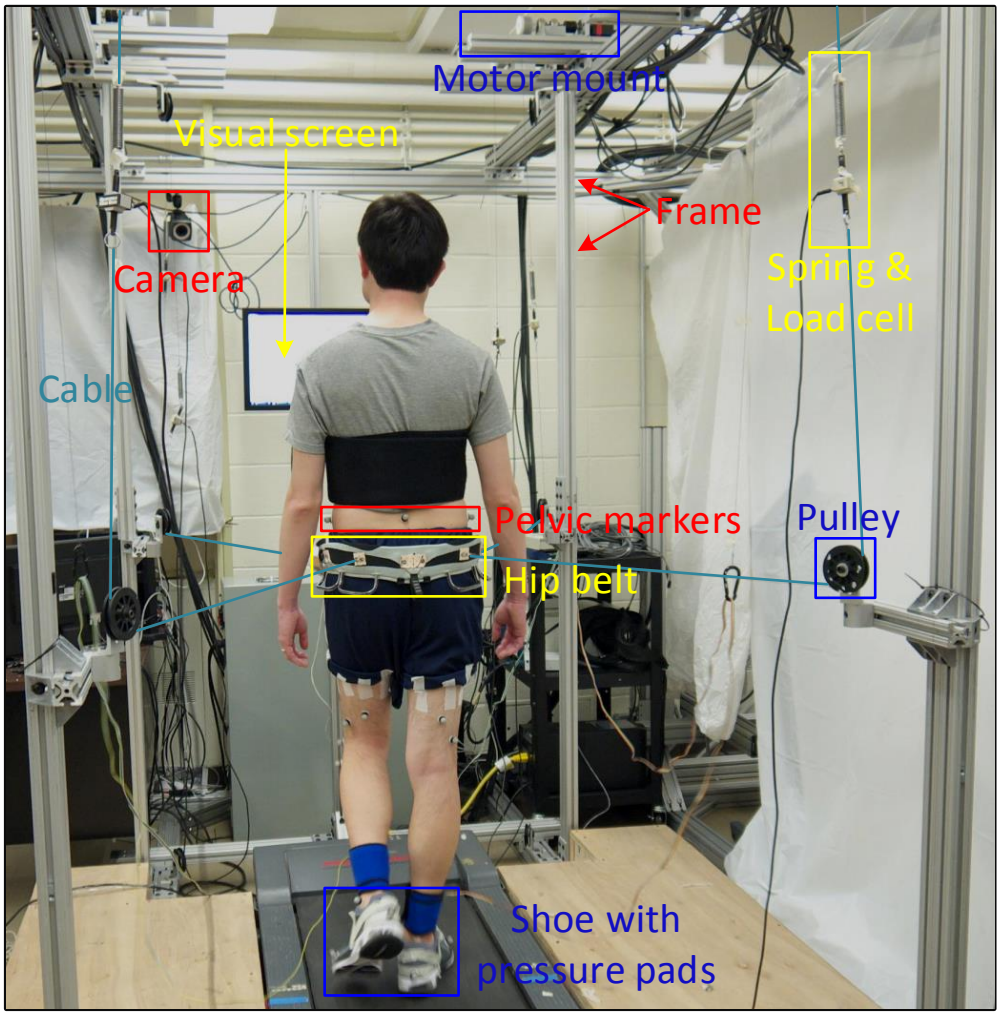

Figure 3.2: A subject walking on a treadmill with four cables attached to the hip belt.

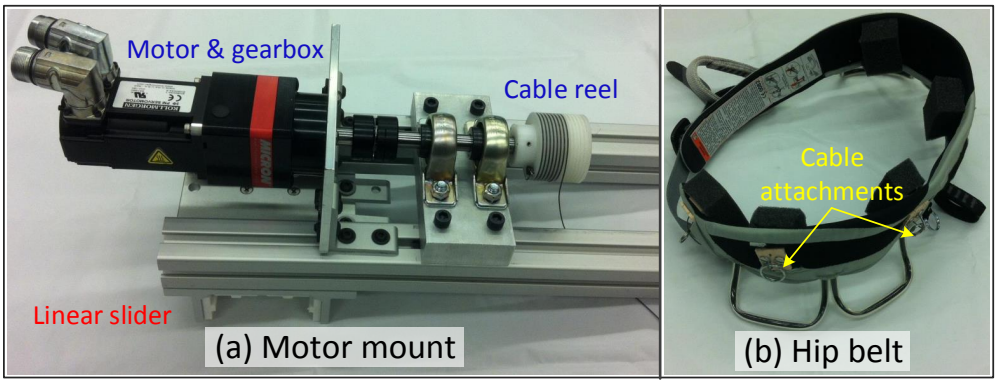

Figure 3.3: (a) An independent unit, comprising a motor, gearbox, cable reel and bearings, is used for actuating each cable. This unit can be easily moved on the inertial frame to achieve different cable configurations. (b) A fabric hip belt is worn by the subject to attach cables at the pelvic level.

the flexibility of changing the number of motors and their placements to achieve different cable configurations and provide modularity to the design. All motors were powered in torque mode and a continuous torque of 4 Nm was achieved in each motor through a 10:1 gear reduction. Motors, drivers, and gear boxes were from Kollmorgen (Radford, VA). A cable reel of 5.08 cm (2 $inch$) diameter was mounted on the gearbox shaft so that a maximum continuous tension of 157 N was achieved in each cable. These reels were machined from Delrin® shaft with right-hand threads (Fig. 3.3), such that when the motor rotates counter-clockwise the cable wrap on to the reel. These reels, unlike a cable drum, prevent cables from wrapping on themselves.

The free end of a cable from the cable-reel was connected to a fabric hip belt (climbing harness from Black Diamond Equipment, Utah), worn by a human subject. This facilitates application of pulling force at each cable connection point on the hip belt. The resultant of these pulling forces generates the desired external wrench on the pelvis. To measure the instantaneous cable tension, a load cell was installed in series with each cable. With a 12 V DC amplifier, each load cell can record up to 890 N (TMO-1 and MLP-200 respectively from Transducer Techniques, California). A spring of stiffness 2.5 N/mm (14.21 lb/in) was also installed in series with each cable to reduce the output impedance. A ten-camera motion capture system (Bonita-10 series from Vicon, Denver) was used as a part of the controller to track the human motion and cable attachment locations during the experiment. The controller was implemented on a Labview PXI real-time system (National Instruments, Austin, TX).

3.1.2 System Model

The A-TPAD is a cable-driven parallel system with m actuated cables connected to the human pelvis having $n = 6$ degrees-of-freedom (DOFs), refer to Fig. 3.4. Each cable is modeled as a pure force at the attachment point. These cables together exert a wrench on the pelvis. Therefore, if $T \in \Re^{m\times 1}$ represents the tension in the cables and $W_e \in \Re^{n\times 1}$ is the external wrench on the pelvis, these are related to each other as

$$AT = W_e \tag{3.1}$$

where $A \in \Re^{n\times m}$ is the structure matrix, which depends on the system geometry and can be computed knowing the coordinates of the cable attachment points. For a six DOF system, when

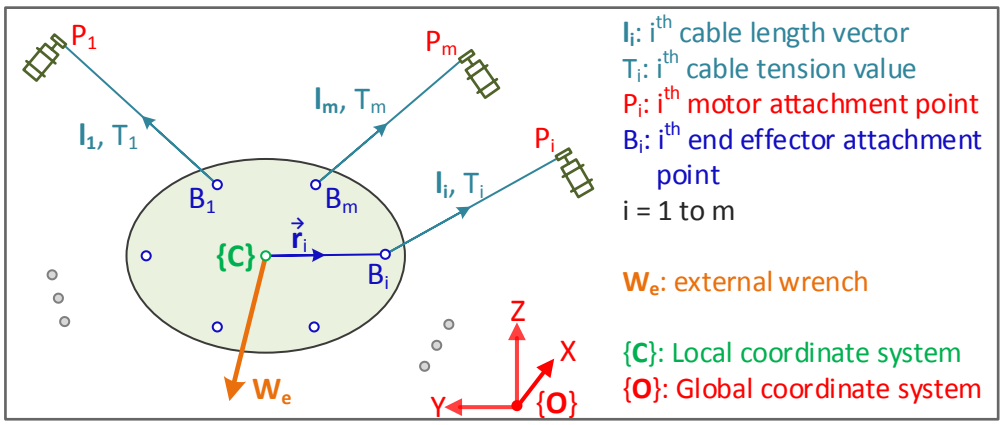

Figure 3.4: The A-TPAD is a cable-driven parallel system with m actuated cables connected to the human pelvis having $n = 6$ DOFs. One end of each cable is attached to the pelvis and the other end to a motor, shown as $\mathbf{B}_i$ and $\mathbf{P}_i$ respectively. These cables together exert an external wrench, W_e, on the pelvis.

W_e is computed at the point C, refer to Fig. 3.4, the matrix A is given by the following expression.

$$A = \begin{bmatrix} \dots & \hat{\mathbf{l}}_i & \dots \\ \dots & \mathbf{r}_i \times \hat{\mathbf{l}}_i & \dots \end{bmatrix}_{6\times m} \tag{3.2}$$

where $\hat{\mathbf{l}}_i$ is the i^{th} unit cable length vector oriented away from the connecting rigid body and $\mathbf{r}_i$ is the vector from the point C to the i^{th} cable attachment point on the rigid body.

The structure matrix, A, can be related to the Jacobian matrix of the cable-driven parallel manipulator using a vector closed loop formulation. From Fig. 3.4, the cable length vector can be expressed as,

$$\vec{\mathbf{l}}_i = \vec{OP}_i - \vec{OC} - \mathbf{r}_i \tag{3.3}$$

On differentiating Eq. (3.3) and taking a scalar product with a unit vector along the cable, we get

$$\dot{\vec{\mathbf{l}}}_i.\hat{\mathbf{l}}_i = -\left(\dot{\vec{OC}} + \omega \times \mathbf{r}_i\right).\hat{\mathbf{l}}_i$$

where $\omega \in \Re^{3\times 1}$ and $\dot{\vec{OC}} \in \Re^{3\times 1}$ are the angular and translational velocities of the end-effector respectively expressed in the global coordinate frame, $\{O\} : XYZ$. The cable length velocity can

then be expressed as

$$\begin{bmatrix} \vdots \\ \dot{l}_i \\ \vdots \end{bmatrix}_{m\times 1} = - \begin{bmatrix} \vdots & \vdots \\ \hat{\mathbf{l}}_i^{\mathrm{T}} & (\mathbf{r}_i \times \hat{\mathbf{l}}_i)^{\mathrm{T}} \\ \vdots & \vdots \end{bmatrix}_{m\times 6} \begin{bmatrix} \dot{\vec{OC}} \\ \omega \end{bmatrix}_{6\times 1} = -A^T \begin{bmatrix} \dot{\vec{OC}} \\ \omega \end{bmatrix} \tag{3.4}$$

where $J = -A^T$ is defined as the Jacobian matrix relating the cable length velocities to the end-effector translational and angular velocities.

3.1.3 Tension Planner

A cable in a cable-driven robot can only apply a pulling force on the end-effector and therefore positive cable tension must be maintained to retain control. It has been shown that for an n DOFs system, at least $n+1$ cables are required for generating a desired wrench, $W_e \in \Re^{n\times 1}$, [69, 70]. Thus, the A-TPAD is modeled as a redundantly restrained cable robot, i.e., $m \geq (n+1)$. This makes Eq. (3.1) under-determined. Assuming A to be full rank, the general solution can be written in terms of the minimum norm solution ($\overline{T}$) and the null space of the structure matrix A, [71].

$$T = \overline{T} + N(A)\lambda \tag{3.5}$$

$$where \quad \overline{T} = A^T(AA^T)^{-1}W_e, \tag{3.6}$$

$N(A)$ is the null space of matrix A and $\lambda \in \Re^{(m-n)\times 1}$ is an arbitrary vector. The minimum norm solution is given by the Pseudo-inverse.

For $T \succeq 0$[1], i.e., each element of T is positive, Eq. (3.5) defines a convex region in the space of tension values. Though, infinitely many tension solution sets are possible in the case of redundantly constraints cable robots. Optimality criteria are therefore developed to find a feasible solution set. Different criteria have been proposed to find the cable tension distribution in the literature, few of these works include [16, 19, 21, 71–75]. In the current work, a quadratic programming based optimization scheme, with a lower and an upper bound on the cable tension values, T_{min} and T_{max},

[1] $\succeq$ stands for the componentwise inequality. For u, v two vectors in $\Re^n$, $u \succeq v \Leftrightarrow u_i \geq v_i, i = 1, \ldots, n$.

Table 3.1: Cable attachment locations on the frame

	$\mathbf{P}_1$	$\mathbf{P}_2$	$\mathbf{P}_3$	$\mathbf{P}_4$
X (m)	0.60	0.60	-0.60	-0.60
Y (m)	0.80	-0.80	0.80	-0.80
Z (m)	-0.10	-0.10	-0.10	-0.10

is implemented to find the cable tension set, T, to apply W_e.

$$minf \tag{3.7}$$

$$f = \frac{1}{2}(T - T_p)^T(T - T_p)$$

$$s.t. \quad AT = W_e, \quad and \quad T_{min} \preceq T \preceq T_{max}$$

where T_p is a positive constant, which is added to the objective function to ensure non-zero cable tension values. A quadratic programming algorithm provides a continuous solution and is suited for real-time applications. It has been successfully used for cable tension planning in various real-time applications [16,19,21,71,72]. However, it suffers from non-predictable worst case run-time [73,74]. Such issues can be minimized by appropriately selecting the cable configuration to apply the desired wrench profile. In the following section, we briefly describe some cable configurations that can be achieved with the A-TPAD.

3.1.4 Cable Configuration and Desired Wrench

During an experiment, the wrench capability of the A-TPAD depends on the actuator limits and the pelvic position relative to the cable attachment locations on the frame. We define the feasible workspace as the set of pelvic poses a subject can have during walking on a treadmill in which the A-TPAD can apply a specific external wrench using limited cable tensions. The system design provides flexibility to change the cable configuration to achieve a desired wrench vector. Four cases have been shown in Fig. 3.5. For configuration A, four cables connect the hip belt to the lower part of the frame. Thus, at most three components of the external wrench vector on the pelvis can be controlled (Eq. (3.5)). One possible choice of wrench can be: forces in the X and Y directions, and a downward vertical force (-F_Z) as shown in Fig. 3.5. Similarly, configuration B can be used to apply a planar wrench vector on the pelvis (F_X, F_Y, and M_Z). Use of six cables in configuration C

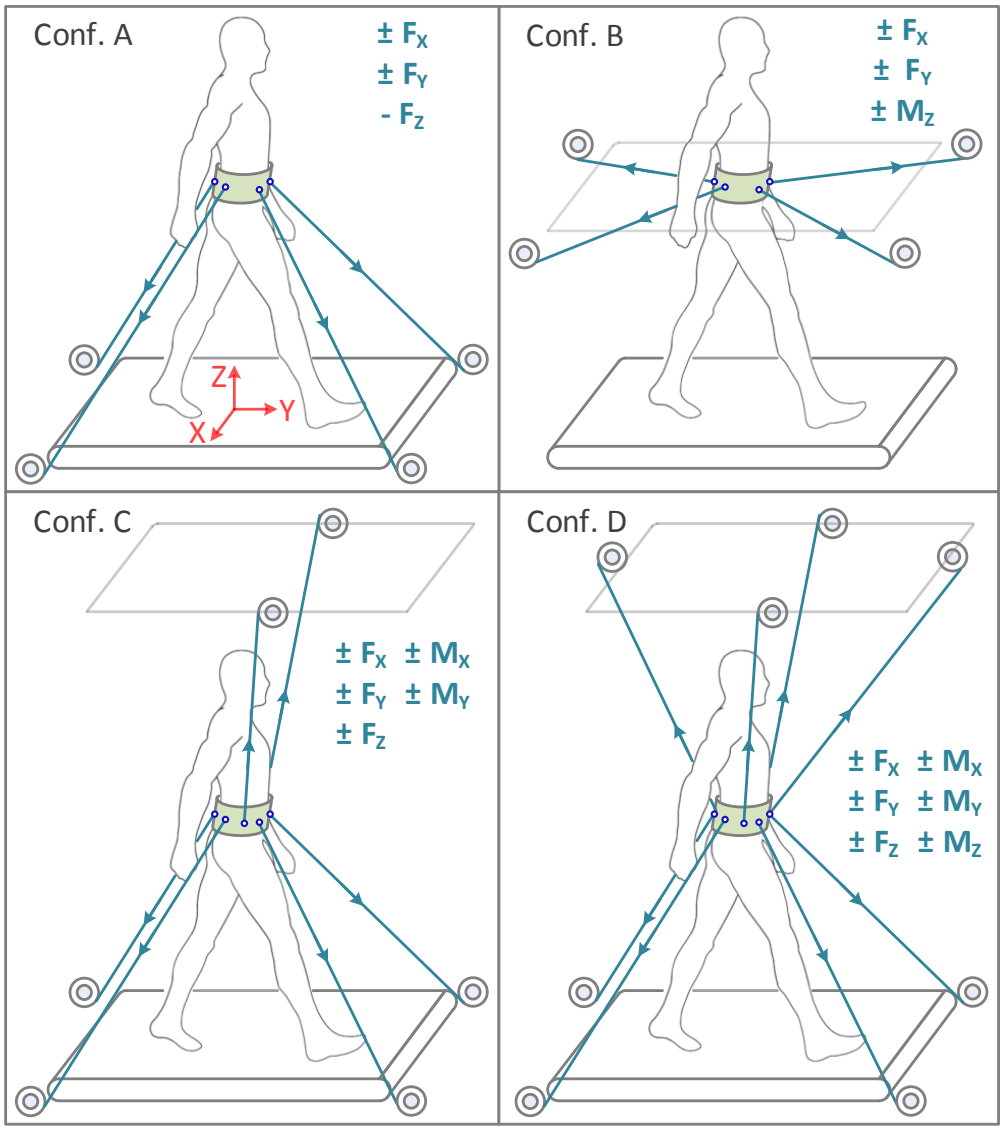

Figure 3.5: The system allows the flexibility to choose the number of motors and the locations of routing pulleys to achieve different cable configurations. Four examples are shown. In Conf. A and B, at most three components of the external wrench vector on the pelvis can be controlled. Use of six cables in Conf. C allows control of five components of the wrench vector, and eight cables in Conf. D allows control of all six wrench components. For each configuration one possible choice of wrench is indicated.

allows the control of any five components of the wrench vector, and eight cables in configuration D allows the control of all six wrench components on the pelvis. Similarly, other cable configurations are also feasible with the A-TPAD, and the choice of a cable configuration depends on the goal of the experiment.

To analyze the A-TPAD feasible workspace, a simulation in Matlab (Mathworks, Natick, MA) can be conducted using baseline pelvic trajectories to optimize the cable attachment locations on the frame. For cable configuration A and cable attachment locations on the frame, $P_i's$ as presented in Table 3.1, where the treadmill center is the origin, the system can apply a 10% of a subject's body weight (BW) vertical downward force on the pelvis for a wide range of subject heights (5-6.4 ft) and weight (55-95 kg) such that F_X and F_Y lie within $\pm 1\%$ BW and the moment components at the pelvic center remain under 4 Nm. Indeed, this simulation procedure can be used for other cable configurations to best locate the cable attachment points to apply a particular wrench on the pelvis.

3.2 Controller

The goal of the A-TPAD is to apply a desired wrench to a subject's pelvis during walking. This is achieved in two steps: (i) the desired cable tension calculation, and (ii) the desired cable tension implementation using the controller architecture shown in Fig. 3.6 [27].

3.2.1 High Level Controller

The part of the controller that calculates the desired cable tension values to apply a desired wrench is referred to as the high level controller (Fig. 3.6). A real-time motion capture system is used to track the retro-reflective markers placed at cable attachment locations and various human anatomical positions, as shown in Fig. 3.7. The marker data are accessed on a host computer running Vicon's Nexus software, where three markers define a rigid body kinematically and a single marker defines a point in the global coordinate system. Using a .NET assembly reference to the Vicon data software development kit (SDK), cable attachment locations are sent to a remote Labview PXI system.

The computation steps are explained through Algorithms 1 and 2. Algorithm 1 is executed once at the start of the training. The pelvic markers ($H|_O$), located at three anatomical loca-

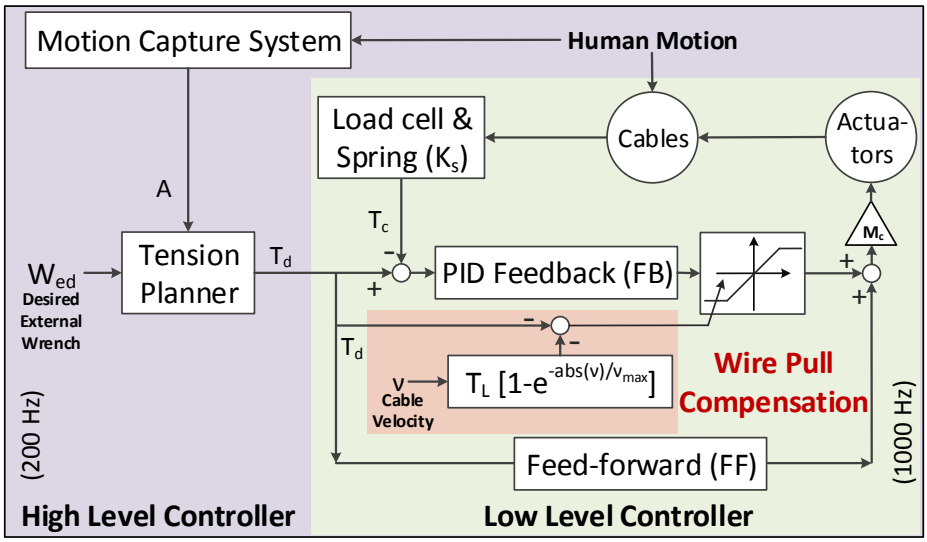

Figure 3.6: The control architecture of the A-TPAD is divided into two parts [27]. The high level controller tracks the human motion and cable attachment locations and uses an online optimization scheme to calculate the desired cable tension values, T_d, necessary to apply desired external wrench, W_{ed}. The low level controller implements the T_d values using a unit gain FF and PID based FB terms. A wire pull compensation is added to resolve the cable slackening problem and improve the controller performance.

Algorithm 1 Markers: Static

```
procedure STATIC
    Acquire:
    H|_O ← pelvic markers
    B|_O ← brace cable point markers
    P|_O ← frame cable point markers
    if H|_O, B|_O or P|_O = ∅ then                ▷ missing markers
        goto Acquire.
    else
        {C}:XYZ ← H|_O.                           ▷ refer to Fig. 3.7
        r_i|_C ← {C}:XYZ and B|_O.
        Save r_i|_C and P|_O.
        close;
```

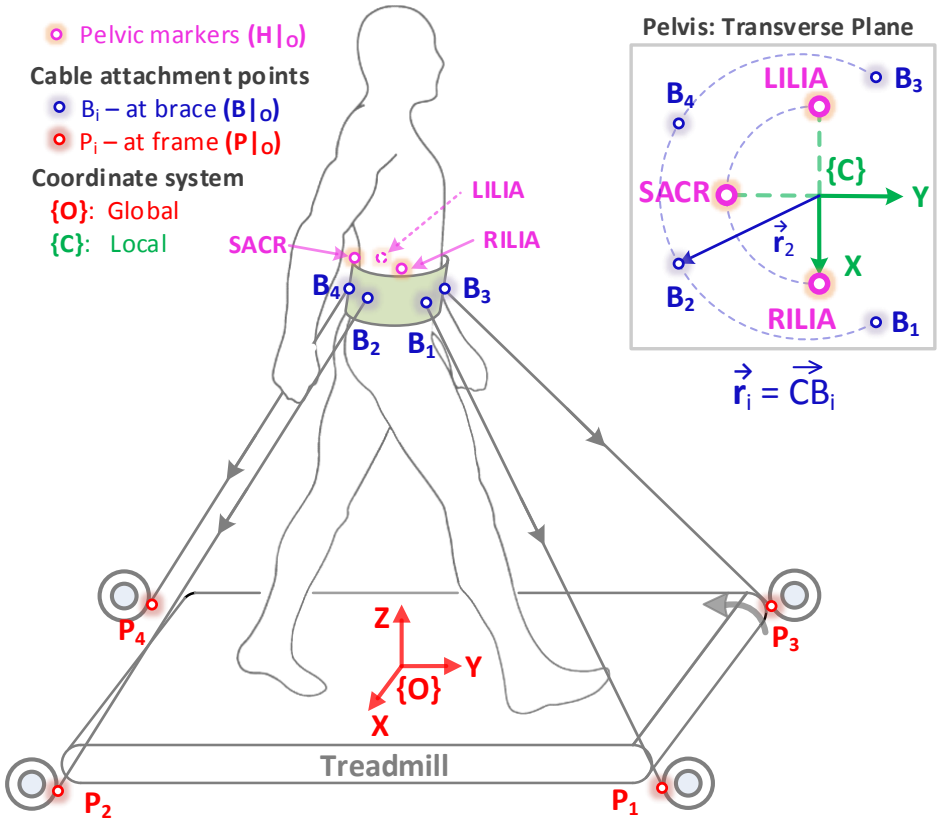

Figure 3.7: Pelvic ($H|_O$), brace ($B|_O$), and frame ($P|_O$) markers are shown for a cable configuration. All these markers are required only once during the static trial (Algorithm 1), i.e., when the subject is standing still and straight. While walking, dynamic trial, only pelvic markers ($H|_O$) are retained (Algorithm 2).

Algorithm 2 Markers: Dynamic

procedure DYNAMIC
  Available : $P|_O$ and $\vec{\mathbf{r}}_i|_C$
  Acquire:
  $H|_O \leftarrow$ pelvic markers
  if $H|_O = \emptyset$ **then** ▷ missing markers
    $T_d(j) \leftarrow T_d(j-1)$ ▷ previous step solution
    return $T_d(j)$
    goto Acquire.
  else
    $\{C\}{:}XYZ \leftarrow H|_O$.
    $B|_O \leftarrow \{C\}{:}XYZ$ and $\vec{\mathbf{r}}_i|_C$.
    $\vec{\mathbf{l}}|_O = P|_O - B|_O$.
    $A \leftarrow \vec{\mathbf{r}}_i|_O$ and $\vec{\mathbf{l}}|_O$. ▷ refer to Eq. (3.2)
    Tension Planner:
    $W_{ed} \leftarrow$ user defined.
    $T_p \leftarrow T_d(j-1)$.
    $min\ \left[\frac{1}{2}(T-T_p)^T(T-T_p)\right]$ ▷ refer to Eq. (3.7)
    $s.t.\ AT = W_{ed},$ and $T_{min} \preceq T \preceq T_{max}$.
    if $T = \emptyset$ **then** ▷ no current solution
      $T_d(j) \leftarrow T_d(j-1)$
      return $T_d(j)$
      goto Acquire.
    else
      $T_d(j) \leftarrow T$
      return $T_d(j)$
      goto Acquire.

tions as shown in Fig. 3.7, are used to calculate the local coordinate system {C}:XYZ. From the brace markers ($B|_O$), vector $\vec{\mathbf{r}}_i$ is then expressed in {C}:XYZ as $\vec{\mathbf{r}}_i|_C$, as described in lines 9-10 of Algorithm 1. The values of $\vec{\mathbf{r}}_i|_C$ and $P|_O$ are then used to calculate the structure matrix, A, as described in lines 10-13 of Algorithm 2 using Eq. (3.2). The Algorithm 2 was executed at 200 Hz. Based on the desired external wrench vector, W_{ed}, the desired cable tension values, T_d, are calculated using the quadratic programming formulation, as described in lines 14-18 of Algorithm 2 using Eq. (3.7). During the experiment, the values of T_p were taken to be the cable tension values calculated in the previous step to keep smoother cable tension profile (line 16 of Algorithm 2). For those instances, when the optimization problem did not yield the solution or when the markers were occluded, tension values calculated in the previous step were used (line 19 and 5 of Algorithm 2 respectively).

3.2.2 Low Level Controller

The part of the controller that implements the desired cable tension is implemented at 1000 Hz and referred to as the low level controller. A force mode control scheme is used to follow the desired tension values. An open loop reference feed-forward (FF) term with a unit gain and a closed loop PID based feedback (FB) term are used (Fig. 3.6). The net commanded voltage to the motor, V_T, is given by the expression

$$V_T = M_c \left(T_{FB} + T_{FF}\right) \tag{3.8}$$

$$\text{where } T_{FB} = \left[K_p e + K_i \int e(\tau) d\tau + K_d \frac{dT_c(t)}{dt}\right],$$

$$T_{FF} = T_d, \text{ and } e = T_d - T_c$$

where T_{FB} and T_{FF} are the outputs of the FB and FF terms, T_d and T_c are the desired and current cable tension values, and e is the tension error. M_c is a positive constant for each motor, called the motor constant, which relates the commanded voltage to the cable tension values linearly. Figure 3.8 shows the calculation of M_c for a motor. K_p, K_i and K_d are the gains for the proportional, integral and derivative terms respectively. The values of these gains depend on the used spring stiffness, K_s, and their values when $K_s = 2.5\ N/mm$ were 3.5, 0.001 and 0.0004 respectively.

The FB output can have both positive and negative values depending on the sign of the difference

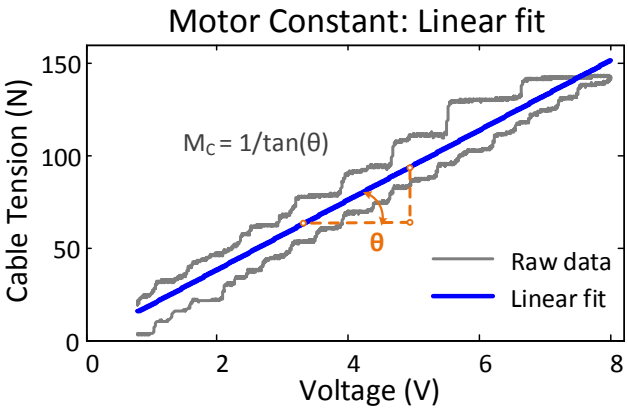

Figure 3.8: Positive voltage was applied on a motor to pull a cable connected to a fixed rigid support at the other end. The collected cable tension and motor voltage data were linearly fitted to calculate the motor constants for each motor, M_c.

between the desired cable tension, T_d, and current cable tension, T_c values. Since each cable in a cable-driven system can only be operated in tension, an uncontrolled negative FB output can result in the cable slackening which can further lead to cable coming off the cable-reel. To prevent such occurrences, a limit on the minimum output of the FB term should be enforced. One possible choice is $(T_{FB})_{min} = -T_d$. However, such limit can potentially add the actuator dynamics to the user. This is demonstrated through a simple test in Fig. 3.9(a). A cable was pulled and pushed approximately 1 ft by hand at different frequencies, which were monitored using a metronome. The commanded desired tension value, T_d, was 20 N, and the applied cable tension values, T_{nc}, were recorded using a load cell. The controller performance was not adequate during the cable pulling phase. This was due to the imposed limit on the minimum FB output. The high T_{nc} values during this phase meant that the actuator dynamics was very apparent to the subject.

From this test, it was observed that the cable velocity sign changes with the direction of hand motion. In particular, positive cable velocities were reported during the cable pushing phase and negative cable velocities were reported during the cable pulling phase. Notably, the cable velocity magnitude increased with the increase in the motion frequency. Therefore, a *wire pull compensation*, WPC, term was implemented to express the minimum FB output limit for each motor as a function of the cable velocity, $\nu(t)$, as shown in Fig. 3.6. The $(T_{FB})_{min}$ is given by the following expression.

$$(T_{FB})_{min} = -T_d - \overbrace{T_{\mathrm{L}}\left(1 - e^{\frac{-\|\nu(t)\|}{\nu_{max}}}\right)}^{T_{lim}}, \tag{3.9}$$

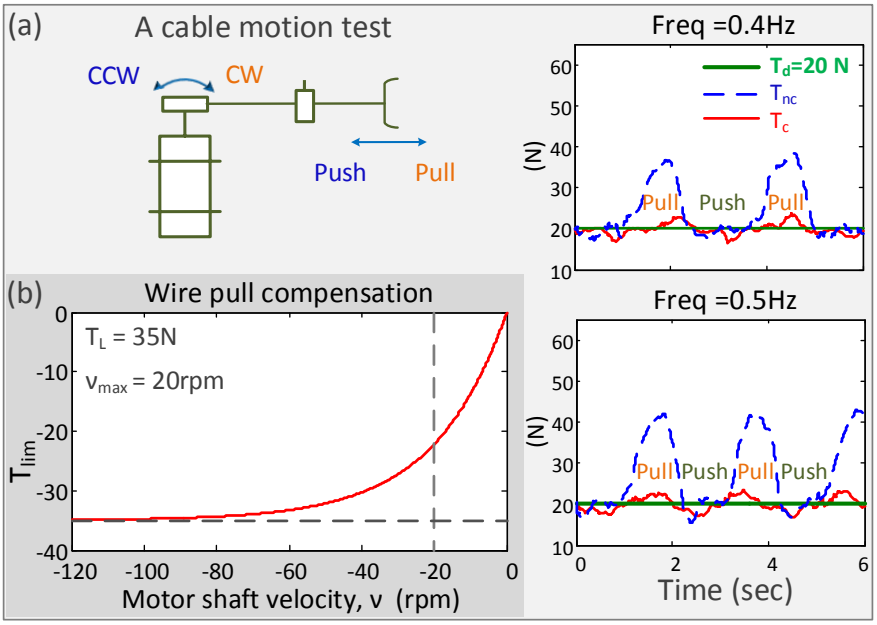

Figure 3.9: (a) A cable was pulled and pushed approximately 1 ft by hand at 0.4 and 0.5 Hz frequencies, which were monitored using a metronome. The actual and desired ($T_d = 20N$) cable tension values are plotted, where T_c and T_{nc} are the cable tension values with and without the wire pull compensation term. (b) T_{lim} is zero when the subject is not moving and approaches $-T_{\text{L}}$ exponentially as the cable velocity becomes more negative.

where T_{L} and ν_{max} are two positive parameters. These parameters were tuned during a human walking test to achieve a responsive controller. The variations of T_{lim} with $\nu(t)$ are shown in Fig. 3.9(b). T_{lim} is zero when the subject is not moving, i.e. $\nu = 0$, and approaches $-T_{\text{L}}$ exponentially as the negative cable velocity magnitude increases. In Fig. 3.9(a), the effect of adding this term on the controller performance is shown by T_c. It is observed that the controller performance improved significantly during the cable pulling phase, which is almost similar to the cable pushing phase.

3.3 Dummy pelvis experiment

Before A-TPAD human testing, an experiment was conducted using a rigid plate setup, referred to as the dummy pelvis setup, to test the system performance.

3.3.1 Setup

The setup included two 1 ft by 1 ft square Delrin® plates attached together with a six axis force-torque sensor (Mini45 from ATI Industrial Automation, North Carolina), as shown in Fig. 3.10.

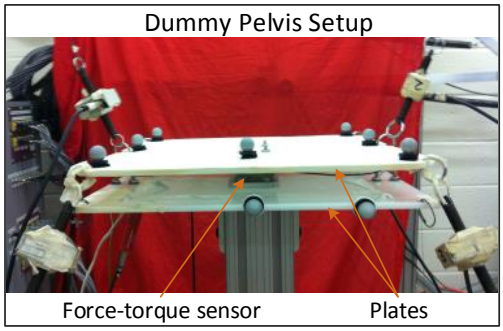

Figure 3.10: The dummy pelvis setup includes two Delrin® plates attached together using a six axis force-torque sensor. Cables are attached to the upper plate to apply the desired external wrench.

Table 3.2: Root mean square error

RMSE	$F_x(N)$	$F_y(N)$	$F_z(N)$	$M_x(Nm)$	$M_y(Nm)$	$M_z(Nm)$
$W_s - W_c$	0.66	1.75	2.77	0.38	0.19	0.07
$W_d - W_c$	0.54	1.35	3.14	-	-	-
$W_d - W_s$	0.58	1.55	2.13	-	-	-

Cables from the motors were attached to the upper plate. The force-torque sensor recorded the force-moment vector at the center of the upper plate with respect to the lower plate. Retro-reflective markers were placed on the upper plate to record the cable attachment points. Three markers were also placed on the lower plate to define a local coordinate frame, which was used to resolve the measured force-moment vector in the global coordinate system.

3.3.2 Experiment

Four cables, as shown by configuration A in Fig. 3.5(a), were used to apply a three dimensional sinusoidal force on the upper plate while the moment components at the plate center were kept within a small range. The quadratic optimization in Eq. (3.7) was solved for the following parameters.

$$\begin{aligned} F_X &= 1\ sin(2\pi f\tau)N \\ F_Y &= 4\ sin(2\pi f\tau)N \\ F_Z &= -45 + 6\ sin(2\pi f\tau)N \\ |M_{X,Y,Z}| &\preceq 2Nm \\ 10 \preceq T &\preceq 60N \end{aligned} \tag{3.10}$$

where τ is the time and f is the frequency ($f = 1.5\ Hz$ during the experiment).

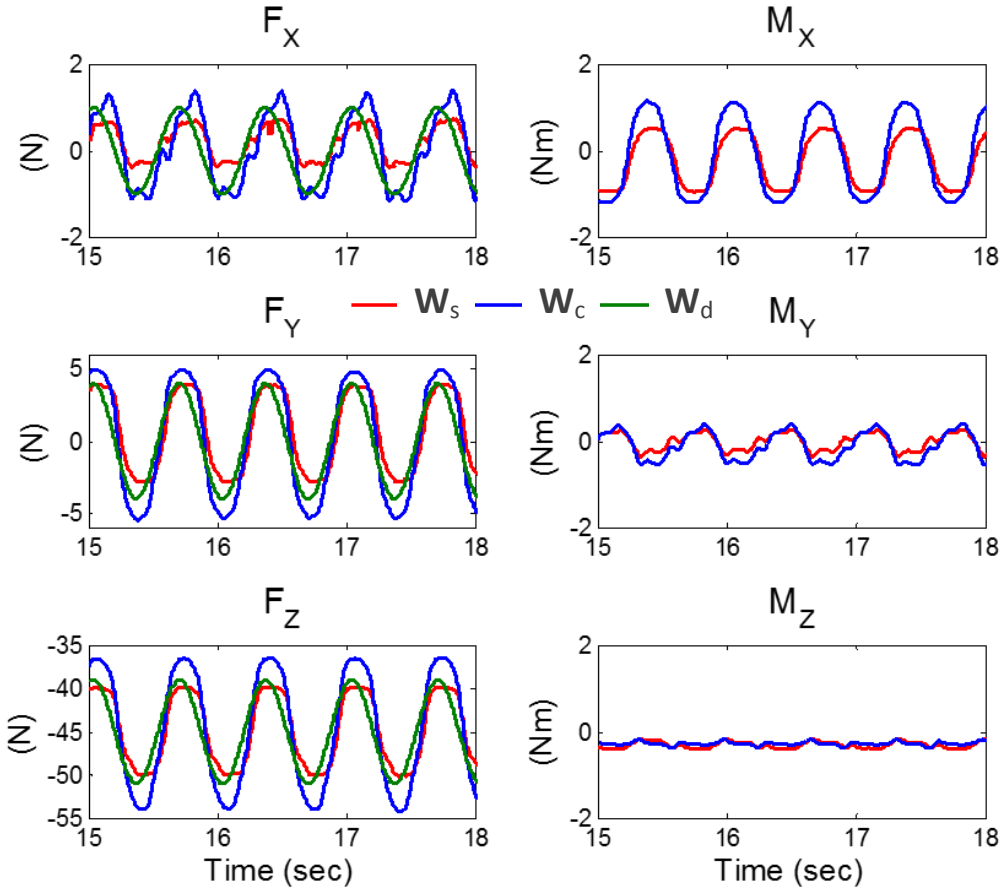

Figure 3.11: Force-moment vector values for a part of the dummy pelvis experiment. W_s denotes the values recorded by the force-torque sensor in the global coordinate system. W_c are the force-moment values calculated using Eq. (3.1) and W_d are the desired force values calculated using Eq. (3.10).

The force-moment values recorded by the force-torque sensor, W_s, were converted to the global coordinate system using the lower plate marker data. The applied force-moment vector, W_c, was also calculated using the actual cable tension values recorded by the load cells and the structure matrix, A, using Eq. (3.1). The W_s and W_c values are shown in Fig. 3.11 for a part of the experiment. The desired force values, W_d, from Eq. (3.10) are also shown in the plot. Root mean square errors, RMSE, were calculated between the W_s, W_c, and W_d values, refer to Table 3.2.

The system was able to follow the desired force profile at the commanded frequency and the moment values remained within the desired limit of $\pm 2Nm$ in the three directions. The force values of W_c and W_s matched closely, with RMSE under 1, 2, and 3 N in the X, Y, and Z directions, respectively. Similarly, the RMSE between the moment values was under 0.5 Nm in all the three directions. Ideally, W_c and W_s values should have matched perfectly but the small compliance in the plate setup resulted in a small displacement of the upper plate at the connecting points whenever the cable tension reversed its direction leading to the observed disparities.

Part III

Human Experiments

Chapter 4

Stance Phase Intervention

The A-TPAD is a cable-driven pelvic robot that can apply and control external forces in magnitude, direction, and duration. It therefore provides a platform to scientifically study human gait adaptation when external wrench (combined force and moment) is applied to the human pelvis. These studies can motivate new gait rehabilitation paradigms that can potentially be used to correct gait deficits in human walking. In this chapter, we present two human experiments using A-TPAD, where external forces were applied to the pelvis to target the stance phase gait parameters. The chapter concludes by outlining potential benefits of the proposed stance phase interventions for gait rehabilitation of neurologically impaired patients.

4.1 Weight Bearing

In most gait rehabilitation studies in literature, the primary goal has been to correct either the swing phase gait measures [3,4,45,67,76], such as the hip and knee flexion-extension, or the spatio-temporal gait measures [77], such as the step length symmetry. Existing understanding of human walking pattern suggests that the inability of an individual to bear weight on the lower limbs during the stance phase of walking affects the overall gait performance [39,40,78–80].

In literature, interventions targeting weight bearing have been used to improve the ability of stroke survivors to bear weight on the affected limb mostly during stationary tasks [78–80]. These studies have not been extended to walking trials, in part because of the lack of a device with the ability to apply weight bearing intervention without adding external constraints. Further, existing

robotic devices typically apply external forces to the legs during the swing phase only, and do not target weight bearing during the stance phase. While some studies have reported the effect of adding weight bags on the lower limbs during walking [64, 78], the added weights increase not only the overall body weight but also the body's mass/inertia properties; thereby affecting walking dynamics undesirably. In this section, we describe an experimental paradigm using the A-TPAD to apply symmetric downward forces during walking without adding external mobility or inertial constraints.

In patients with neural impairments, the inability to generate sufficient lower limb muscle power during the stance phase also limits the ability to control the center of mass (COM) over the affected limb [40]. Further, it is the body's balance that controls the duration of limb support periods during walking [34, 40, 81]. For example, individuals with hemiparesis demonstrate longer swing phase and shorter stance phase on the affected side. Therefore, in this section, we also describe a second paradigm using the A-TPAD to apply an asymmetric force vector during walking. In this paradigm, the applied force vector was directed along a moving vector parallel to the right leg. Thus an external anterior-posterior force was applied to the pelvis in addition to an external weight bearing downward force. As a result, an external forward pull was applied to the pelvis for a part of a gait cycle and an external backward pull was applied for the rest of the gait cycle, thereby creating the need for subjects to modify the lower limb support periods while walking.

For both the symmetric and asymmetric weight bearing paradigms, the cable configuration (Fig. 3.1) where four cables connect the hip belt to the lower part of the frame, was used to apply the external wrench to the pelvis. This configuration reduces the possibility of cable interference with hand motion during walking.

4.1.1 Symmetric Weight Bearing

In the symmetric weight bearing paradigm, the cables in the A-TPAD were controlled to apply a net vertical downward force (F_Z) to the pelvis with a magnitude equivalent to 10% of a subject's body weight (BW) [27]. The components of the net force applied to the pelvis in the medial-lateral (F_X) and anterior-posterior (F_Y) directions were maintained within 1% BW. In addition, the moment components resolved at the pelvic center were maintained within 4 Nm, where the pelvic center was calculated as the centroid of the three pelvic anatomical markers (details of anatomical markers

are in Appendix B). Thus, the commanded wrench components and tension limits to the controller during the experiment are given as,

$$\begin{aligned} |F_{X,Y}| &\preceq 1\%BW \\ F_Z &= -10\%BW \\ |M_{X,Y,Z}| &\preceq 4Nm \\ 5 \preceq T &\preceq 60N \end{aligned} \tag{4.1}$$

Thus, an external vertical downward force was applied over the stance and swing phases of both legs. The desired wrench in Eq. (4.1) could be interpreted as a 10% increase in the acceleration due to gravity. Unlike a body weight support system, this intervention promotes training with increased body weight - the body mass remains unaltered. We hypothesize that subjects will adapt their gait kinetics in response to the applied force and will walk with higher forces transmitted through their legs.

4.1.2 Asymmetric Weight Bearing

In the asymmetric weight bearing paradigm, the A-TPAD was used to apply an asymmetric external force vector to the pelvis which was directed along a moving vector parallel to the right leg [28]. The force vector had a constant magnitude, equivalent to 10% of a subject's body weight (BW), and was directed along a vector from the right iliac crest (RILIAC) to the right ankle (RANK). The desired external wrench for the human experiment is expressed as,

$$\begin{aligned} \vec{F_d} &= \|F\|\,\widehat{u} \\ |M_{X,Y,Z}| &\preceq 6Nm \end{aligned} \tag{4.2}$$

where $\widehat{u}$ is a unit vector defined from the RILIAC anatomical position on the pelvis to the RANK, refer to Fig. 4.1(a). The magnitude of the external force applied to the pelvis was constant ($\|F\|$ = 10% BW). External moments resolved at the pelvic center were kept under ±6 Nm.

A stick diagram representation of the desired external force in the sagittal plane is illustrated in Fig. 4.1(b). The force components values in the anterior-posterior (Y) and vertical (Z) directions change based on RANK position with respect to RILIAC. Baseline motion data of three healthy

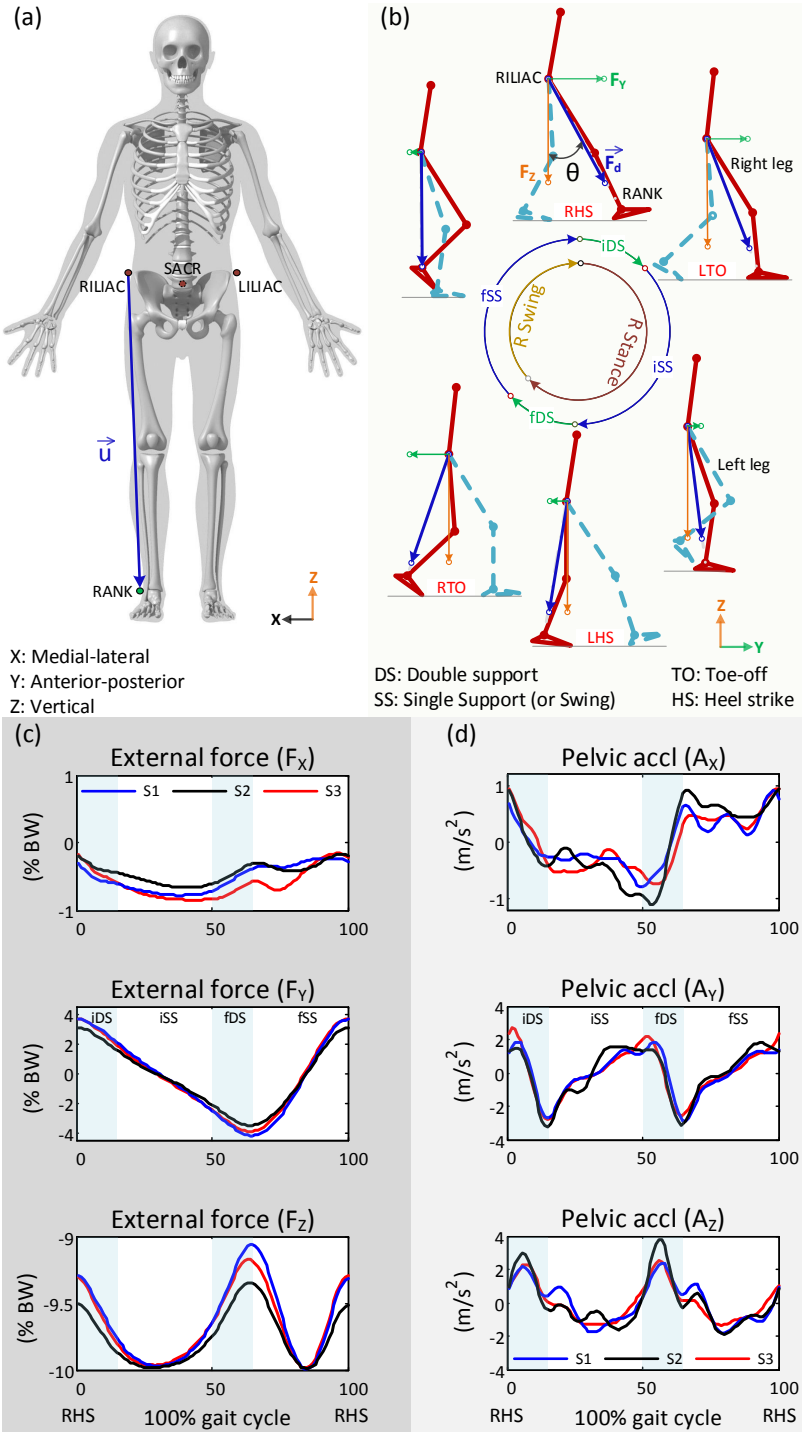

Figure 4.1: (a) Shown are anatomical marker locations on the pelvis and ankle. The vector, $\vec{u}$, is defined from the right iliac crest (RILIAC) on the pelvis to the right ankle (RANK) [28]. (b) The sagittal plane stick diagram represents the desired force components over different instances of a gait cycle. The sketch also defines the gait events and phases. The angle θ defines the desired force inclination from the vertical axis and is termed as the right limb angle. (c) The desired external force components calculated as per Eq. (4.2), and (d) the pelvic baseline acceleration pattern for three healthy subjects are shown.

subjects from earlier studies with passive TPAD are used here to further explain the external force pattern over a gait cycle. The RILIAC and RANK coordinate data over a gait cycle are used to calculate $\vec{F_d}$ using Eq. (4.2) and are plotted in Fig. 4.1(c). Similarly, the pelvic center acceleration calculated from the pelvic marker data is plotted in Fig. 4.1(d).

Medial-lateral direction (X): For healthy individuals, the foot movement in the medial-lateral direction is typically small over a gait cycle. Thus, the F_X values calculated from the reference data show small variation (Fig. 4.1(c)). For the three subjects, F_X values are negative which imply that RANK is medial to RILIAC throughout the gait cycle. The pelvic acceleration in this direction, A_X, is negative during the left swing (iSS) and positive during the right swing (fSS) phase (Fig. 4.1(d)). Therefore, the applied external force opposes the pelvic medial-laternal motion during the right swing and assists during the left swing. However, since the magnitude of F_X is small (under 1% BW) we do not expect significant changes in the medial-lateral pelvic motion.

Anterior-posterior direction (Y): The F_Y values are either positive or negative over a gait cycle, which imply external forward or backward pull on the pelvis respectively (Fig. 4.1(b,c)). Based on the RANK position relative to RILIAC, F_Y attains maximum positive magnitude at right heel strike events (RHS: 1 and 100% of the gait cycle) and maximum negative magnitude at right toe-off (RTO: around 63% of the gait cycle). Subjects accelerate forward during the SS (or swing) phases and decelerate in the forward direction during the DS phases; refer to A_Y plot in Fig. 4.1(d). Comparing the F_Y and A_Y plots, the applied external forces resist the pelvic motion during the right stance and assist the pelvic motion during the right swing. As the F_Y values vary between 4% to -4% BW and the swing duration significantly shorter than the stance duration, we expect an asymmetric change in the anterior-posterior pelvic motion during a gait cycle. Further, we expect that this asymmetry in the pelvic motion while walking will require subjects to modify the limb-support periods. We hypothesize that such force patterns will promote longer right stance duration and reduce right swing duration. Such a force pattern is chosen to target a hemiparetic gait pattern, which is characterized by longer swing phase and shorter stance phase on the affected limb.

Vertical direction (Z): The F_Z component is directed downward over the complete gait cycle as $\vec{u}$ points downward (Fig. 4.1(a-c)). From the A_Z plot, the pelvic accelerates upward during the

DS phases and decelerates in the upward direction during the SS phases (Fig. 4.1(d)). From the healthy subjects data, the F_Z values reach the maximum magnitude of 10% BW at mid swing and minimum magnitude around RHS. Since the F_Z is always directed downward and its variations over the gait cycle are smaller than 1% BW, we expect that subjects will reduce the vertical pelvic motion and will adapt their gait kinetics as a result.

Thus, selecting $\vec{u}$ to decide the external force direction provides a force vector that is mainly distributed in the sagittal plane during a gait cycle.

4.2 Human Experiments

4.2.1 Protocol

Nineteen healthy male subjects, all right handed, participated in the experiments. Ten subjects with age range 20-35 years (mean age: 27 yrs and SD: 3.7 yrs) and mean weight 72 kg (SD: 12.7 kg) were part of Experiment 1: symmetric weight bearing, and nine subjects with age range 20-35 years (mean age: 26.6 yrs and SD: 3.8 yrs) and mean weight 71.5 kg (SD: 10.4 kg) were part of Experiment 2: asymmetric weight bearing. The training protocol was approved by the Columbia University Internal Review Board and involved Baseline (BL), Training (T), and Post-training (PT) sessions, as shown in Fig. 4.2. Each subject was suited with retro-reflective markers to record human motion data. The marker set and associated limb frame assignment are discussed in detail in Appendix B. Surface Electromyography (EMG) activities from the lower limb muscles were measured bilaterally, namely Gastrocnemius Medialis (MG), Soleus (SOL), Tibialis Anterior (TA), Vastus Lateralis (VL), Rectus Femoris (RF) and Biceps Femoris (BF) of each leg. The electrode location and recording process has been elaborated in Appendix C. A fabric hip belt with cable attachment points was worn by the subject, and a three axis accelerometer was mounted on the subject's pelvis. Force sensitive resistor (FSR) pressure pads with 440 N limit (Flexiforce, Tekscan, Massachusetts) were mounted on the subject's shoe insoles to measure foot pressure data.

During the Baseline session, each subject walked on a treadmill for four minutes at a constant speed of 3.8 $kmph$. Data collected during the last minute of this session was treated as the reference data and labeled as BL. Thereafter, cables were attached to the hip belt to apply the desired external wrench to the pelvis. During the Training session, each subject walked for sixteen minutes at the

Figure 4.2: Experimental protocol for the human experiment included baseline, training and post training sessions. The numbers in the block indicate the data collection trial number for each session.

same treadmill speed of 3.8 $kmph$. As the subject walked, the controller adjusted the tension values of each cable to continue applying the desired external wrench. Data were recorded for six intervals, each lasting one minute: at the start, 3^{rd}, 6^{th}, 9^{th}, 12^{th}, and 15^{th} min. These data collection instances were referred to as T1, T2, T3, T4, T5, and T6 as shown in the Fig. 4.2. To evaluate subjects' adaptation to the applied force vector, a catch trial was added at the middle of the training session (in between trials T3 and T4) for Experiment 2. During the Catch trial, the A-TPAD did not apply the desired force on the pelvis but maintained only a minimum tension in each cable to prevent cable slackening. Data collected during this trial were labeled as C1. Following the training session, the cables were removed immediately and each subject walked for another ten minutes at same treadmill speed of 3.8 $kmph$ as part of the Post-training session. Data were recorded four times for one minute duration at the start, 3^{rd}, 6^{th}, and 9^{th} min. These data collection instances were referred to as PT1, PT2, PT3, and PT4.

4.2.2 Data Processing

During the experiment, each subject's kinematics, EMG, foot pressure, pelvic acceleration, and applied wrench data were recorded. The time histories of all gait parameters were normalized in time to 100% of the gait cycle, where a gait cycle was defined as the interval from a right heel strike event (RHS) to subsequent right heel strike. The farthest anterior position of the heel marker with respect to the sacrum marker was used to define the heel strike (HS) event and the farthest posterior position of the toe marker with respect to the sacrum marker was used to define the toe-off (TO) event. These events were used to estimate the durations of double support (DS) phases, single support (SS) phases, stride time, and stance time during each gait cycle. Gait symmetry between the two legs was analyzed by calculating the stance-swing ratio (SSR), the stance period ratio (SPR), and the double support ratio (DSR). Gait cadence was defined as the number of

steps per minute. Lower limb sagittal plane joint angles were estimated from the human segment marker data. The foot pressure data of each leg were normalized by the maximum and minimum pressure values of the baseline trial. Since the pressure sensors cover only a part of the subject's foot, the pressure values were not related to the subjects' weight and were not statistically analyzed. Thus, the changes in the pressure values were only qualitatively related with the ground reaction forces during the experiment. EMG signals were post-processed using a band-pass filter (4th order Butterworth, 40-450 Hz) and a full-wave rectification. The signal was filtered using a low pass filter (n=4, fc = 6 Hz). For every subject, EMG data of each muscle were normalized to the peak values recorded during the baseline session. EMG root mean square (RMS) amplitudes and linear envelope peak values during the major burst were computed to estimate the level of muscle activation during the different trials of the experiment.

An asymmetric measure was defined to evaluate the gait symmetry, given as

$$\text{Asymmetric measure} = 100 \times \frac{(R-L)}{(R+L)} \text{ or } 100 \times \frac{(f-i)}{(f+i)} \tag{4.3}$$

where R and L represent the values of right and left limb parameters respectively. The values of a gait measure, which are not associated with a particular limb, were divided into initial, i, (1 to 50% gait cycle) and final, f, (51 to 100% gait cycle). A zero value of the asymmetric measure implies perfect symmetry while a positive/negative value means higher/lower R (or f) value compare to L (or i) values. Asymmetry measures were calculated for the stance phase duration and hip flexion-extension range of motion (ROM) between the two legs, and the anterior-posterior and vertical pelvic center motion over a gait cycle. The centroid of a triangle formed by three pelvic anatomical markers was calculated to define the position of the pelvic center. A right limb angle that represents the applied external force inclination from the vertical axis in the sagittal plane was calculated from the RILIAC and RANK markers, shown as θ in Fig. 4.1(b).

To study the response of the group to the applied external wrench, gait measures from the last five gait cycles for trials BL, T6, and PT4, and from the first five gait cycles for trials T1, C1, and PT1 were analyzed. The data were first checked against the sphericity violation using the Mauchly's test and the Huynd-Feldt correction was applied when the data violated the condition. One way repeated measure ANOVA was performed to determine the statistical significance (defined as $p <$

0.05). The Bonferroni-Holm significant difference test was performed when a statistical significance was identified. The chosen combinations for statistical difference comparison for Experiment 1 were BL-T1, BL-T6, BL-PT1, BL-PT4 and T6-PT1. The chosen combinations for statistical difference comparison for Experiment 2 were BL-T1, BL-T6, BL-PT1, BL-C1, T1-C1 and T6-PT1. A significant difference between the values of a gait parameter during BL and T1 is referred as the effect of training with force. In addition, if the values during PT1 (or C1) were also significantly different from BL, then it is referred as an aftereffect. A negative aftereffect is defined as when the changes between BL-PT1 or BL-C1 were of opposite nature than BL-T1, adapted from [82]. Values plotted in the following section are given as means ± standard errors. An asterisk mark indicates a significant difference between the means of the two sessions.

4.3 Experiment 1 - Symmetric Weight Bearing

4.3.1 Results

Figure 4.3(a) shows the vertical component of the applied force-moment vector, F_Z, on the pelvis of a representative subject during the training session. Periodic variations in the F_Z values at almost twice the gait frequency were observed over the gait cycle. The highest F_Z magnitudes, lowest F_Z magnitudes, and root mean square error (RMSE) between the desired and applied F_Z values for the group were tested for the statistical significance (Fig. 4.4). Repeated measure ANOVA did not report any significant changes in the values of these parameters between trials T1, T3 and T6 (RMSE: $p = 0.6$, Highest: $p = 0.07$ and Lowest: $p = 0.33$). The F_Z values during a gait cycle were between -8.3 and -12.9% BW, and the RMSE values were below 0.5% BW during the training trials, T1 to T6, for all subjects. In addition, the rest of the force and moment components of the applied wrench at the pelvic center remained within the desired levels of 1% BW and 4 Nm respectively during the training session.

Figure 4.3(b) shows the vertical motion of the pelvic center, P_Z, of a representative subject during different experimental trials. Lower P_Z values over a gait cycle compared to trials BL and PT4 were observed during the trial T6. A significant effect of the training with the applied force-moment vector was observed in the pelvic range of motion, ROM, values in the vertical direction ($p \leq 0.05$, Fig. 4.5). The post-hoc pairwise analysis reported that the vertical pelvic ROM values

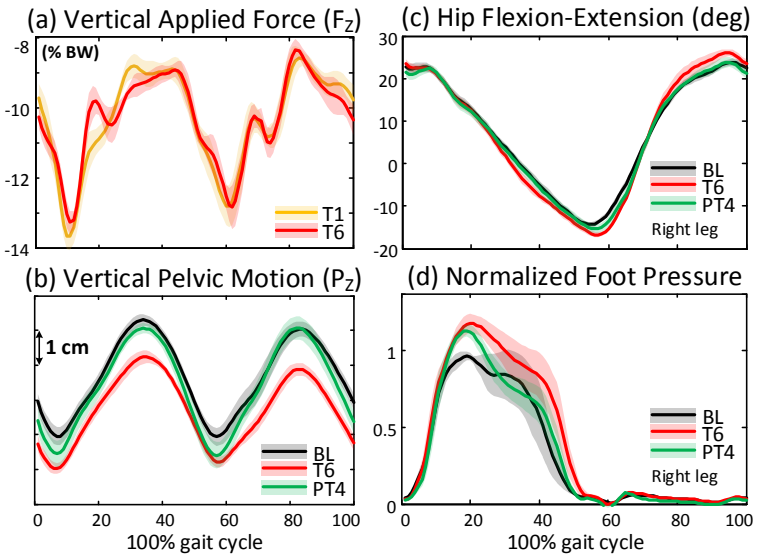

Figure 4.3: Gait parameters for a representative subject during different experimental sessions plotted over a gait cycle. The solid line represents the mean value during a trial and the shaded area plots the trial variation for that gait parameter. A gait cycle is defined from RHS to subsequent RHS.

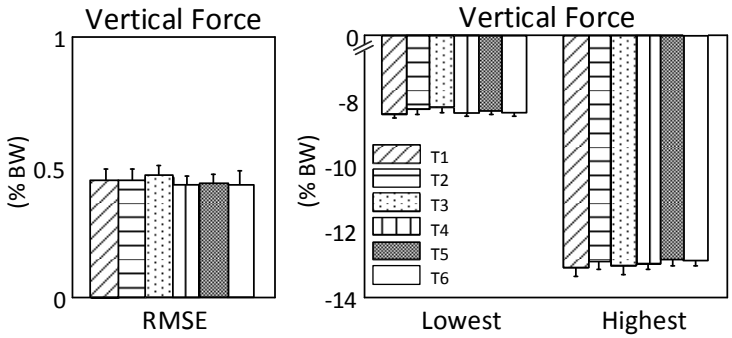

Figure 4.4: Body weight normalized vertical force, F_Z, on the subject's pelvis for the group. $RMSE$ is the root mean square error between the applied and the desired force values. Lowest is the minimum F_Z magnitude and highest is the maximum F_Z magnitude applied during a gait cycle. No significant changes were observed in these values.

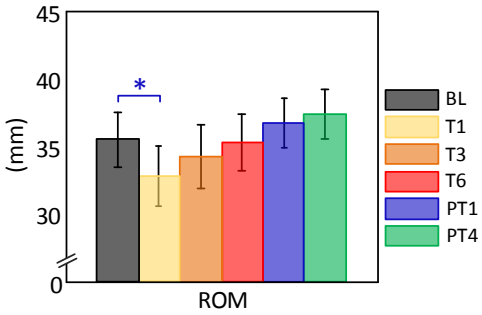

Figure 4.5: Pelvic range of motion, ROM, in the vertical direction during a gait cycle for the group. Significant changes were reported between the average ROM values during BL and T1.

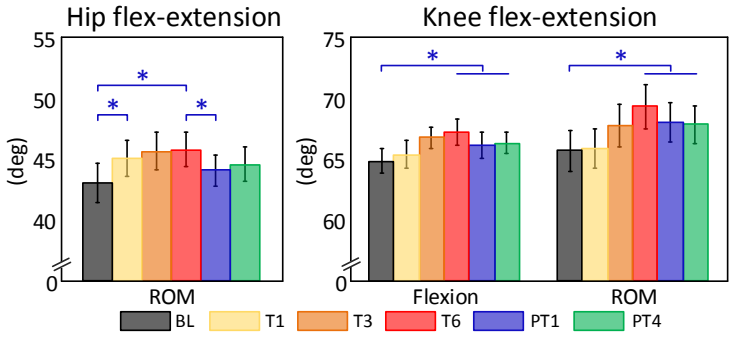

Figure 4.6: Hip and knee flexion-extension *ROM* and maximum knee flexion values for the group. Average hip *ROM* values changed significantly between following pairs BL-T1, BL-T6 and T6-PT1. Average knee flexion values and knee flexion-extension *ROM* values reported following significant pairwise comparisons BL-T6, BL-PT1 and BL-PT4.

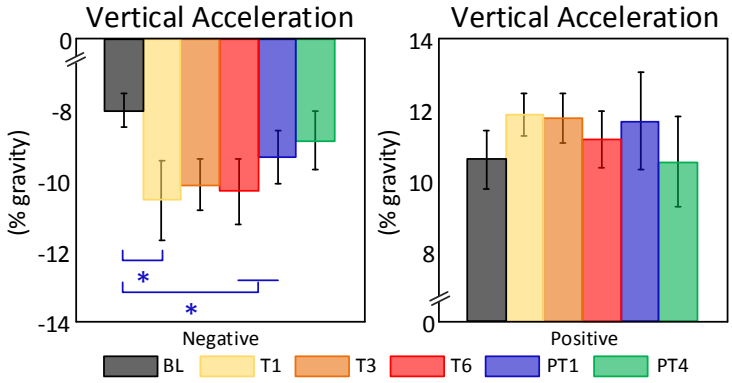

Figure 4.7: Pelvic acceleration peak values in the vertical direction, minus the acceleration due to gravity, over different sessions of the experiment. The acceleration values were negative during the *SS* phases and positive during the *DS* phases. Significant changes were reported in the negative acceleration peak values between following pairs BL-T1, BL-T6 and BL-PT1.

Table 4.1: Percentage changes in the gait parameter values. '*' represent the pairwise comparisons reaching significance.

	$100 \times (Trial - BL)/BL$				
Trial→	**T1**	**T6**	**PT1**	**PT4**	**p**
Cadence	3.41*	0.47	-0.28	-1.43	<0.05
Stance Phase Duration					
R Leg	0.6	1.27*	0.84	0.36	<0.001
Stride Duration					
R Leg	-2.66*	-0.36	0.23	2.12	<0.001
SS Duration					
R Leg	-1.2	-2.53*	-1.67	-0.72	<0.001

were significantly lower than the baseline values during the trial T1. With the progression of the training session, ROM values increased to the baseline level. During the post-training trials, these values were higher than the baseline level, but these differences were not statistically significant.

Figure 4.3(c) shows the hip flexion-extension values of a representative subject during different experimental trials. Increase in the hip flexion and extension values were observed during the trial T6. Statistical analysis on the hip flexion-extension ROM values reported significant changes during the experiment ($p \leq 0.05$, Fig. 4.6). Significant increase in the hip ROM values was reported during the trials T1 and T6 over the baseline values. The average hip ROM values during the post-training trials were not significantly different from the baseline values. Significant changes were also observed in the knee maximum flexion values and knee flexion-extension ROM values ($p \leq 0.05$). These values increased as the training session progressed with significant differences between the trials BL and T6. These values remained higher during the post-training trials as confirmed by the pairwise comparison between PT1-BL and PT4-BL.

Figure 4.3(d) plots the right heel foot pressure values of a representative subject during different experimental trials. Higher pressure values were observed during the trials T6 and PT4 as compared to the trial BL. The magnitude of the vertical pelvic acceleration values recorded by the accelerometer, minus the acceleration due to gravity, was positive during the double support, DS, phases and negative during the single support, SS, phases of a gait cycle. A significant change was reported in the negative vertical acceleration peak values ($p \leq 0.05$, Fig. 4.7). The pairwise analysis reported significantly higher negative acceleration peak magnitudes during the trials T1 and T6 compared to the baseline values. The magnitude of the negative acceleration peak also remained significantly higher during the trial PT1 compared to BL. The changes in the positive acceleration peak values were not statistically significant ($p = 0.58$), refer to Fig. 4.7.

No significant changes were reported in the DSR, SPR and SSR values during the experiment ($p = 0.7$, $p = 0.08$ & $p = 0.09$ respectively), implying that gait symmetry was retained. Significant changes were reported in the stride time and the gait cadence values ($p \leq 0.05$, Table. 4.1). Stride time values decreased and cadence values increased significantly during the trial T1 as compared to the baseline values. The values of these parameters returned to the baseline level with the progression of the training session. During the post-training trials, aftereffects were observed in these values, though pairwise comparison did not show any significance difference. Statistical

analysis also reported significant change in the stance phase and SS phase duration values ($p \leq 0.05$, Table. 4.1). Subjects spent a larger part of the gait cycle in the stance phase during the training session, with significant differences between the trials BL and T6. Stance phase duration values were also higher during the post-training session compared to the baseline values. The SS phase duration values decreased significantly during the trial T6 as compared to the baseline values.

4.3.2 Discussion

During the human experiment, subjects' immediate response to the applied forces was to reduce the pelvic vertical range of motion (ROM) significantly. In addition, subjects increased gait cadence by reducing stride time. With the progression of training with the applied forces, subjects adapted their gait pattern such that these parameters returned back to the baseline level. Notably, gradual increase in the stance phase duration values and knee flexion-extension values were reported during the training session. During the post-training session, negative aftereffects in the pelvic vertical ROM, gait cadence and stride time values were reported. In addition, higher knee flexion-extension and stance phase duration values were retained when forces were removed. The changes in these gait parameters can be categorized as: (i) Parameters that changed immediately with the force application, and subjects were able to bring these parameters back to the baseline level after some experience with the applied force such that the removal of force resulted in the opposite change in these parameter values. Such negative aftereffects in response to a force intervention training reflect subject adaptation, and imply temporary recalibration of the existing motor commands as explained in [82, 83]; (ii) Parameters that changed gradually during the training session, and subjects retained these changed values when the forces were removed. These results show that healthy subjects adapt gait kinematics in response to the applied downward force.

In this current experiment, gait symmetry was retained. In addition, the pelvic vertical acceleration values reported significant increase during the training session. Particularly, subjects generated higher pelvic acceleration during the single support phase of the gait cycle. This was due to the external downward force on the subjects' pelvis, which required extra push-off effort from the subjects. Subjects retained these large magnitudes of pelvic acceleration when the external forces were removed. The increase in the pelvic acceleration and stance phase duration values further implies that subjects applied higher ground reaction forces during the experiment.

Table 4.2: Applied force values during the training trials

		T1	T3	T6	p-value
RMSE (% BW)	F_X	0.28	0.33	0.29	= 0.1
	F_Y	0.92	0.95	0.90	= 0.6
	F_Z	1.30	1.26	1.33	= 0.5
Maximum (% BW)	F_X	0.34	0.19	0.19	= 0.1
	F_Y	4.25	4.38	4.47	= 0.1
	F_Z	-8.35	-8.20	-8.03	= 0.1
Minimum (% BW)	F_X	-1.02	-1.36	-1.28	= 0.001
	F_Y	-3.44	-3.57	-3.68	= 0.3
	F_Z	-12.55	-12.72	-12.71	= 0.6
Maximum (Nm)	M_X	4.81	4.41	4.65	= 0.4
	M_Y	-1.46	-1.52	-1.46	= 0.8
	M_Z	-8.35	-8.20	-8.03	= 0.4
Minimum (Nm)	M_X	-2.68	-3.35	-3.36	= 0.04
	M_Y	-3.42	-3.95	-3.8	= 0.06
	M_Z	-1.32	-1.62	-1.51	= 0.02

These results show that healthy subjects adapted gait kinetics in response to the applied downward force. The proposed force paradigm has important consequences in terms of improving weight bearing capability in patients [78–80]. Such training paradigms are further useful in improving bone health of legs [43]. Patient groups, such as stroke survivors, children with cerebral palsy and amputees [35, 37, 41, 43], shy away from supporting their weight on the weak limbs. These patients generally develop compensatory strategies which lead to gait asymmetry, poor balance, hip hiking, etc. The weight bearing paradigm using A-TPAD provides a novel way to approach these problems.

4.4 Experiment 2 - Asymmetric Weight Bearing

4.4.1 Results

The maximum and minimum values of the three force components during a gait cycle averaged over the group during the training trials T1, T3 and T6 are reported in Table 4.2. The F_X, F_Y and F_Z values varied from -1.4 to 0.35% BW, -3.7 to 4.5% BW, and -12.75 to -8% BW respectively during a gait cycle over the training session. The root mean square error (RMSE) between the desired and applied force values in the medial-lateral (X), anterior-posterior (Y), and vertical (Z) directions were under 0.5, 1, and 1.4% BW respectively (Table 4.2). One way repeated measure ANOVA did not report any significant change in the force values between trials T1, T3, and T6 in

the three directions except for the minimum F_X values. The minimum F_X values during trial T1 were statistically different from the corresponding values during trials T3 and T6. The maximum and minimum values of the external moment components resolved at the pelvic center averaged over the group during trials T1, T3, and T6 are also reported in Table 4.2. The applied external moment components were within the desired level of $\pm 6\ Nm$ over the training session.

The pelvic center anterior-posterior and vertical displacements are plotted in Fig. 4.8(a) during different experimental trials for a representative subject. Asymmetric changes were observed in the anterior-posterior pelvic motion over a gait cycle during the trials T1, T6, C1, and PT1. As seen in Fig. 4.8(a), y_f values were larger during trials T1 and T6, while y_i values were larger during trials C1 and PT1. Here, y_i and y_f represent pelvic center range of motion (ROM) during the left and right swing phases respectively. A significant effect of the training with the applied force vector was reported in the values of anterior-posterior pelvic motion asymmetric measure, $\frac{y_f - y_i}{y_f + y_i}$, ($p \leq 0.05$, Fig. 4.8(b)). The post-hoc pairwise analysis reported that the asymmetric measure values were significantly positive in the presence of the applied force vector (T1 and T6) and significantly negative when the applied force vector was removed (C1 and PT1), as compared to the baseline (BL) values.

The pelvic center motion in the vertical direction was asymmetric during trials T1, T6, C1, and PT1, with reduced pelvic motion range in the final part of the gait cycle, z_f; refer to Fig. 4.8(a). Significant asymmetric changes were reported in the vertical pelvic motion ($p \leq 0.05$, Fig. 4.8(b)). The asymmetric measure in the vertical direction, $\frac{z_f - z_i}{z_f + z_i}$, had significant negative values during the training trials (T1 and T6) and catch trial (C1) compared to the baseline values. Negative values of the asymmetric measure were also reported during the post-training sessions, but these values were not statistically different from the baseline values. The percentage changes in the pelvic center ROM values in the medial-lateral direction, P_X ROM, are reported in Table 4.3. Compared to baseline values, the P_X ROM values were significantly reduced only during the catch trial.

Significant changes were reported in the values of the stance phase asymmetric measure, $\frac{R-L}{R+L}$, where R and L denote the right and left stance phase durations as a percentage of gait cycle, ($p \leq 0.05$, Fig. 4.9). The stance phase asymmetric measure values were negative during T1 and positive during T6, but were not statistically different from the baseline values. The post-hoc pairwise analysis reported that the asymmetric measure values during the catch and post-training

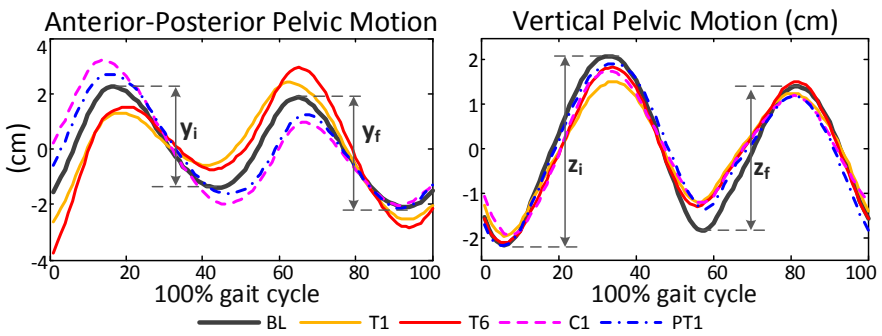

(a) Pelvic motion over the gait cycle

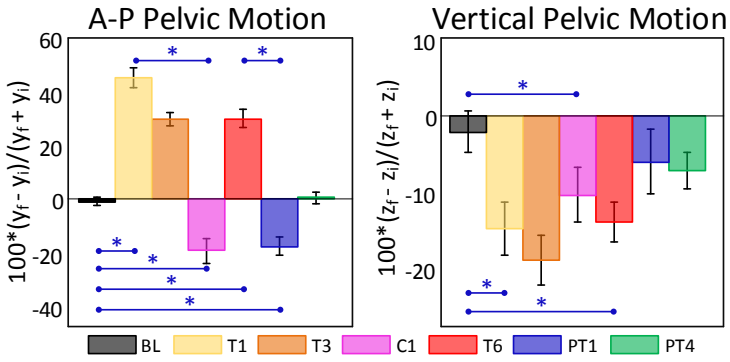

(b) Pelvic motion asymmetric measure

Figure 4.8: (a) Pelvic center anterior-posterior and vertical displacements during different experimental trials for a representative subject. A gait cycle was defined from RHS to subsequent RHS. (b) Anterior-posterior and vertical pelvic motion asymmetric measures for the group during different trials of the experiment. Significant changes were reported between BL-T1, BL-C1, BL-T6, BL-PT1, T1-C1, and T6-PT1 for the anterior-posterior asymmetric measure values. Significant changes were also reported between BL-T1, BL-C1, and BL-T6 for the vertical asymmetric measure values.

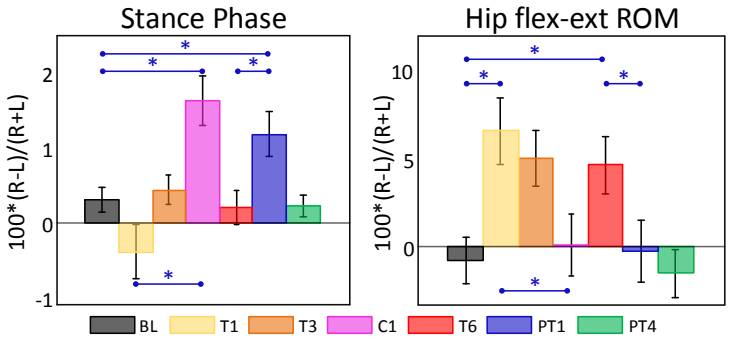

Figure 4.9: Stance phase asymmetric measure for the group during different trials of the experiment. Significant changes were reported between BL-C1, BL-PT1, T1-C1, and T6-PT1 for the stance phase asymmetric measure values. Hip flexion-extension range of motion (ROM) asymmetric measure changed significantly during the training session. Significant changes were reported between BL-T1, BL-T6, T1-C1, and T6-PT1 for the hip flexion-extension ROM asymmetric measure values.

Table 4.3: Percentage changes in the gait parameter values.
$100 \times (Trial - BL)/BL$

Trial→	**T1**	**C1**	**T6**	**PT1**	**p**
P_X ROM	6.1	-17.9*	-9.1	-8.2	<0.001
Cadence	3.8*	2.2	0.9	-2.2	<0.05
Stance Phase Duration					
R Leg	-0.4	1.2	0.5	1.6*	<0.001
L Leg	0.9*	-1.4*	0.7*	-0.2	<0.001
Right Limb Angle					
ROM	-3.4	-2.2	2.3	-1.6	<0.05
EMG RMS Values					
LMG	14.1	6.9	5.3	-0.4	=0.07
LSOL	12.5	-8.9	9.0	6.2	=0.24
LTA	4.1	-8.1	0.3	-13.2	<0.05
LVL	29.4	-2.1	15.4	-19.2	<0.001
LRF	37.1	6.8	7.7	-27.2*	<0.001
LBF	5.7	2.1	-3.8	-13.8	=0.12
RMG	10.3	14.1	-5.4	-0.5	<0.05
RSOL	17.4	15.9	6.6	3.2	<0.05
RTA	-3.2	23.2	-0.5	4.3	<0.05
RVL	6.9	52.3	34.7	1.3	<0.001
RRF	8.3	61.9	27.9	5.8	<0.001
RBF	7.6	17.5	22.3	2.9	=0.37
EMG Peak Values					
LRF	20.8	4.1	9.4	-28.1	<0.05
LBF	14.3	2.7	2.5	-10.6	=0.21
RRF	7.6	65.4	41.6	12.9	<0.05
RBF	-3.2	12.3	16.5	8.9	=0.33

Note: '*' represents a pairwise comparison between a gait measure value during '*Trial*' and BL reaching statistical significance.

trials (C1 and PT1) were significantly different from the baseline values. The percentage changes in the left and right stance phase duration values are reported in Table 4.3. The left stance values during the training trials (T1 and T6) were significantly higher than the baseline values. Longer right stance durations were reported in the absence of the applied force, such that a significant difference was reported between trials BL and PT1. Further, subjects walked with higher cadence values during the training session ($p \leq 0.05$), such that cadence values during T1 were significantly higher than BL (Table 4.3). Cadence values decreased during trials C1 and PT1 but were not statistically different from the trial BL.

The hip flexion-extension range of motion (ROM) asymmetric measure values, $\frac{R-L}{R+L}$, where R and L denote the right and left hip flexion-extension ROM, changed significantly during the

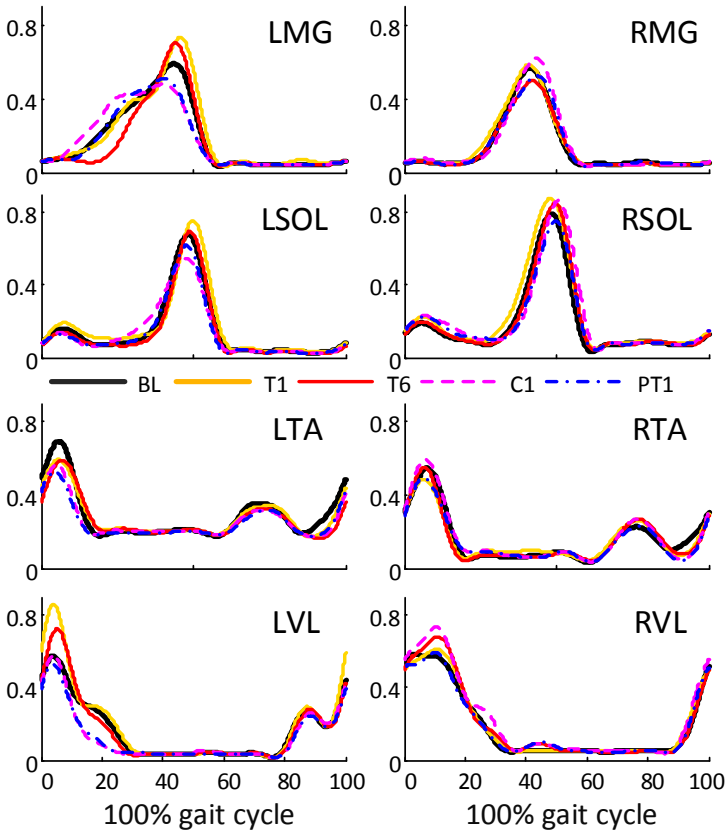

Figure 4.10: Left and right lower limb EMG envelopes during different experimental trials for a representative subject.

experiment ($p \leq 0.05$, Fig. 4.9). These values were significantly positive during the training trials (T1 and T6) compared to the baseline values, mainly due to larger right hip flexion-extension ROM values. However, the values during the catch and post-training trials were close to the baseline values. The changes in the values of right limb angle ROM during the experiment were also statistically significant ($p \leq 0.05$, Table 4.3). These values decreased during T1 and then increased with the progression of the training session, though statistical significance was reported only between the values of trials T6 and PT1.

Lower limb EMG envelopes for a representative subject over different experimental trials are shown in Fig. 4.10. The left leg muscle activation increased at the start of the training (T1). With the progress of training, the activation level for most of the left muscles was reduced, and more importantly when the force was removed, the left leg muscle activation was lower than the BL level, especially during C1. In particular, the LTA peak values and LRF RMS values during BL were significantly higher than the corresponding values during PT1 (Fig. 4.11, Table 4.3). The peak

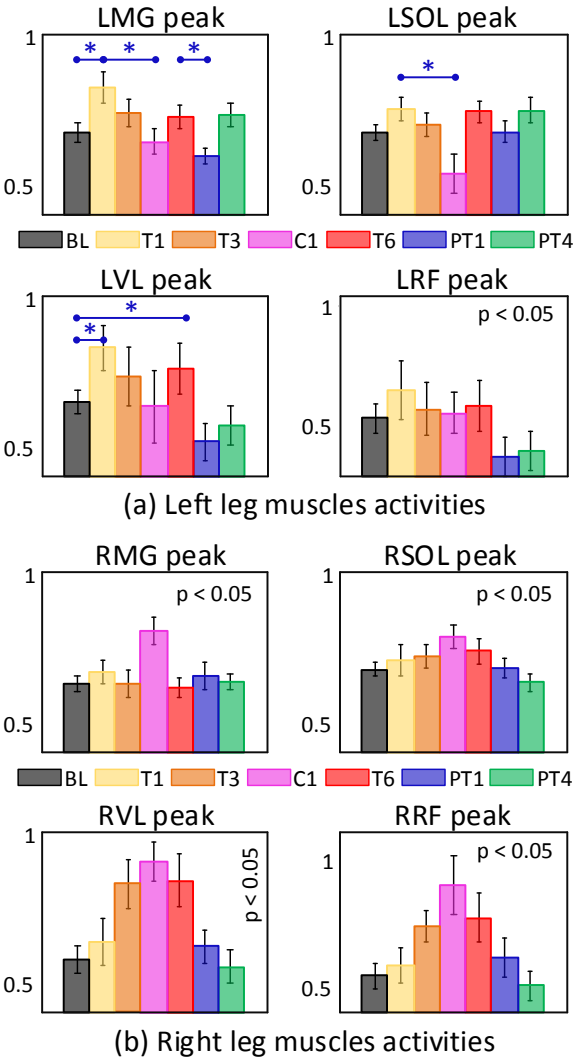

Figure 4.11: (a) Left, and (b) right limb muscles peak values during the major burst over different trials of the experiment. The left limb EMG peak values pairwise comparisons reaching significance are indicated using '*'. One way repeated ANOVA reported significant changes in the RMG, RSOL, and RVL peak values, but no pairwise significance was reported in the chosen pairs.

values during BL were significantly lower than T1 for LMG, and significantly lower than T1 and T6 for LVL. Additionally, the peak values during C1 were significantly lower than BL for LTA, and significantly lower than T1 for LMG and LSOL (Fig. 4.11). The right leg muscle activation, unlike the left leg, increased gradually with the progression of the training, refer to Fig. 4.10, 4.11 and Table 4.3. These values were higher then the BL values during the C1. One way repeated measure ANOVA reported significant changes in various muscles peak values during the major burst and RMS values ($p \leq 0.05$) but the pairwise analysis did not report significant changes in the chosen pairs. As noted from Table 4.3, no significant changes were reported in the BF activation pattern of both legs during the experiment.

4.4.2 Discussion

Adaptation to the asymmetric force vector

In this work, the applied force was mainly confined in the sagittal plane of walking. The vertical force component provided an external downward force to the pelvis over the full gait cycle, and the anterior-posterior force component provided an external forward pull to the pelvis for a part of a gait cycle, and external backward pull for the rest of the gait cycle. As explained in Section 4.1.2, at any instant during a gait cycle, the applied force values were based on the RANK position relative to RILIAC. Therefore, the absence of significant changes in the F_Y and F_Z values during training trials implied no adaptation in RANK sagittal plane motion relative to RILIAC. This is further supported by the absence of significant changes in the right limb angle values during the training trials. Notably, the subjects' immediate response to the applied force vector was to modify the pelvic motion in the sagittal plane. Asymmetric changes were observed in both the anterior-posterior and vertical directions. This was perhaps because the force vector was applied to the pelvis, and adaptation of a distal segment's motion, e.g. the right foot, might have been complex to achieve.

For a healthy individual, the pelvic motion has almost twice the gait frequency and is fairly symmetric in the anterior-posterior and vertical directions during a gait cycle [32]. In the current experiment, the applied F_Y component resisted the pelvic motion during the right stance phase and assisted the pelvic motion during the right swing phase of a gait cycle. As a result, subjects adopted

an asymmetrical pelvic motion in the anterior-posterior direction, which was significantly different from their baseline pattern. The asymmetry in the anterior-posterior pelvic motion lessened as the training session progressed, but remained significantly different relative to the baseline values. In the vertical direction, the F_Z component provided an external downward force throughout the gait cycle. As expected, subjects reduced their vertical pelvic range of motion during the training session. Notably, this reduction was significant during the final part of the gait cycle. This was because at RTO there was a backward F_Y component on the pelvis, therefore the net effect of F_Z and F_Y at RTO required an extra push-off effort. Since subjects use the pelvis to transfer forces from the lower extremity to the trunk during the forward propulsion of the body [32, 84], subjects reduced their vertical pelvic motion during the right swing phase. Thus, the observed asymmetric adaptation in the sagittal plane pelvic motion was the result of anterior-posterior component of the applied force.

Asymmetric changes were also observed in the hip flexion-extension ROM during the training session. These changes were mainly due to larger right hip flexion-extension values, which would have been required to maintain the foot clearance during the right swing phase as the vertical pelvic ROM was reduced. Further, asymmetric changes were also reported in the stance durations. In particular, longer left stance and shorter right stance durations were reported at the start of training session. With the progression of training with force, increase in the right stance duration resulted in positive stance phase asymmetric measure values. Similar to the asymmetric anterior-posterior pelvic motion, these changes in the stance durations were due to the anterior-posterior component of the applied force.

Subjects' adaptation to the applied force vector was reflected in the catch and post-training trials. Particularly, during the catch trial, when the applied force was removed at the middle of the training session without the subjects' knowledge, significant changes in the gait parameter values were observed. Similar mechanisms to evaluate a subject's immediate adaptation to an external intervention have been implemented in various studies. For example in [67], the applied velocity dependent resistance on lower limb was removed during the training session without subjects' knowledge. The changes in the pelvic anterior-posterior motion and stance phase asymmetry measure values during C1 and PT1 were opposite to the changes observed in the respective values during trial T1. Such negative aftereffects in response to a force intervention training reflect sub-

jects' adaptation, and imply temporary recalibration of the existing motor commands as explained in [82,83]. Thus, healthy subjects temporarily adopted an asymmetric gait with longer right stance durations compared to their baseline walking pattern after the removal of the force vector. Additionally, subjects also showed reactive adaptation to the applied intervention. In particular, the changes in the hip flexion-extension ROM asymmetric measure were not observed during the catch and post-training trials. As explained in [67, 77], such changes are feedback driven compensatory responses to the applied intervention and are referred to as reactive adaptation.

Lower limb muscle activation changes were not as significant as various kinematics parameters, but were in accordance with these changes. The shank muscles (Gastrocnemius, MG, and Soleus, SOL) contribute to the body support during a gait cycle [32]. Additionally, the SOL also contributes to the forward propulsion of the body [64]. In the current experiment, the changes in the shank muscle activity were in accordance with the reported changes in the limb stance periods. In particular, higher activities of the left shank muscles, LSOL and LMG, at the start of the training session were in response to the applied F_Y force component. With the progression of the training session, decrease in the left shank muscles activity and increase in right shank muscles activity were observed. Moreover, the increase in RSOL activity during the training session was required to provide the extra push-off effort at RTO. Further, just after the heel-strike of a gait cycle, the activation of thigh muscles (Vastus Lateralis, VL, and Rectus Femoris, RF) allow the body to rise against the body weight [32]. In the current experiment, there was an external downward force on the pelvis in addition to the subjects' weight. Therefore, increase in the RF and VL activation levels was required to balance the applied external vertical downward force, which essentially provided an external weight bearing during walking.

Gait interventions at pelvis

In most existing motor based gait rehabilitation approaches, the gait intervention is either applied during the swing phase movement of the affected limb [3, 4, 45, 67, 76], or is applied at the foot level using a split-belt treadmill to provide a speed constraint during walking [77]. The goal of these studies has been to target the spatio-temporal gait symmetry through these interventions. During normal walking, the movement of lower limbs is achieved through cyclic activation of leg muscles. These muscle activations generate joint torques which are in response to the net external

forces on the body, gravitational and ground reaction forces (GRF). Therefore, an intervention that targets the asymmetry in kinetic variables, such as limited weight bearing, could have the potential to improve overall gait performance [39, 40]. Researchers have studied weight bearing during standing tasks and through compelled weight shift for hemiparetic patients [78–80]. In this regard, our presented force-based training paradigm, which targets weight bearing during walking and promotes longer stance duration of the targeted leg, is a novel contribution.

4.5 Conclusion

The external forces used in these studies provide a motor adaptation approach to gait rehabilitation. This is because the applied force vector modifies the gait requirements while walking and drives the human CNS to make corrections to minimize the induced errors by modifying the motor commands. In these paradigms, external forces were applied to the pelvis as pelvic motion plays an important role during the gait cycle, particularly in the weight transfer between limbs and in forward propulsion of the body [32]. The vertical component of the force vector provided an external weight bearing during walking in both studies. In contrast, the anterior-posterior component in the second study resulted in asymmetric changes in the pelvic motion, thus creating a need for subjects to adapt the lower limb support periods. Both of these requirements are critical during gait and are effectively accomplished during a healthy individual's walking [32–34]. However, due to lack of muscle power and control, individuals with neural impairments, such as hemiparetic stroke patients, are unable to bear weight during the affected limb stance phase. This inability results in gait asymmetry, higher energetics, and risks of falls, among other compensatory adaptations [34–42].

We believe these paradigms, when extended to individuals with limited weight bearing ability or hemiparesis, can be very useful. Training done in multiple sessions with an force vector, where magnitude can be regulated, can provide improvements in weight bearing capability with positive effects on gait symmetry and walking speed. In gait rehabilitation literature on stroke survivors [67,76,77,85], it has been shown that despite compromised nervous system these patients are able to adapt their gait pattern in response to the applied intervention. In the following chapter, we present a single-session experiment conducted with hemiparetic stroke patients using the asymmetric weight bearing paradigm.

Chapter 5

Gait Rehabilitation Studies

The weight bearing paradigms using the A-TPAD discussed in the previous chapter have the potential to improve stance phase gait performance of neurologically impaired patients. In this chapter, we describe a single-session study conducted with hemiparetic stroke patients using the asymmetric weight bearing paradigm and discuss the results in the context of gait rehabilitation.

5.1 Gait Pattern of Hemiparetic Stroke Patients

Stroke is caused by a blocked artery (ischemic stroke) or the leaking/bursting of a blood vessel (hemorrhagic stroke) resulting in interrupted or reduced blood supply to the brain [29, 86]. Depending on the area of brain and the duration for which it was deprived of blood supply, a stroke occurrence can result in temporary or permanent disabilities. In most cases, these instances affect an individual's ability to generate voluntary muscle contractions of normal magnitude and result in inappropriately timed muscle activity [35–37].

Eight out of every ten stroke survivors demonstrate one-sided weakness - referred to as hemiparesis [86]. The gait patterns of hemiparetic stroke patients have been characterized by shorter stance phase, prolonged swing phase, and reduced joint excursion on the affected side as compared to the unaffected side. These patients also demonstrate reduced ability to bear weight on the affected leg, which results in lower ground reaction force (GRF) values over a gait cycle. Thus, hemiparetic gait is characterized by distinct gait asymmetries in the gait kinematics as well as kinetics. These abnormalities and asymmetric gait pattern increase the risk of falls for these patients and put them

at increased risk of serious injuries, such as hip fractures [34]. Consequently, restoration of gait symmetry has been the main focus of various gait rehabilitation interventions [3,67,76,77]. Most of the existing studies in the literature focus on the swing phase gait parameters and spatio-temporal gait parameters to target the asymmetric gait kinematics of these patients. As pointed out in the previous chapter, the goal of the current work is to target the asymmetric gait kinetics. Thus, the stance phase interventions were developed using the A-TPAD to improve the weight bearing during walking.

Sufficient weight bearing on a limb during walking is crucial for maintaining the gait symmetry, as the inability to bear weight on one leg affects the swing initiation as well as the positioning of the contra-lateral leg for the weight acceptance. In addition, during steady-state walking, an individual applies forces against the ground to accelerate and decelerate the body's COM during the stance phase, which are generally represented as propulsive and braking efforts and are computed from the time integration of the anterior-posterior (A-P) GRF values over particular sections of the stance phase. Unlike healthy individuals who demonstrate almost equal propulsive and braking efforts on even-terrains, hemiparetic stroke patients demonstrate reduced propulsive effort from the affected leg due to the inappropriately timed muscle activation and the inability to bear weight [87,88]. This results in asymmetric A-P GRF patterns with lower propulsive impulse and higher braking impulse from the affected leg within the stance phase. To compensate for the reduced propulsion effort from the affected leg, these patients apply higher propulsive effort from the unaffected leg, thereby adapting an asymmetric gait pattern. In addition, these patients also develop other compensatory strategies like hip circumduction on the affected side to compensate for the reduced push-off effort, thus generating higher level of hip joint torque than able-bodied individuals [35].

In the following sections, we investigate the effects of the proposed asymmetric weight bearing paradigm on gait symmetry of hemiparetic stroke patients by exploring gait kinetics adaptation.

5.2 Motor Adaptation

In literature, the human nervous system is believed to be capable of predicting upcoming movement requirements based on an internal body representation [82,83,89]. When external forces are applied, these requirements are modified due to induced movement errors. The human nervous system

updates the internal representation through experience to modify the motor commands [67, 89, 90]. This therefore explains an individual's ability to adapt the walking pattern under constantly human musculo-skeletal structure changes as well as varying external environmental conditions. In the motor adaptation research community, numerous studies have been conducted to understand human walking adaptation. In the previous chapter, we presented walking adaptation when external forces were applied to the pelvis. One of the main goals of any walking adaptation study is to use this understanding for gait rehabilitation of neurologically impaired patients.

In the gait rehabilitation literature on stroke survivors [67, 76, 77, 85], it has been shown that despite a compromised nervous system, these patients are able to adapt their gait pattern in response to an applied intervention. In these studies, various strategies have been developed to modify the walking conditions for these patients to induce new movement errors. These interventions drive the patients' central nervous system (CNS) to make corrections to minimize the induced errors by modifying the motor commands. For example, in [77], an error augmentation paradigm was implemented using a split-belt treadmill to further increase the step length asymmetry of hemiparetic stroke patients'. Temporary improvements in the step length symmetry were reported as a result of the applied intervention. Similarly, in [76] unilateral resistance was applied on the lower limb of stroke patients by attaching weights during the swing phase. It was reported that mild to moderate hemiparetic stroke patients were able to improve gait symmetry temporarily post training. Such recalibration of established motor commands during walking hold great potential in the rehabilitation processes.

5.3 Single Session Study

To conduct the stroke patient experiment, a second version of the A-TPAD was developed for the Columbia University Medical Center. The design and control methodologies were similar to the ones described in Chapter 3. In addition, a split-belt treadmill with force plates from Bertec (Columbus, OH) was installed to measure the ground reaction forces (GRF) for each leg during the experiment.

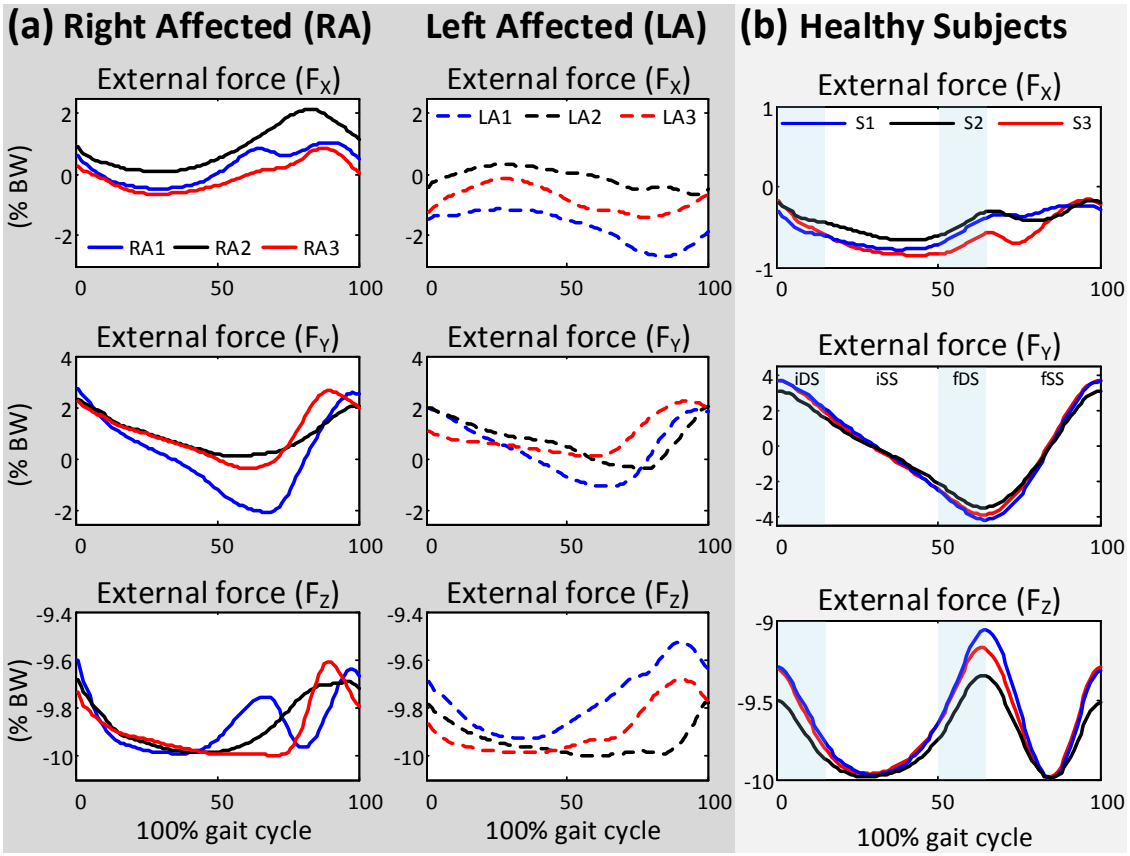

Figure 5.1: (a) The desired external force values during a gait cycle calculated from 6 hemiparetic baseline markers data: 3 have right leg affected (RA) and other 3 have left leg affected (LA). Pelvic marker R/LILIAC and ankle marker R/LANK were used to calculate the force vector. (b) The desired external force values for three healthy subjects (copy of Fig. 4.1(c)).

5.3.1 Asymmetric Weight Bearing

An asymmetric weight bearing force intervention was used for the stroke experiment. In the healthy subject experiment described in the previous chapter, a force vector with a magnitude equivalent to 10% of subject's body weight (BW) was directed along the right leg (Section 4.1.2). For stroke patients, the magnitude of the force vector was also chosen to be 10% of the body weight (BW), and the force vector was directed along the affected leg of the patient. Thus, for a stroke patient with weaker right leg the force was directed along a vector from the right iliac crest, RILIAC, to the right ankle, RANK; while for a weaker left leg patient the vector was applied from the left iliac crest, LILIAC, to the left ankle, LANK.

In Fig. 5.1(a), the components of the desired external force vector are described using baseline pelvic and foot markers data from six hemiparetic patients: 3 with right leg affected (RA) and other

3 with left leg affected (LA). Due to the significant differences between the baseline gait pattern of hemiparetic stroke patients and healthy individuals, significant differences are noted between the desired force components of stroke patients and healthy individuals as shown in Fig. 5.1 (Fig. 5.1(b) is a copy of Fig. 4.1(c)). In the medial-lateral direction (X) for example, the range of external force is large compared to F_X values for healthy subjects. This could be because stroke patients develop compensatory strategies along the affected side, such as hip circumduction which results in increased lateral movement of the affected leg. The anterior-posterior force component, F_Y, range is smaller than that of the healthy subjects due to reduced hip and knee flexion-extension range of motion on the affected side. The vertical force component, F_Z, for the healthy subjects showed two oscillations over a gait cycle, refer to Fig. 5.1(b). For the hemiparetic gait pattern, the variations in the F_Z values during the second half of the gait cycle are greatly reduced. This reflects reduced foot vertical clearance of the affected leg during early swing phase.

The force vector direction along a moving vector parallel to the affected limb of the patients was selected to provide extra weight bearing on the affected limb. In addition, it was expected that the anterior-posterior component of the applied force will promote longer affected leg stance duration during walking. This force intervention therefore provides a novel approach to target gait training of hemiparetic stroke patients, as they typically shy away from loading their affected limb which could further weaken the limb and inhibit the patient's voluntary movements. With this paradigm, we hypothesized that while walking with external asymmetric weight bearing, these patients will train their affected leg to show temporary improvements in the stance phase duration and weight bearing capability. These changes will be reflected further in improved gait symmetry measures between the affected and unaffected legs.

5.3.2 Experimental Protocol

Ten hemiparetic stroke patients participated in the study. Five patients had a right affected leg and the remaining five had a left affected leg. These patients are referred as 'RA' for right affected and 'LA' for left affected in this chapter. The patient information is presented in Table 5.1. The training protocol, approved by the Columbia University Internal Review Board, included Baseline (BL), Training (T), and Post-training (PT) sessions, as shown in Fig. 5.2. At least three rest breaks one minute in duration were provided during the experiment, and additional rest breaks

Figure 5.2: Experimental protocol for the single session stroke experiment. The experiment included baseline, training and post training sessions with rest sessions in between. The numbers in the block indicate the data collection trial number for each session.

Table 5.1: Patients information, RA - right leg affected and LA - left leg affected.

	Age	Gender	Type of Stroke	AFO Used	Walking Speed
RA 1	65	M	Ischemic	No	0.4 m/s
RA 2	62	F	Ischemic	No	0.2 m/s
RA 3	62	F	Hemorrhagic	Yes	0.2 m/s
RA 4	48	F	Hemorrhagic	No	0.4 m/s
RA 5	41	M	Ischemic	No	0.7 m/s
LA 1	52	M	Hemorrhagic	Yes	0.4 m/s
LA 2	58	M	Ischemic	No	0.1 m/s
LA 3	72	F	Ischemic	No	0.2 m/s
LA 4	50	F	Ischemic	Yes	0.6 m/s
LA 5	59	M	Hemorrhagic	Yes	0.5 m/s

were permitted if the patient felt fatigued. Each subject was suited with retro-reflective markers to record the motion data. The marker set and associated limb frame assignments are discussed in detail in Appendix B. A fabric hip belt with cable attachment points was worn by the subject, and a hand sling was used to hold the affected arm during the experiment. A safety harness was used throughout the experiment to prevent accidental falls. Patients who used an ankle foot orthosis (AFO) during their daily activities were allowed to use it during the experiment.

During the Baseline session, each subject walked on a treadmill for three minutes at a self selected speed. Data collected during the last minute of this session was treated as the reference data and labeled as BL. Thereafter, cables were attached to the hip belt to apply the desired external wrench to the pelvis. During the Training session, each subject walked for sixteen minutes in total at the same treadmill speed. A rest break of one minute was allowed after eight minutes. As the subject walked, the controller adjusted the tension values of each cable to continue applying the desired external wrench. Data were recorded six times for one minute duration at the start, 3.5^{th}, and 7^{th} min of both part of training. These data collection instances were referred to as T1, T2, T3, T4, T5, and T6 as shown in the Fig. 5.2. Following the training session, the subject was

given a one minute rest and cables were removed. During the Post-training session, each subject walked for another ten minutes at the same treadmill speed. Data were recorded four times for one minute duration at the start, 3^{rd}, 6^{th}, and 9^{th} min. These data collection instances were referred to as PT1, PT2, PT3, and PT4. Before the baseline session, each subject was asked to stand still for a few seconds to record a static data set.

5.3.3 Data Processing

During the experiment, each subject's kinematics, ground reaction forces, and applied wrench data were recorded for the analysis. The time histories of all gait parameters were normalized in time to 100% of the gait cycle, where a gait cycle was defined as the interval from a right heel strike event (RHS) to subsequent right heel strike. The heel strike and toe-off events were determined from the ground reaction force (GRF) values obtained from the treadmill force plates. The GRF data were recorded at 1000 Hz and post-processed using a low-pass filter (4^{th} order Butterworth, cut-off 20 Hz). The GRF data were normalized by each subject's body weight for the analysis. The gait events were also used to estimate the durations of the double support (DS) phase, single support (SS) phase, stride time, and stance time during each gait cycle. Lower limb sagittal plane joint angles were estimated from the human segment marker data. Since the pelvic markers were placed on the brace during walking and some patients used their AFOs, the hip and ankle joint angles data were not compared between subjects.

An asymmetric measure was defined to evaluate the gait symmetry, given as

$$\text{Asymmetric measure} = 100 \times \frac{(A-U)}{(A+U)}, \tag{5.1}$$

where A and U represent the values of the affected and unaffected limb parameters respectively. A zero value of the asymmetric measure implies perfect symmetry while a positive/negative value means higher/lower A values compared to U values. Eq. (5.1) was used to calculate the asymmetry in the stance phase, GRF, and step length values of the two legs. Step length was defined as the anterior-posterior distance between the heel marker of each leg at heel strike of the leading leg.

To study the performance and response of the group to the applied external wrench, gait measures from the last five gait cycles for trials BL, T6, and PT4, and from the first five gait cycles

for trials T1 and PT1 were analyzed. The data were first checked against the sphericity violation using the Mauchly's test and the Huynd-Feldt correction was applied when the data violated the condition. One way repeated measure ANOVA was performed to determine the statistical significance (defined as $p < 0.05$). The Bonferroni-Holm significant difference test was performed when a statistical significance was identified. The chosen combinations for statistical difference comparison were BL-T1 and BL-T6 to evaluate the effects of force training, and BL-PT1 and BL-PT4 to evaluate the post-training effects. A significant difference between the values of a gait parameter during BL and T1 is referred as the effect of training with force. In addition, if the values during PT1 were also significantly different from BL, then it is referred as an aftereffect. A negative aftereffect is defined as when the changes between BL-PT1 were of opposite nature than the changes between BL-T1, adapted from [82]. Values plotted in the following section are given as means ± standard errors. An asterisk mark indicates a significant difference between the means of the two sessions.

5.4 Results

The ground reaction force values normalized by the patient's body weight in the vertical direction, GRF_Z, is shown in Fig. 5.3 for a RA patient during different trials of the experiment. Asymmetric differences can be observed in the BL distribution of GRF_Z values between the two legs. In particular, the duration over which the right leg was in contact with ground was shorter and the normal impulse magnitude (the time integral of the GRF_Z values) was lower. During the training trials, T1 and T6, higher normal impulse magnitudes were observed from both legs. This was due to the external vertical component of the applied force to the pelvis. Notably, higher normal impulse magnitudes from the right leg were retained during the post-training trials, PT1 as well as PT4.

Full-normal impulse (I_{FN}) and partial-normal impulse (I_{PN}) values were calculated from the vertical GRF values for each leg, which are the time integral of the GRF_Z values over a gait cycle and the time integral of the GRF_Z values with magnitudes $\geq 80\%$ BW respectively as shown in Fig. 5.3. To quantify the effect of applied intervention on the group performance, asymmetric measures, $100 \times \frac{(A-U)}{(A+U)}$, were calculated for both I_{FN} and I_{PN} values, presented in Fig. 5.4. Since the ability

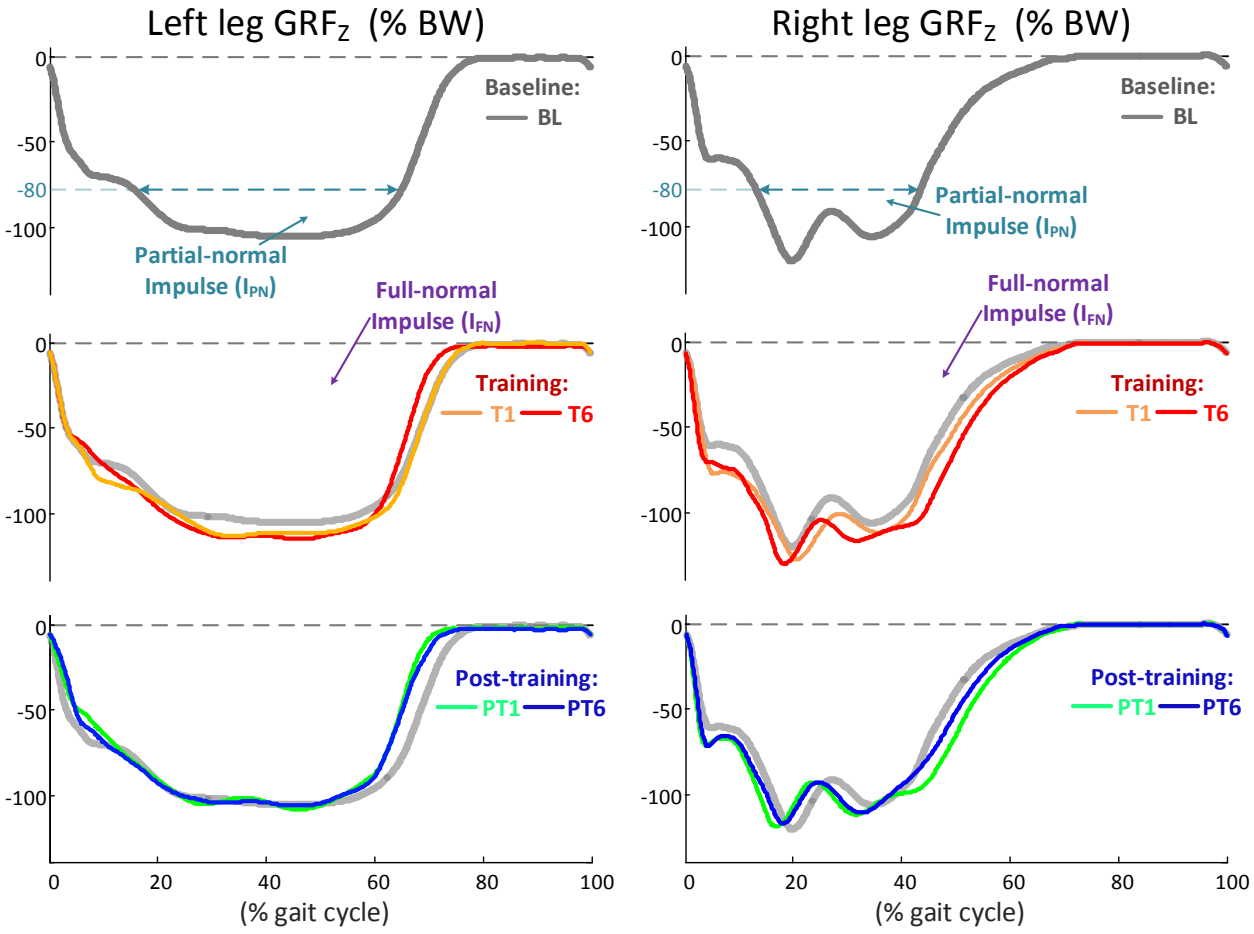

Figure 5.3: Ground reaction force component normalized with body weight in the vertical direction (GRF_Z) for a right affected (RA) patient during different trials of the experiment.

Table 5.2: Full-normal impulse values, $I_{FN}/10$ ($\%BW \times GaitCycle$), for each patient.

	Affected Leg						**Unaffected Leg**					
Sub ↓	**BL**	**T1**	**T3**	**T6**	**PT1**	**PT4**	**BL**	**T1**	**T3**	**T6**	**PT1**	**PT4**
RA 1	46.15	53.94	53.47	54.23	47.55	44.98	47.49	51.83	52.15	52.32	48.66	50.13
RA 2	36.85	42.29	44.19	44.47	36.80	42.22	63.44	68.79	66.99	66.54	63.88	59.46
RA 3	45.41	52.56	49.61	50.80	45.41	44.25	54.77	57.70	60.14	58.53	54.28	54.52
RA 4	44.27	49.32	47.52	52.92	50.17	47.18	62.75	66.88	70.42	65.15	58.66	59.63
RA 5	44.53	47.78	51.22	47.42	44.74	45.10	58.41	65.49	63.23	66.44	58.34	58.11
LA 1	41.41	47.86	45.90	46.79	42.60	42.38	59.03	64.78	65.53	65.53	60.33	59.35
LA 2	40.01	45.40	44.42	47.88	42.57	42.72	58.76	65.49	64.57	62.77	59.07	59.28
LA 3	39.11	42.75	45.63	41.58	39.23	39.41	63.96	69.57	67.75	71.19	64.40	65.35
LA 4	42.30	47.03	50.73	49.60	44.77	44.71	62.51	67.12	64.83	65.60	58.04	61.16
LA 5	39.87	44.98	44.81	45.29	40.13	43.83	53.82	59.65	58.96	58.78	54.74	52.89

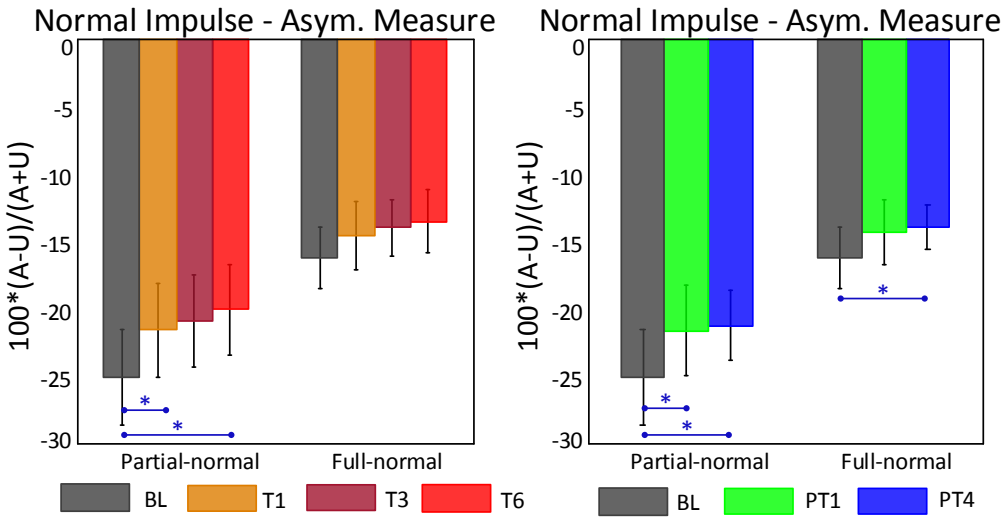

Figure 5.4: The time integral of the GRF_Z values during a gait cycle (I_{FN}) and the time integral of the GRF_Z values with magnitudes $\geq$ 80% BW (I_{PN}) from both legs were used to calculate the asymmetric measures for the group. Significant changes were observed between BL-T1, BL-T6, BL-PT1, and BL-PT4 for I_{PN} values; and between BL-PT4 for I_{FN} values.

of a hemiparetic stroke patient to bear weight on the affected leg is significantly limited, negative I_{FN} and I_{PN} asymmetric measure values were observed. Further, as I_{PN} is calculated from GRF_Z values $\geq$ 80% BW, larger I_{PN} asymmetric measure values were observed. The I_{FN} values for each patient are presented in Table 5.2. The repeated measure ANOVA reported significant changes in the values of I_{FN} and I_{PN} ($p < 0.05$). With the post-hoc analysis, we observed that the I_{PN} asymmetric measure decreased significantly from BL to T1 and BL to T6, as well as from BL to PT1 and BL to PT4. Similarly, significant lower values of I_{FN} asymmetric measure were reported during PT4 trial compared to BL. The reduction in the I_{FN} asymmetric measure values during the training trials failed to reach the post-hoc comparison significance. The lower values of normal impulse asymmetric measures reflect improved GRF symmetry in the vertical direction during walking.

The ground reaction force component normalized with body weight in the anterior-posterior (A-P) direction, GRF_Y, is shown in Fig. 5.5 for a RA patient during different trials of the experiment. The GRF_Y values also showed asymmetry during the BL trial. In particular, lower propulsive impulse magnitudes and higher braking impulse magnitudes were observed from the right leg as compared to left leg. Here, the braking impulse, I_B, represents the time integral of positive GRF_Y values, and the propulsive impulse, I_P, represents the time integral of negative GRF_Y values. With

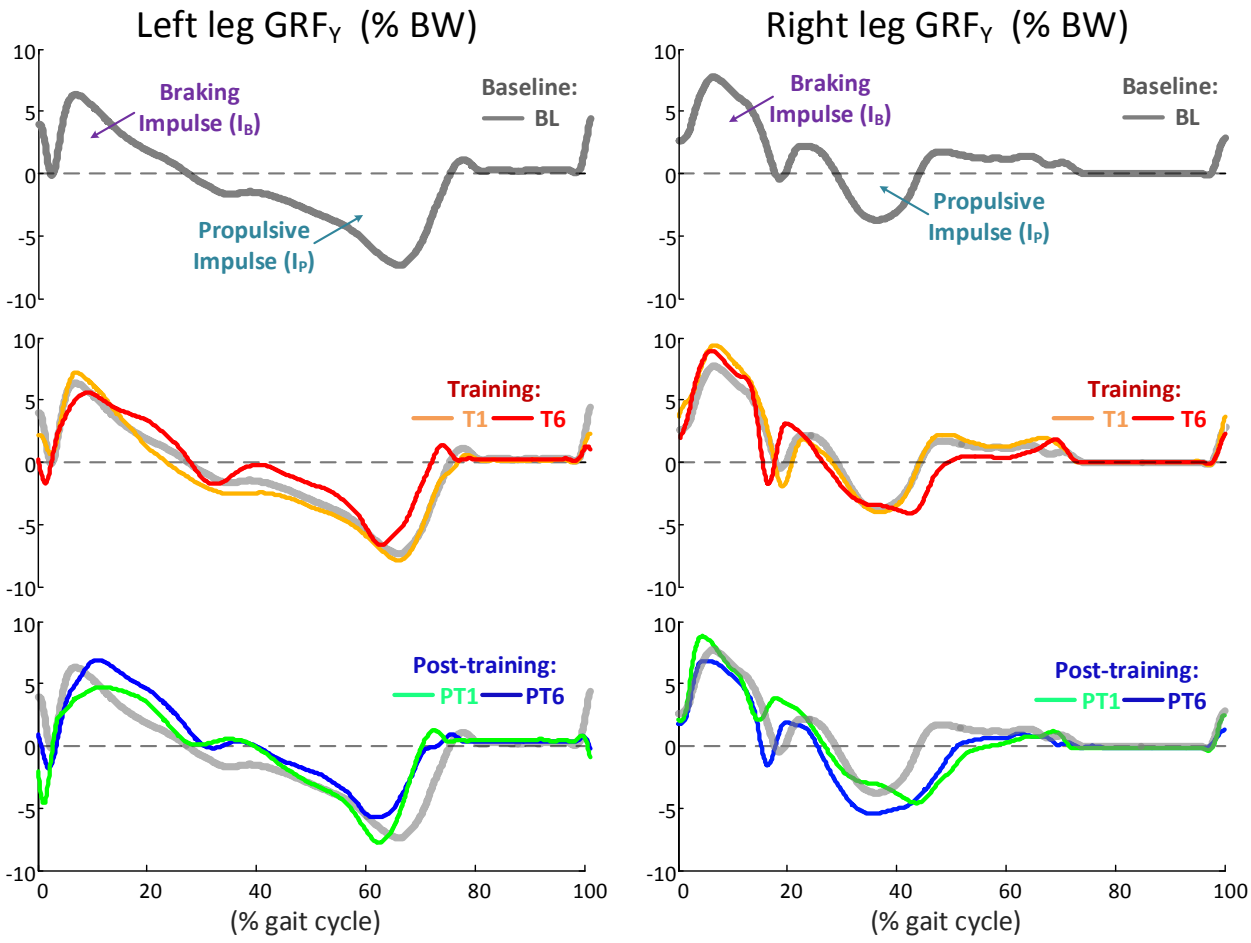

Figure 5.5: Ground reaction force component normalized with body weight in the anterior-posterior (GRF_Y) direction for a RA patient during different trials of the experiment.

the external force training, where an external anterior-posterior force was applied that followed the affected leg motion, higher I_P values were observed during the T6 trial (Fig. 5.5). In addition, the patient continued to generate higher I_P magnitudes even when the external force was removed, PT1 and PT4 trials.

The GRF_Y braking and propulsive impulse values were calculated from both legs for the group and the corresponding asymmetric measure values, $100 \times \frac{(A-U)}{(A+U)}$, are presented in Fig. 5.6. The I_P values for each patient are presented in Table 5.3. The statistical analysis reported significant reduction in the I_P asymmetric measure during the post-training trials compared to baseline ($p < 0.05$), BL-PT1 and BL-PT4. This was due to higher I_P values from the affected leg, refer to Table 5.3. Reduction in the I_P values during training trails did not reach significance. The I_B asymmetric measure values also decreased during the training and post-training trials, but the repeated measure

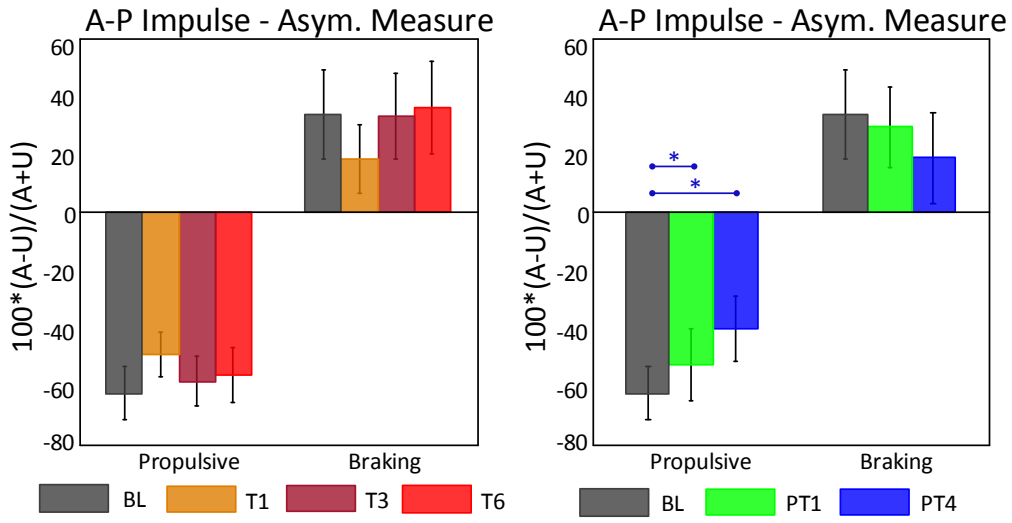

Figure 5.6: The time integral of positive GRF_Y values represents the braking impulse (I_B) applied by the patients, and the time integral of negative GRF_Y values represents the propulsive impulse (I_P) applied by the patients. These values from both legs were used to calculate the asymmetric measures for the group. Significant changes were observed between BL-PT1 and BL-PT4 for I_P values.

analysis showed significance only between the baseline and training trials ($p < 0.05$). However, the pairwise comparison did not reach the significance. Similar to the vertical direction, these lower values of GRF_Y impulse asymmetric measures also reflect improved GRF symmetry in the A-P direction during walking.

Stance phase durations for both legs over the group are shown in Fig. 5.7. The asymmetry in the stance phase duration is very apparent, indicated by shorter affected leg stance phase values. No statistically significant changes were reported in the stance phase asymmetric measure values

Table 5.3: Propulsive impulse values, I_P ($\%BW \times GaitCycle$), for each patient.

	Affected Leg						**Unaffected Leg**					
Sub ↓	**BL**	**T1**	**T3**	**T6**	**PT1**	**PT4**	**BL**	**T1**	**T3**	**T6**	**PT1**	**PT4**
RA 1	7.28	7.10	6.70	5.50	4.05	10.44	22.29	16.41	22.14	21.14	25.76	19.44
RA 2	0.24	4.05	0.44	0.88	0.35	2.86	18.53	10.45	15.50	18.07	23.39	19.56
RA 3	1.97	4.47	4.04	3.32	5.84	5.96	8.71	5.69	9.80	11.74	14.48	13.18
RA 4	3.91	4.67	5.68	6.22	6.96	9.10	16.45	19.10	17.72	11.08	12.89	10.03
RA 5	11.07	8.20	11.81	7.44	9.54	9.72	33.38	30.26	30.55	24.38	30.41	35.72
LA 1	10.69	5.99	8.49	9.82	11.59	12.09	11.77	8.78	12.13	11.34	12.31	13.42
LA 2	3.59	0.95	2.76	4.05	5.39	9.17	8.72	3.52	5.90	7.60	4.02	6.65
LA 3	0.03	1.69	0.00	0.00	0.06	1.14	20.01	7.85	10.23	11.72	13.79	10.90
LA 4	1.11	0.49	1.14	1.29	1.20	1.23	22.60	16.28	20.80	21.84	22.02	22.71
LA 5	4.46	8.50	6.87	6.82	5.81	7.63	21.30	20.65	22.27	18.29	19.96	17.29

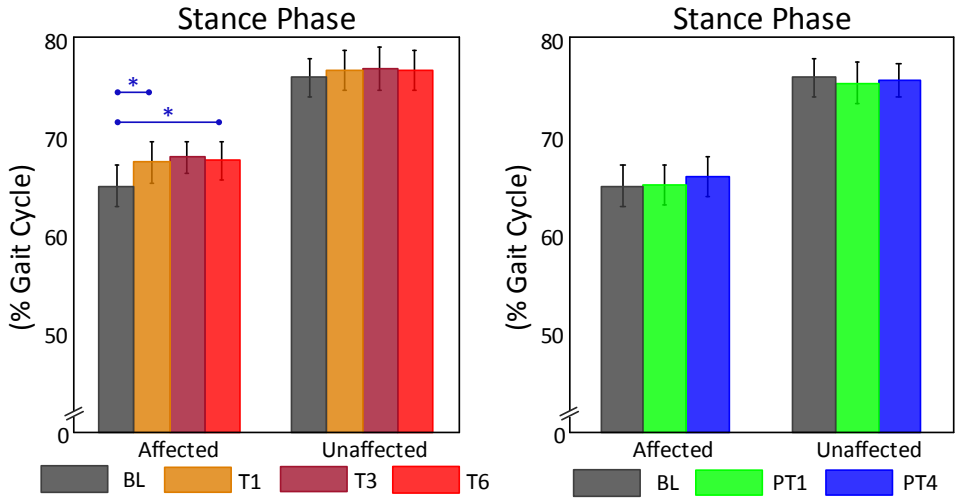

Figure 5.7: The stance phase durations of the affected and unaffected legs during different trials of the experiment. Significant changes were observed between BL-T1 and BL-T4 for affected leg stance phase durations.

during the experiment. Notably, the applied external force training promoted significant increase in the affected leg stance phase values ($p < 0.05$). The pairwise comparison reported significant changes between BL-T1 and BL-T6. One interesting note is that subjects retained the longer affected stance phase values even after the removal of the force and also showed reduction in the unaffected leg stance phase values. However, statistical significance was not reported between the baseline and post-training trials.

Double support phase duration and single support phase duration asymmetric measure values are presented in Fig. 5.8. For a RA patient, iDS and iSS were taken as A (affected leg parameter) in Eq. (5.1), where iDS denotes the part of a gait cycle from right heel strike to left toe off (double support) and iSS denotes the part of a gait cycle from left toe off to left heel strike (right leg single support phase) respectively. Similarly, for a LA patient, fDS and fSS were taken as A in Eq. (5.1), where fDS denote the part of a gait cycle from left heel strike to right toe off (double support) and fSS denotes the part of a gait cycle from right toe off to right heel strike (left leg single support phase) respectively. The DS asymmetric measure values increased during the training trials as compared to baseline values, while a decreasing trend was reported in its values during the post-training trials. The SS asymmetric measure values reduced during both the training and post-training trials compared to the baseline values. However, the statistical analysis did not report significant differences in these values.

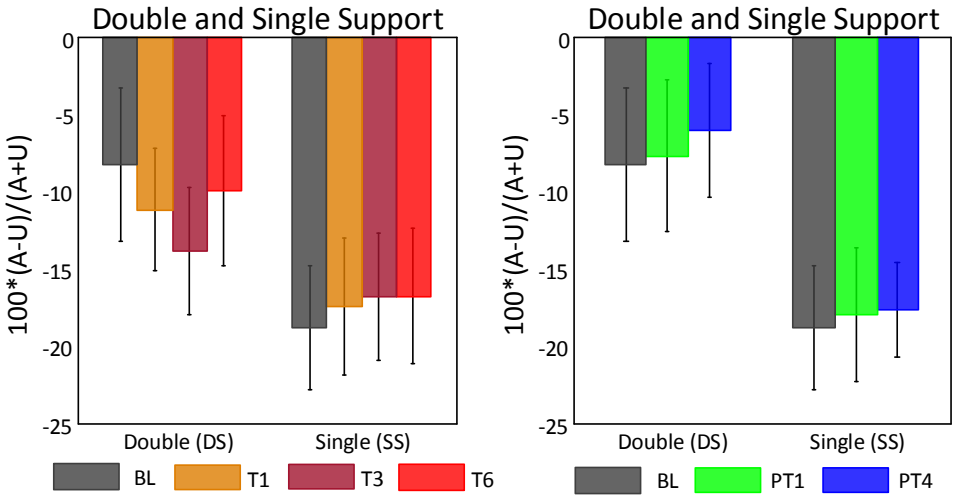

Figure 5.8: The double and single support phase durations of the affected and unaffected legs were used to calculate the asymmetric measure during different trials of the experiment. No significant changes were observed in these values.

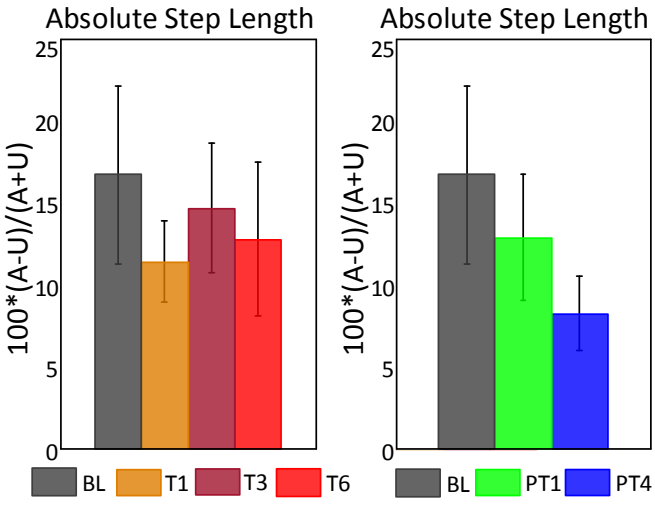

Figure 5.9: The step length values of the affected and unaffected legs were used to calculate the asymmetric measure during different trials of the experiment. No significant changes were observed in these values.

Table 5.4: Step length values (mm) for each patient.

	Affected Leg						Unaffected Leg					
Sub ↓	**BL**	**T1**	**T3**	**T6**	**PT1**	**PT4**	**BL**	**T1**	**T3**	**T6**	**PT1**	**PT4**
RA 1	377.5	339.3	337.4	368.9	383.6	333.8	392.7	439.0	423.9	397.1	357.1	457.9
RA 2	206.9	194.6	215.3	261.2	173.8	217.3	74.5	102.7	82.3	88.2	82.7	133.2
RA 3	187.0	191.3	169.6	191.0	255.1	169.9	197.5	214.1	188.0	183.0	161.3	193.0
RA 4	316.7	273.7	317.5	307.2	340.1	301.3	245.9	241.5	245.5	307.1	315.1	304.3
RA 5	562.0	566.6	563.4	488.7	526.6	530.4	463.0	413.3	457.0	347.1	427.8	431.6
LA 1	233.6	194.8	294.8	305.7	295.4	366.0	360.1	245.2	333.8	361.1	375.3	416.7
LA 2	191.9	138.3	143.4	151.2	122.2	131.0	151.6	129.2	103.1	108.5	122.6	150.8
LA 3	291.7	148.4	206.9	232.8	233.2	203.0	103.6	180.7	117.4	150.0	126.6	187.2
LA 4	504.2	475.8	507.6	505.2	550.5	513.7	437.1	395.0	459.5	444.3	452.6	442.3
LA 5	384.4	374.4	388.7	398.3	418.2	402.7	425.6	445.2	445.8	415.5	406.4	404.5

Step length values for each leg were also calculated and are presented in Table 5.4 for each patient. It was observed that six patients had longer affected step length values during the baseline while four patients (RA1, RA3, LA1, and LA5) had longer unaffected step length values during the baseline. Thus, the absolute values of the step length asymmetric measure were used for the statistical analysis, which are presented in Fig. 5.9. The absolute values of the step length asymmetric measure decreased during both the training as well as post-training trials. However, the repeated measure ANOVA analysis did not report significant differences in these values.

5.5 Discussion and Conclusion

In this chapter, we presented a single session hemiparetic stroke experiment using a novel asymmetric weight bearing paradigm to target the asymmetries in gait kinetics measures. During the experiment, an external force vector directed along the affected leg was applied to the patient's pelvis. All patients successfully completed the sixteen minutes training session with the 10% BW external force applied to their pelvis. As this was the first study of this kind, the duration of the training and the magnitude of external force were chosen based on healthy subject experiment. As the patients did not complain about fatigue during the experiment, this study suggests that the selected external force magnitude and training duration were reasonable for hemiparetic patients, who typically shy away from loading their affected limb during walking.

The results of the current study showed improved weight bearing capabilities along the affected side during the training session. In particular, the hemiparetic stroke patients generated higher

GRF_Y propulsive impulse as well as GRF_Z normal impulse during the stance phase of the affected leg. This was expected during the training, as the anterior-posterior force component necessitated higher propulsive effort at the affected leg push-off and the vertical component of the applied force vector provided external downward force during walking. Notably, patients continued to generate higher GRF_Y propulsive and GRF_Z normal impulse values even after the removal of the external force. This ability of patients to generate higher GRF values from the affected leg in the absence of external intervention reflects the translation of training effects and demonstrate gait kinetics adaptation. In the existing weight bearing paradigms reported in the literature [78–80], improvements in the vertical GRF symmetry have been reported mostly during the standing tasks. Since walking is a dynamic process with continually changing requirements, the results of these studies have not been shown to translate to walking. In this regard, the novelty of current work is in providing external weight bearing training with an anterior-posterior force component which follows the patient's affected limb motion during walking.

The proposed force intervention also promoted longer affected leg stance phase durations. This was because the F_Y component of the applied external force resisted the pelvic motion during the affected leg stance phase and assisted the pelvic motion during the affected leg swing phase. This resulted in patients spending more time on their affected leg during the training session. However, this single session force training was not enough to result in longer affected stance phase durations during the post-training trials. The training with asymmetric weight bearing force vector also showed positive effects in reducing the step length, double support, and single support asymmetry measures. One possible reason for these changes not being significant could be that the current force training was only limited to a single-session. It is therefore expected that a multi-session study with this force intervention could induce long-term gait improvement in hemiparetic stroke patients.

Chapter 6

Walking Effort Study

In this chapter, we describe an intervention to apply external gait synchronized forces on the pelvis to reduce the user's effort during walking. The external forces were directed in the sagittal plane to assist the trailing leg during the forward propulsion and vertical deceleration of the pelvis during a gait cycle. The results of an experiment with five healthy subjects using the proposed force intervention are provided in the chapter.

6.1 Human Walking Mechanics

Walking is the main mode of locomotion among legged animals. Humans accomplish walking through successful inter-limb coordination and cyclic activation of leg muscles. Human walking is a mechanically-complex task that involves a state of continuous imbalance, where each step is taken to regain the body's balance [32]. In particular, sufficient foot clearance is required when one leg is in the swing phase to prevent scuffing with the ground. At the end of the swing phase, the leg must be positioned ahead of body. This is accomplished through bearing weight on the leg in contact with ground (stance phase). At the end of a leg's stance phase, sufficient push-off force is needed to initiate the swing phase of that leg as well as to propel the body's center of mass (COM) forward.

Given the ease with which healthy individuals accomplish these patterns, researchers have described the steady-state walking as the most metabolically economic locomotion mode [32, 91–94]. Despite this, a significant amount of research effort has explored ways to augment the metabolic cost of walking to make walking easier. The main motivation for these efforts is to restore per-

formance in individuals with lower limb impairments, such as lower limb amputees, and to enable increased human endurance while performing demanding tasks while walking, such as carrying weight. To achieve these goals, researchers have developed external devices with passive and active force generating elements to complement the functioning of lower limb during walking.

In the literature, simple inverted pendulum walking models have been developed to understand the human walking dynamics [91–93]. This is because during walking leg motions are coordinated to move the body's COM forward while keeping at least one foot in contact with the ground at all times, thereby inducing an arc shaped trajectory to the COM in the sagittal plane. In these mathematical models, step to step transition has been identified as the most critical event. In this phase, the trailing leg performs positive work to smoothly change the COM direction of motion in the vertical and anterior-posterior directions. Studies on lower limb joint moments identify ankle and hip joints as the source of the positive work with ankle joint being the dominant contributor [93, 95].

The majority of the works reported on reducing the walking effort have thus focused on developing an exoskeleton or prosthetic device to complement the ankle joint, [94–102]. The exoskeletons have been tested on able bodied individuals to study the changes in the metabolic cost under altered walking conditions, such as walking on an incline. Similarly, the prosthetic devices have been tested with amputees to study changes in the metabolic cost and coordination between the intact and affected leg. In the literature, researchers have also developed mechanisms to study the role of applying external forces on the thigh segments to complement the hip joint during walking. For example, in [103], a modified version of active leg exoskeleton (ALEX II) was used to assist a hip joint. In a separate study [104], a prototype of a device was presented to assist the hip joints during the swing phase.

Among these works, very few studies have been successful in reducing the overall metabolic cost of walking compared to those with able bodies [94] or individuals using conventional prosthesis [96]. One important factor in using these exoskeletons or prosthetic devices is that they change the human dynamics, in particular due to the added mass on the leg and mismatch in timing when the external forces are applied [95, 101]. Since humans adapt their walking pattern under different external conditions, it becomes critical to understand the adapted pattern. For example, in [102], a study with a powered ankle exoskeleton was conducted to report that external assistance at ankle

push-off reduces the metabolic cost by primarily reducing the affected leg hip power during the swing phase, but it does not reduce the overall COM work.

As the main goal of inter-limb coordination and cyclic activation of leg muscles during steady-state walking is to propel the COM forward, studies with external forces that directly alter the COM dynamics can provide better understanding for designing exoskeletons and prosthetic devices to reduce the overall walking effort. In this work, we present a setup and methodology to apply gait synchronized external forces at the pelvis to reduce the user's walking effort.

6.2 Pelvic Intervention using A-TPAD

Due to the proximity of the pelvis segment to the body's COM, pelvic motion plays a central role in all forms of locomotion. The vertical pelvic motion and acceleration profiles during steady-state walking are presented for a healthy individual in Fig. 6.1 over a gait cycle. It is observed that human pelvis undergoes two oscillations along the vertical axis. Each oscillation is accompanied with periodic exchange between the gravitational potential and kinetic energy.

The transition in the pelvic motion direction during the single support (SS) phase is mainly due to the external gravitational force on the body. While the motion transition during the double support (DS) phase is to push the pelvis into the periodic arc shaped trajectory, which is achieved through successful step to step transition. Thus, a significant amount of lower limb muscle effort is needed from the trailing leg to provide forward propulsion during the DS phase and to decelerate the vertical fall of the COM during the SS phase [92, 93, 95, 105].

In this study, an external force vector is applied at the pelvis to reduce the trailing leg effort over a gait cycle.

6.2.1 Desired External Wrench

A-TPAD configuration with four cables was used to apply the external wrench to the pelvis, as shown in Fig. 6.2. Two of these cables connect the hip belt to the top of the frame while the other two cables connect the hip belt to the bottom of the frame. By controlling the tension magnitude in these cables, an external force vector was applied to the pelvis and the moments resolved at the pelvic center were maintained in a desired small range. The medial-lateral component of the

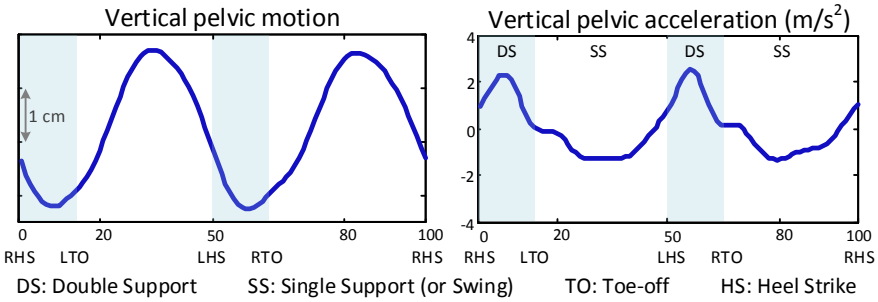

Figure 6.1: A healthy individual's pelvic vertical motion and acceleration profile over a gait cycle during steady-state walking.

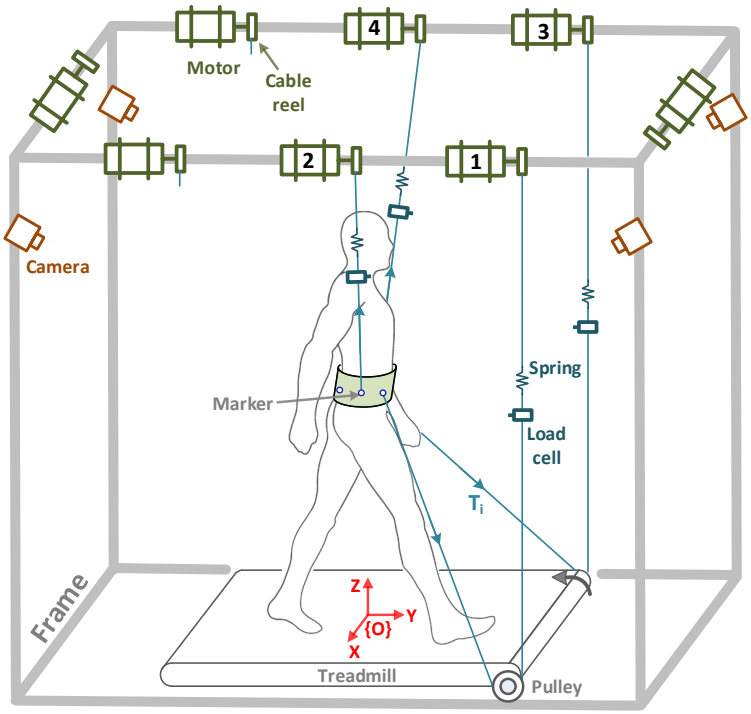

Figure 6.2: The cable configuration used during the A-TPAD experiment is shown. Four cables were used to apply the desired sagittal plane forces. The hip belt was connected to the frame top by two cables and to the frame bottom by other two cables.

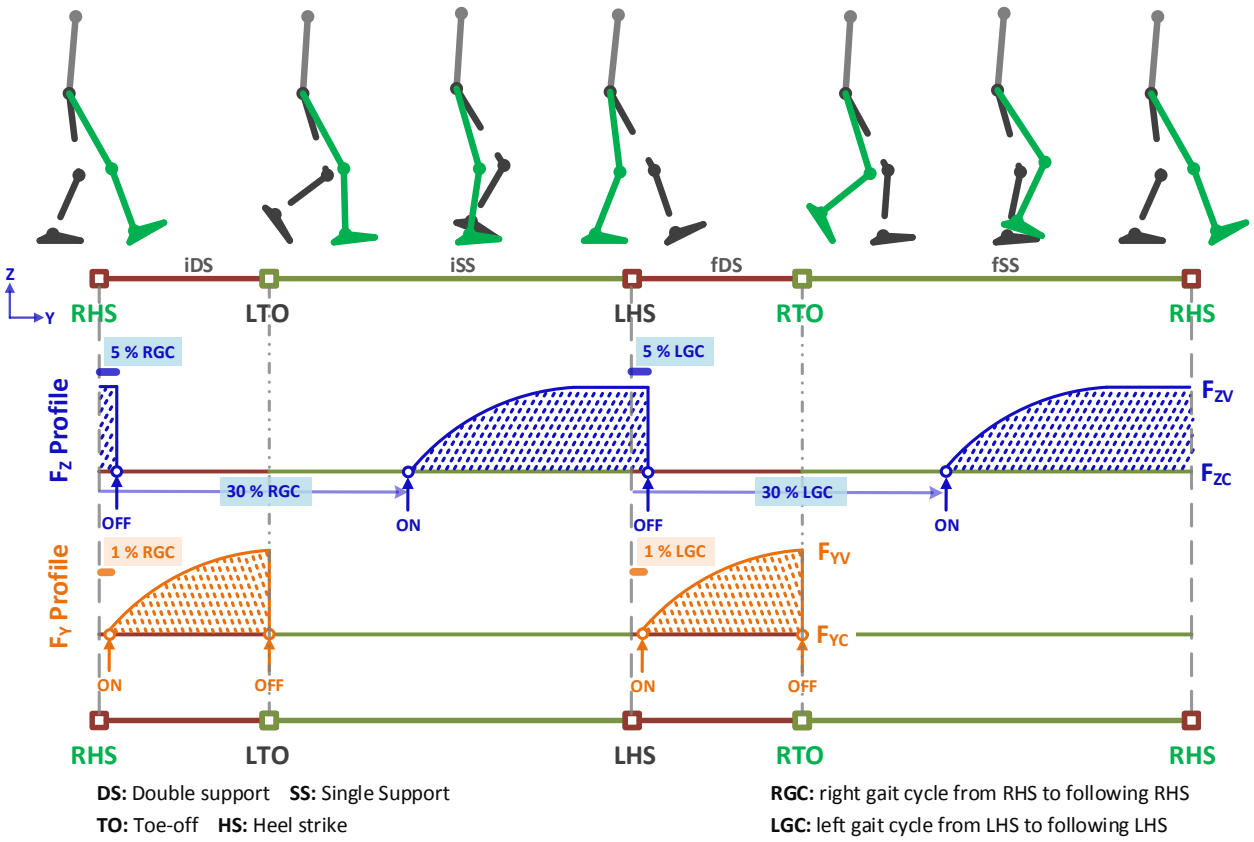

Figure 6.3: The desired sagittal plane external force pattern over a gait cycle that was used during the study. The F_Y and F_Z values were comprised of varying terms (F_{YV} and F_{ZV}) that appeared briefly during the gait cycle and constant terms (F_{YC} and F_{ZC}) that were necessary to maintain positive cable tension during the experiment.

external force, F_X, was controlled to be less than 1% of a subject's body weight (BW) , while the moment components resolved at the pelvic center were maintained within $\pm$ 4 Nm. The sagittal plane component of the force vector (F_Y: anterior-posterior, and F_Z: vertical) were controlled to provide the external assistance during walking, which are described as

$$\begin{aligned} |F_X| &\leq 1\% \text{ BW} \\ F_Y &= F_{YC} + F_{YV} \\ F_Z &= F_{ZC} + F_{ZV} \\ |M_{X,Y,Z}| &\preceq 4 \text{ Nm} \end{aligned} \tag{6.1}$$

where F_{YC} and F_{ZC} are the constant terms. While the F_{YV} and F_{ZV} are the varying terms of the force vector that appear briefly during a part of the gait cycle, refer to Fig. 6.3.

Anterior-posterior force component (F_Y): The varying term F_{YV} was applied to the pelvis during the double support phase of a gait cycle. It was activated at 1% of a gait cycle (GC) past a heel-strike event. The right and left leg gait cycles (RGC and LGC) were identified separately using an adaptive frequency oscillator (Section 6.2.2) to adapt the timing of force actuation to the gait frequency during walking. Once activated, the F_{YV} magnitude grew as a sinusoidal function of time from zero to a maximum value of 2% BW. The F_{YV} term was deactivated exactly at the end of the double support phase, i.e., at the toe-off event which was identified using a foot switch in each shoe. Thus, there were two instances of F_{YV} during a gait cycle: from 1% RGC to LTO and from 1% LGC to RTO as shown in Fig. 6.3. The choice of this profile was made to mimic the biological forward propulsion effort applied by the lower limb muscles, which starts early in the double support phase to generate sufficient propulsion force to accomplish the weight transition and to propel the body's COM forward at push-off [93, 101, 105]. *It was therefore expected that the applied force intervention will reduce the trailing leg's walking effort required for the forward propulsion during the late stance phase.*

Vertical force component (F_Z): The varying term F_{ZV} was activated at 30% GC past the heel-strike event of a leg, and deactivated at 5% GC past the heel strike event of contra-lateral leg. In this time span, the magnitude of F_{ZV} grew as a sinusoidal function of time from zero to reach a maximum value of 3% BW which was maintained until it was deactivated. Thus, the F_{ZV} term was applied twice during a gait cycle: from 30% RGC to 5% LGC and from 30% LGC to 5% RGC as shown in Fig. 6.3. Similar to the F_{YV} profile, the choice of the F_{ZV} profile was motivated from the biological walking effort spent in decelerating the body's COM during the single support phase. As the COM reaches its vertical peak position almost around mid single support phase and starts falling under the gravitational force afterward, a significant trailing leg's muscle activation is required for deceleration to prevent sudden collision with the ground and accomplish foot transition [93, 102]. *It was therefore expected that the applied force intervention will further help in reducing the trailing leg's walking effort during the late stance phase.*

As the F_{YV} and F_{ZV} values were zero for most part of the gait cycle, a constant term F_{YC} with 2% BW magnitude and F_{ZC} with magnitude 4% BW were maintained to keep the cables in tension.

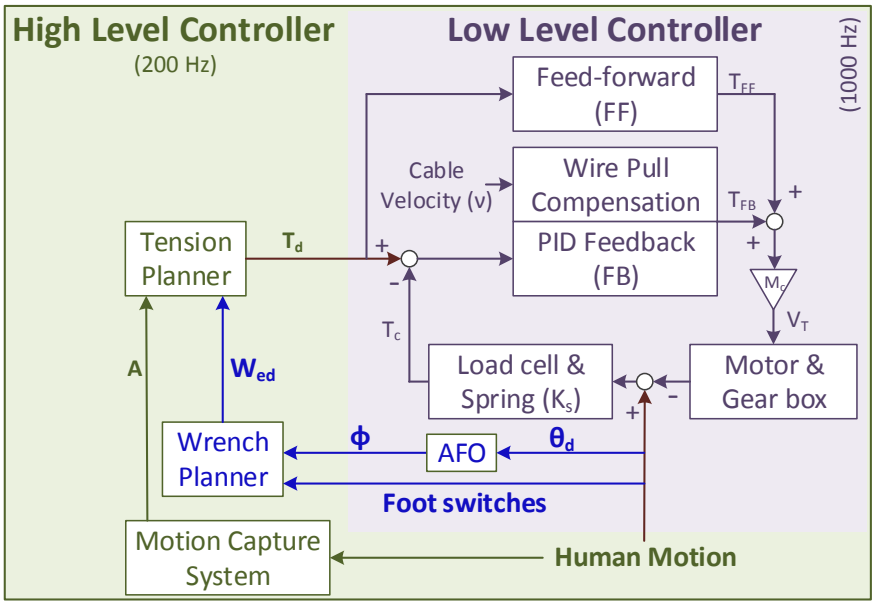

Figure 6.4: The A-TPAD control architecture described in Chapter 3 was updated to include a wrench planner in the high level controller and an adaptive frequency oscillator (AFO) in the low level controller. As explained in Algorithms 3 and 4, the pelvic acceleration was used to determine the gait phase required for the wrench planner to compute the external wrench (W_{ed}) values.

6.2.2 Controller

The A-TPAD control architecture was updated to include an adaptive frequency oscillator in the low level controller and a wrench planner in the high level controller as shown in Fig. 6.4.

AFO: An adaptive frequency oscillator (AFO, [106]) scheme was implemented to detect the gait phase during the experiment, the methodology is presented in Algorithm 3. The use of AFO to detect gait phase during walking has been implemented in various robotic studies using different periodic signals, for example joint angle trajectory was used in [56, 107]. In the current work, an accelerometer was placed on the subject's pelvis during the experiment to record the vertical pelvic acceleration values, a_y. An estimated acceleration signal, $\hat{\theta}$, was constructed using M harmonic oscillators and the previous estimated value, as described in line 6 of Algorithm 3. The amplitude, α, frequency, ω, offset, β, and phase, ϕ, of these harmonic oscillators describe the AFO states, Y. A teaching signal, $F(t)$, was constructed from the vertical pelvic acceleration values (minus the acceleration due to gravity), θ_d, and the $\hat{\theta}$ values (line 7). The first order equations, $\dot{Y}_t$ in line 8, were solved to learn the frequency of $F(t)$. Here, ϵ, ν, and f_{min} are the coupling strength, learning factor, and minimum frequency limit for the AFO respectively. At a time instant, the phase of the

Algorithm 3 Gait Phase Detection

1: **procedure** AFO

2: Input: $M \leftarrow 2; \nu \leftarrow 2; \epsilon \leftarrow 20; f_{min} \leftarrow 1.3$ ▷ f_{min} in Hz

3: Zero values: $Y_0 \leftarrow \begin{bmatrix} \phi_0 \\ \omega_0 \\ \alpha_0 \\ \beta_0 \end{bmatrix} = \begin{bmatrix} 0_{M\times 1} \\ 2\pi \times f_{min} \\ 0_{M\times 1} \\ 0_{1\times 1} \end{bmatrix}_{(2M+2)\times 1}$

4: Acquire: $a_y \leftarrow$ pelvic vertical acceleration ▷ At time instant t

5: $\theta_d \leftarrow (a_y -$ acceleration due to gravity$)$

6: $\hat{\theta}_t \leftarrow (\beta_{t-1} + \sum_{i=1}^{M} \alpha_{t-1}(i) sin(\phi_{t-1}(i)))$ ▷ Estimated signal

7: $F(t) \leftarrow (\theta_d - \hat{\theta}_t)$ ▷ Teaching signal

8: $\begin{bmatrix} \dot{Y}_t(i) \\ \dot{Y}_t(M+1) \\ \dot{Y}_t(M+1+i) \\ \dot{Y}_t(2M+2) \end{bmatrix} \leftarrow \begin{bmatrix} \dot{\phi}_t \\ \dot{\omega}_t \\ \dot{\alpha}_t \\ \dot{\beta}_t \end{bmatrix} = \begin{bmatrix} iY_{t-1}(M+1) + \epsilon F(t) cos(Y_{t-1}(i)) \\ \epsilon F(t) cos(Y_{t-1}(1)) \\ \nu F(t) sin(Y_{t-1}(i)) \\ \nu F(t) \end{bmatrix}_{(2M+2)\times 1}$ ▷ $i = 1 : M$

9: $Y_t \leftarrow \int \dot{Y}_t$

10: $Y_t(1) \leftarrow mod(Y_t(1), 4\pi)$ ▷ Remainder after division - Rolling over the phase value

11: **if** $Y_t(M+1) < 2\pi f_{min}$ **then**

12: $Y_t(M+1) \leftarrow 2\pi f_{min}$ ▷ Controlling the frequency

13: **return** $Y_t(1)$ and $Y_t(M+1)$ ▷ Gait phase and frequency

first harmonic oscillator, $\phi(1)$, approximated the gait phase value [107]. In Fig. 6.5(a), the θ_d and corresponding $\hat{\theta}$ data are shown for a section of the experiment. With only two oscillators ($M = 2$), a good estimate of the frequency of the pelvic acceleration pattern was obtained. The gait phase detection algorithm was tested for different walking speeds and it was observed that any change in the gait frequency was learned within three gait cycles.

Wrench Planner: As the pelvis oscillates vertically at twice the gait frequency, the gait phase values calculated from Algorithm 3 using the vertical pelvic acceleration vary from 0 to 4π during a gait cycle. To estimate the gait cycle with respect to each leg, foot switches (force sensitive resistor pads) were used to detect the heel-strike and toe-off events. The gait events were used to calculate the right and left leg gait phase values, ϕ_{RGC} and ϕ_{LGC}, as described in lines 4 and 5 of Algorithm 4. In Fig. 6.5(b), the foot switch data from both legs along with the calculated left and right gait cycle phase values (ϕ_{RGC} and ϕ_{LGC}) are presented for a section of the experiment. The activation of F_{YV} and F_{ZV} was therefore accomplished as per the conditions described in Section 6.2.1, as described in lines 6-13 of Algorithm 4. Thus, the desired force vector components in the sagittal plane were updated as $F_Y = F_{YC} + F_{YV}$ and $F_Z = F_{ZC} + F_{ZV}$.

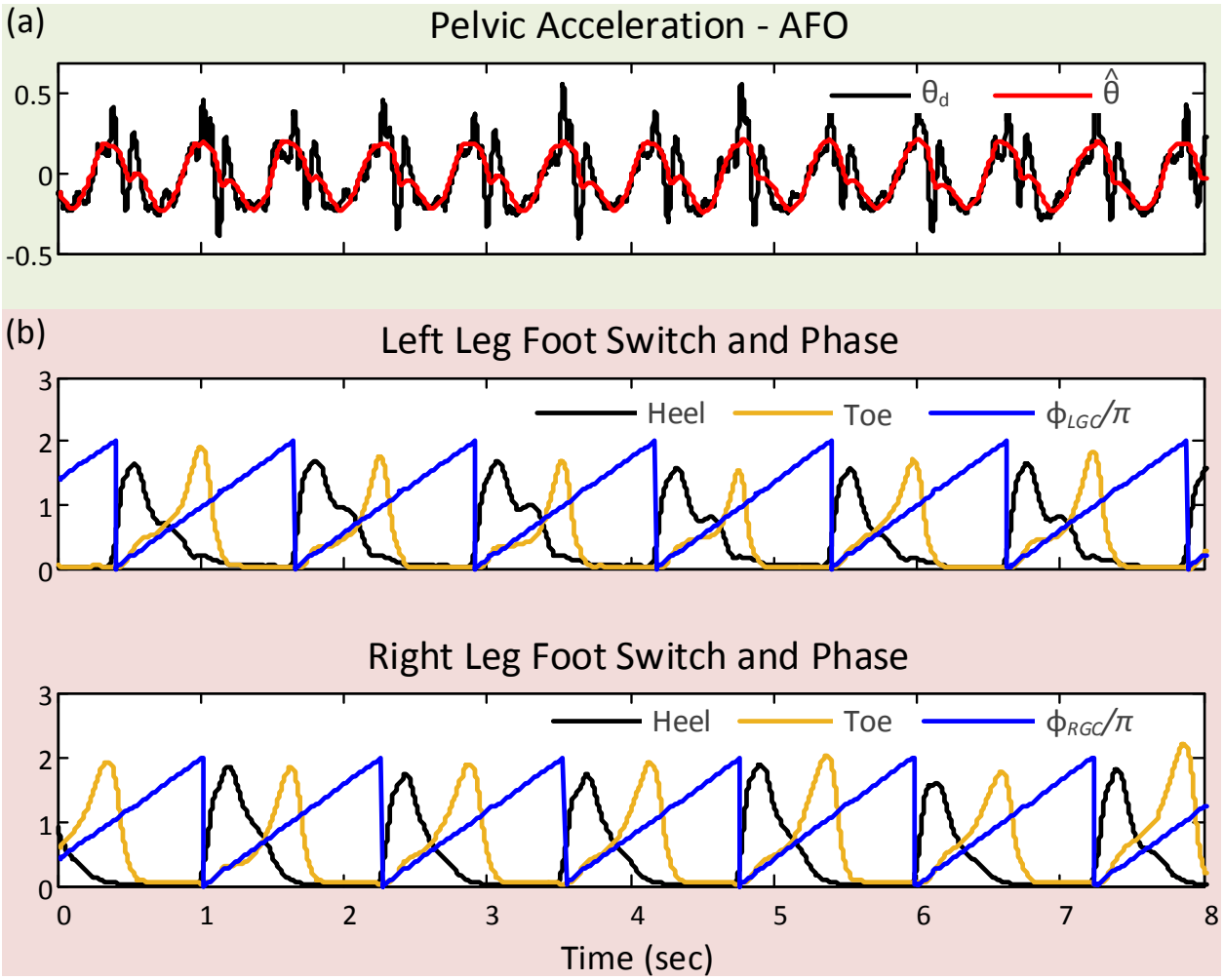

Figure 6.5: (a) The vertical pelvic acceleration profile from the accelerometer (θ_d) and the estimated acceleration values ($\hat{\theta}$) are shown for a section of the experiment. (b) The foot switch data from the heel and toe sensors of both legs are shown. The left and right gait cycle phase values (ϕ_{RGC} and ϕ_{LGC}) as calculated using Algorithm 4 are also presented for a section of the experiment

Algorithm 4 Force Computation

procedure FORCE ON-OFF
    Available: ω and ϕ ▷ Gait phase and frequency
    Acquire: $f_p \leftarrow$ *foot switches*
    $\phi_{RGC} \leftarrow \frac{100\times(\phi-\phi_{RHS})}{4\pi}$ ▷ RHS: right heel strike
    $\phi_{LGC} \leftarrow \frac{100\times(\phi-\phi_{LHS})}{4\pi}$ ▷ LHS: left heel strike
    if $(\phi_{RGC} \geq 30\%$ && $\phi_{LGC} \leq 5\%)$ || $(\phi_{LGC} \geq 30\%$ && $\phi_{RGC} \leq 5\%)$ **then**
        return aF_Z TRUE
    else
        return aF_Z FALSE
    if $(1\% \leq \phi_{RGC} \geq 20\%$ && LTO FALSE) || $(1\% \leq \phi_{LGC} \geq 20\%$ && RTO FALSE) **then**
        return aF_Y TRUE
    else
        return aF_Y FALSE

procedure FORCE VALUES
    if aF_Z TRUE **then**
        return $F_Z \leftarrow (F_{ZC} + \overbrace{A_Z\ sin(\omega t)}^{F_{ZV}})$
    else
        return $F_Z \leftarrow F_{ZC}$
    if aF_Y TRUE **then**
        return $F_Y \leftarrow (F_{YC} + \overbrace{A_Y\ sin(\omega t)}^{F_{YV}})$
    else
        return $F_Y \leftarrow F_{YC}$

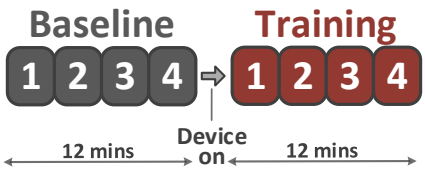

Figure 6.6: Experimental protocol for the human experiment included baseline and training sessions. The numbers in the blocks indicate the data collection trial numbers for each session.

6.3 Human Experiment

6.3.1 Protocol

Five healthy subjects, three male and two female in age range 22-30 years (mean age: 26.6 yrs) and mean weight 67.6 kg (SD: 9 kg), participated in the experiment. The training protocol was approved by the Columbia University Internal Review Board and involved Baseline (BL) and Training (T) sessions, as shown in Fig. 6.6. During both Baseline (BL) and Training (T), each subject walked on a treadmill for twelve minutes at a constant speed of 3.8 $kmph$. Data were collected four times during each session, at 1^{st}, 4^{th}, 7^{th}, and 10^{th} min. Data collection instances are shown by numerals in Fig. 6.6. Cables were attached to the hip belt for the Training session to apply the desired external wrench to the pelvis. As the subject walked, the controller adjusted the tension values of each cable to continue applying the desired external wrench.

For the experiment, each subject was suited with retro-reflective markers to record the human motion data. The marker set and associated limb frame assignments are discussed in detail in Appendix B. Surface EMG activities from the lower limb muscles were measured bilaterally, namely Gastrocnemius Medialis (MG), Soleus (SOL), and Tibialis Anterior (TA) of each leg. The electrode location and recording process has been elaborated in Appendix C. A fabric hip belt with cable attachment points was worn by the subject, and a three axis accelerometer was mounted on the subject's pelvis. Force sensitive resistor (FSR) pressure pads with 440 N limit (Flexiforce from Tekscan, Massachusetts) were mounted on the subject's shoe insoles to measure the foot pressure data. An Oxycon metabolic system from Care Fusion (CA, USA) was used to measure breath by breath volumetric oxygen (VO2) intake. The Oxycon metabolic system was calibrated using ambient air and a certified 16% oxygen and 4% carbon dioxide (CO2) gas tank. A heart rate belt from Polar (NY, USA) was used to obtain the breath by breath heart rate (HR) values. In

addition, a split-belt treadmill with force plates from Bertec (Columbus, OH) was used to measure the ground reaction forces (GRF) for each leg during the experiment.

6.3.2 Data Processing

During the experiment, each subject's EMG, GRF, VO2 intake, HR, and applied wrench data were recorded for the analysis. The time histories of all gait parameters were normalized in time to 100% of the gait cycle, where a gait cycle was defined from a right heel strike event (RHS) to subsequent right heel strike. The GRF data were recorded at 1000 Hz and post-processed using a low-pass filter (4^{th} order Butterworth, cut-off 20 Hz). The GRF data were weight normalized for each subject for the analysis. Further, the peak values of GRF data from each leg and the time integral of GRF values over a gait cycle, referred to as impulse, were compared between the baseline and training sessions.

EMG signals were post-processed using a band-pass filter (4^{th} order Butterworth, 40-450 Hz) and a full-wave rectification. The signals were smoothed using a low pass filter (n=4, fc = 6 Hz). For every subject, EMG data of each muscle were normalized to the peak values recorded during the baseline session. EMG root mean square (RMS) amplitudes and linear envelope peak values during the major burst were computed to estimate the level of muscle activation during the different trials of the experiment. The metabolic system data was normalized with subjects' body weight to get metabolic consumption rate (VO2/kg). The first two minutes of VO2 data collected during the BL and T sessions were discarded due to increased physiological demand of oxygen by the muscles. The remaining ten minutes of data were filtered using a 4^{th} order low pass filter at a cut-off frequency of .04 Hz [108, 109]. The first minute, last minute, and overall ten minutes average VO2/kg were calculated for each session per subject. In addition, a 21-sample (breath by breath) moving average was used to filter the VO2 data, the maximum value of this data was recorded as the peak VO2 for each subject. For the HR data, a 21-sample block average was taken of the raw data. The smoothed HR data were averaged for each session per subject.

To study the performance and response of the group to the applied external wrench, gait measures from the last five gait cycles for trials BL1, BL4, and T4 and from the first five gait cycles for trial T1 were analyzed. The data were first checked against the sphericity violation using the Mauchly's test and the Huynd-Feldt correction was applied when the data violated the condition.

One way repeated measure ANOVA was performed to determine the statistical significance (defined as $p \leq 0.05$). The Bonferroni-Holm significant difference test was performed when a statistical significance was identified. The chosen combinations for statistical difference comparison were BL4-T1 and BL4-T4 to evaluate the effects of force training. For the VO2 and HR parameters, a pairwise t-test assuming unequal variance was performed between BL and T and the significance was defined at $p \leq 0.05$. Values plotted in the following section are given as means $\pm$ standard errors. An asterisk mark indicates a significant difference between the means of the two sessions.

6.4 Results

The ground reaction force components normalized with body weight in the medio-lateral (GRF_X), anterior-posterior (GRF_Y), and vertical (GRF_Z) directions are shown in Fig. 6.7 for a representative subject during different trials of the experiment. Distinctive differences can be observed in the GRF values during the BL and T trials. In particular, the magnitude of GRF_X values during the T1 and T4 trials were lower than the corresponding BL1 and BL4 values, almost during the entire stance phase on each side. In the anterior-posterior direction, the GRF_Y values during the T1 and T4 trials were higher than the baseline values in the early stance phase but were lower in the late stance phase. The time integral of positive GRF_Y values represents the braking impulse, I_B, and the time integral of negative GRF_Y values represents the propulsive impulse, I_P. In the vertical direction, lower GRF_Z values were observed during the training trials around the late stance phase on each side.

Average GRF values from both legs for the group are presented in Fig. 6.8. In the anterior-posterior direction, the GRF_Y propulsive impulse values (time integral of negative GRF_Y values) were reduced during the training trials. The changes were significant for the right leg ($p < 0.05$), and significant differences were reported between BL4-T1 and BL4-T4. In addition, the GRF_Y braking impulse values (time integral of positive GRF_Y values) increased significantly for both left and right legs ($p < 0.05$). Pairwise comparison showed significant changes between BL4-T1 and BL4-T4. Notably, the GRF values were reduced for both legs during the training session. The statistical analysis reported significant reduction in the GRF_Z peak and impulse values (time integral of GRF_Z values over a gait cycle) between BL4-T1 and BL4-T4 pairs for both legs ($p < 0.05$). Further,

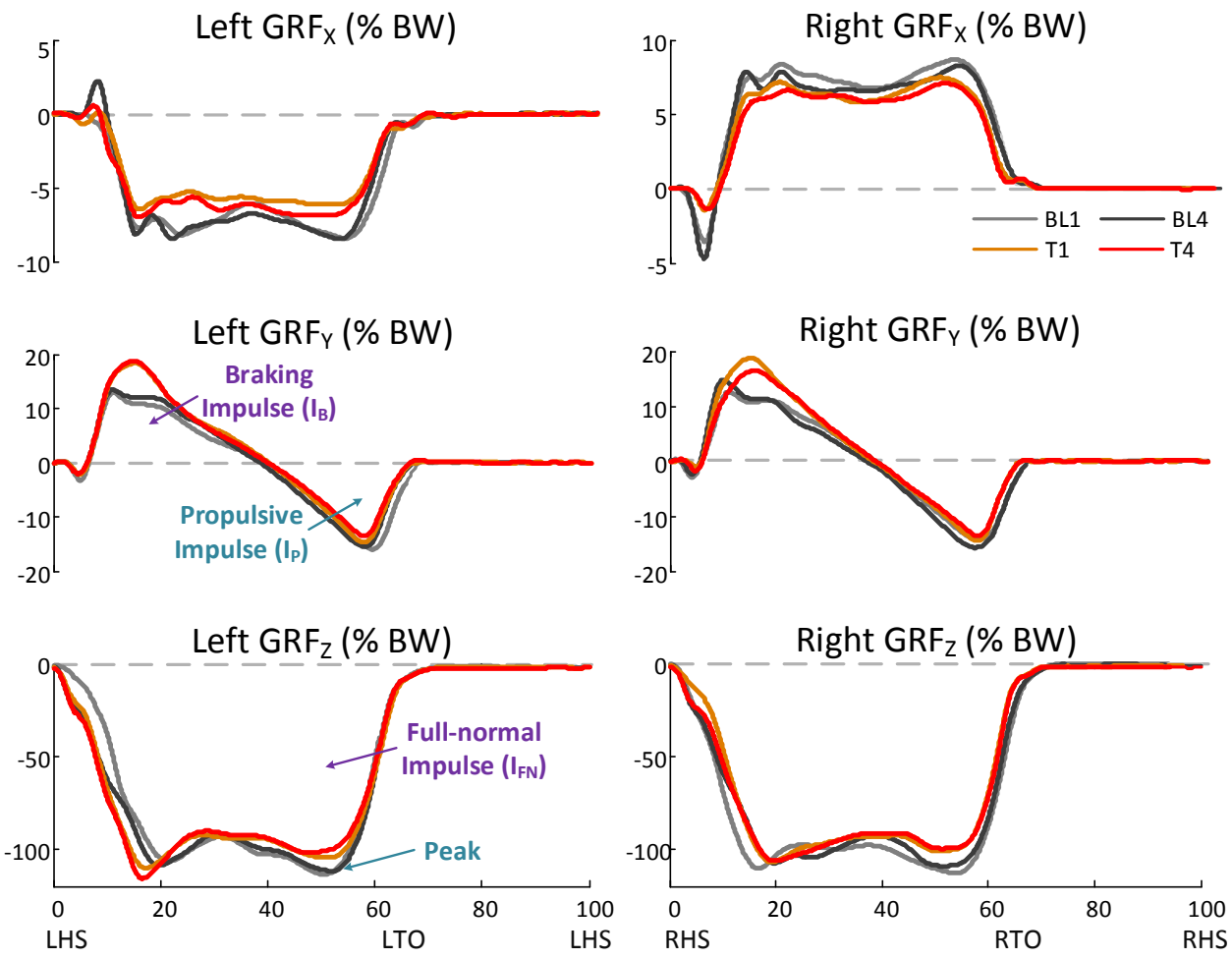

Figure 6.7: Weight normalized ground reaction force components in the medio-lateral (GRF_X), anterior-posterior (GRF_Y), and vertical (GRF_Z) directions are shown for a representative subject during different trials of the experiment.

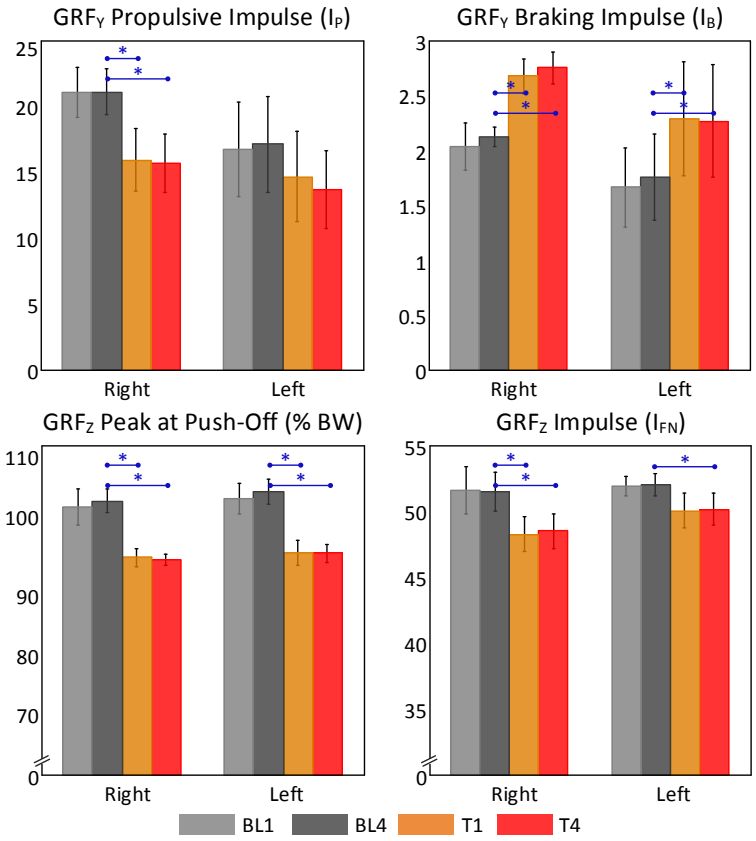

Figure 6.8: The time integral of positive GRF_Y values (I_B, braking impulse) and time integral of negative GRF_Y values (I_P, propulsive impulse), and the peak and time integral of GRF_Z values during a gait cycle are presented for the group. Significant changes were observed between BL-T1 and BL-T4 for the right leg's A-P propulsive and braking impulse, and vertical peak and normal impulse values. In addition, significant changes were observed between BL-T1 and BL-T4 for the left leg's A-P propulsive impulse, and vertical peak and normal impulse values.

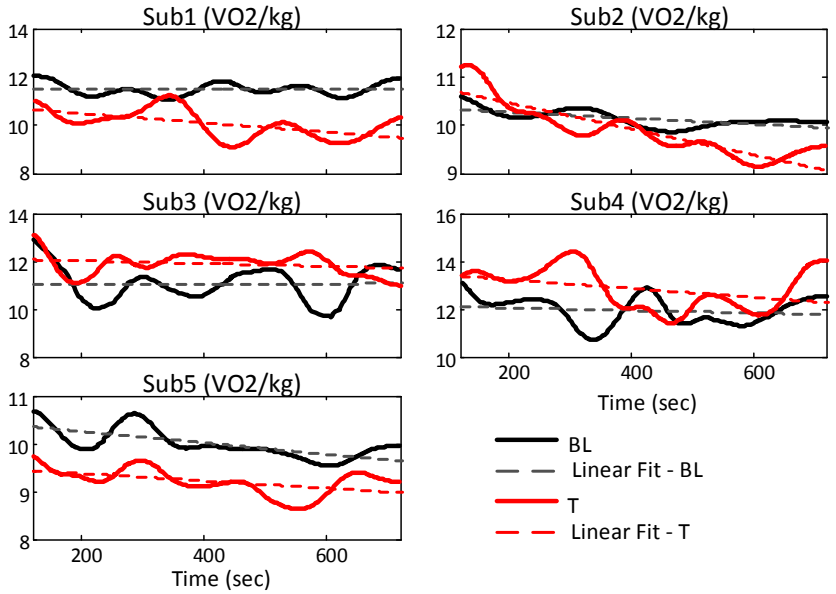

Figure 6.9: Weight normalized volumetric oxygen consumption rate (VO2/kg) for each subject over the ten minutes of the baseline and training sessions. The data were fitted linearly to qualitatively analyze the trend within a session.

the GRF_X peak and impulse values were also calculated during the experiment, but no pairwise statistical significance was reported in the GRF_X values.

The weight normalized volumetric oxygen consumption rates (VO2/kg) are presented in Fig. 6.9 for each subject over the ten minutes of the baseline and training sessions. Lower VO2 consumption values were observed for subjects 1, 2, and 5 during the training session. A linear fit model was used for the VO2/kg data during a session as shown in Fig. 6.9. A decreasing VO2 consumption rate was observed for all subjects as the training with external forces applied to the pelvis progressed. The average VO2/kg values for each subject during the first minute, last minute, and over the full ten

Table 6.1: Weight normalized volumetric oxygen consumption rate (VO2/kg) for each subject.

	Avg. VO2/kg								**Avg. HR**	
	Full trial		1^{st} min		10^{th} min		Peak		Full trial	
	BL	**T**	**BL**	**T**	**BL**	**T**	**BL**	**T**	**BL**	**T**
Sub 1	11.48	10.06	11.85	10.56	11.74	9.98	11.97	11.10	83.23	83.18
Sub 2	10.13	9.87	10.43	11.04	10.07	9.50	10.58	11.15	88.55	87.68
Sub 3	11.05	11.90	12.18	12.12	11.77	11.20	12.60	12.81	101.37	103.67
Sub 4	11.94	12.81	12.45	13.48	12.44	13.67	13.05	14.30	111.46	111.24
Sub 5	9.99	9.21	10.38	9.49	9.92	9.27	10.60	9.65	91.55	86.33
Group Avg.	10.92	10.77	11.46	11.34	11.19	10.72	11.76	11.80	95.23	94.52
Group Std.	0.77	1.43	0.90	1.30	1.01	1.87	1.08	1.53	12.73	13.21

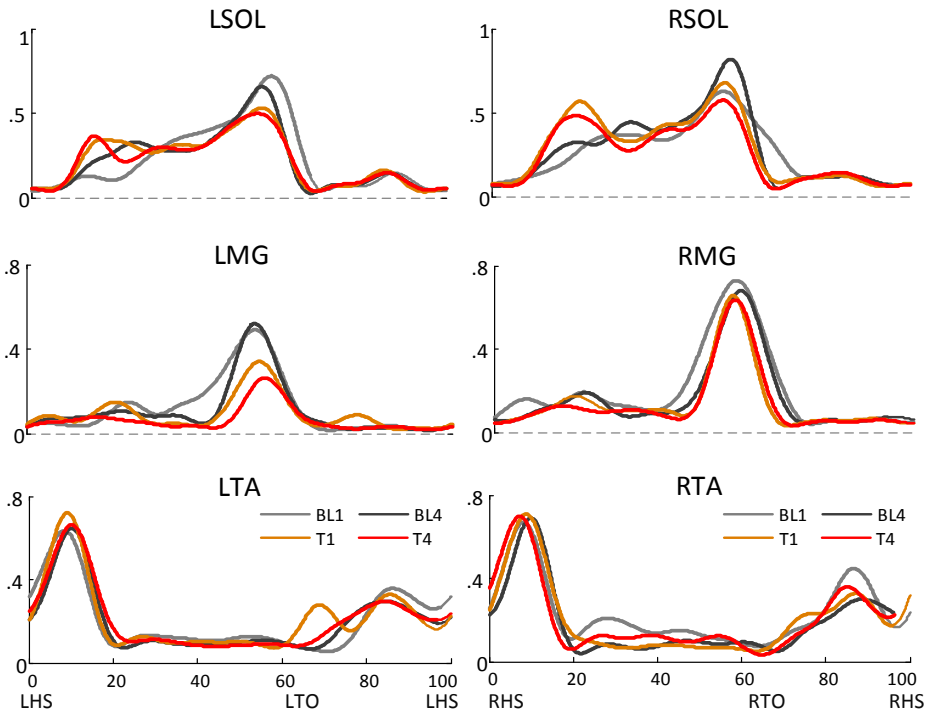

Figure 6.10: Left and right lower limb EMG envelopes during different experimental trials for a representative subject.

minutes are presented in Table 6.1. The group average of these values during the training session were lower than the baseline values. In addition, the peak VO2/kg consumption rate and HR values are also presented in Table for 6.1. The group average of HR values was also reduced during the training session. In particular, VO2 consumption rate and HR values for subjects 1, 2, and 5 decreased in presence of external forces but increased for subjects 3 and 4. Due to these differences in individual subject response to the force training, statistical significance was not observed when the group data were compared between the baseline and training sessions.

The lower limb EMG envelopes are plotted for a represented subject in Fig. 6.10 during different trials of the experiment. Lower SOL activities were reported during the training trials, T1 and T4, compared to the baseline activation levels for both legs. In addition, the activation level of MG was reduced for both legs during the training trials. However, the TA activities during the training trials T1 and T4 were observed to be higher than the baseline activation levels for both legs. The peak activation level during the major burst of a muscle and the RMS values of the lower limb muscles are presented in Fig. 6.11 over the group. Lower peak and RMS values were observed during the training trials for the SOL and MG of each leg. The statistical analysis reported significance

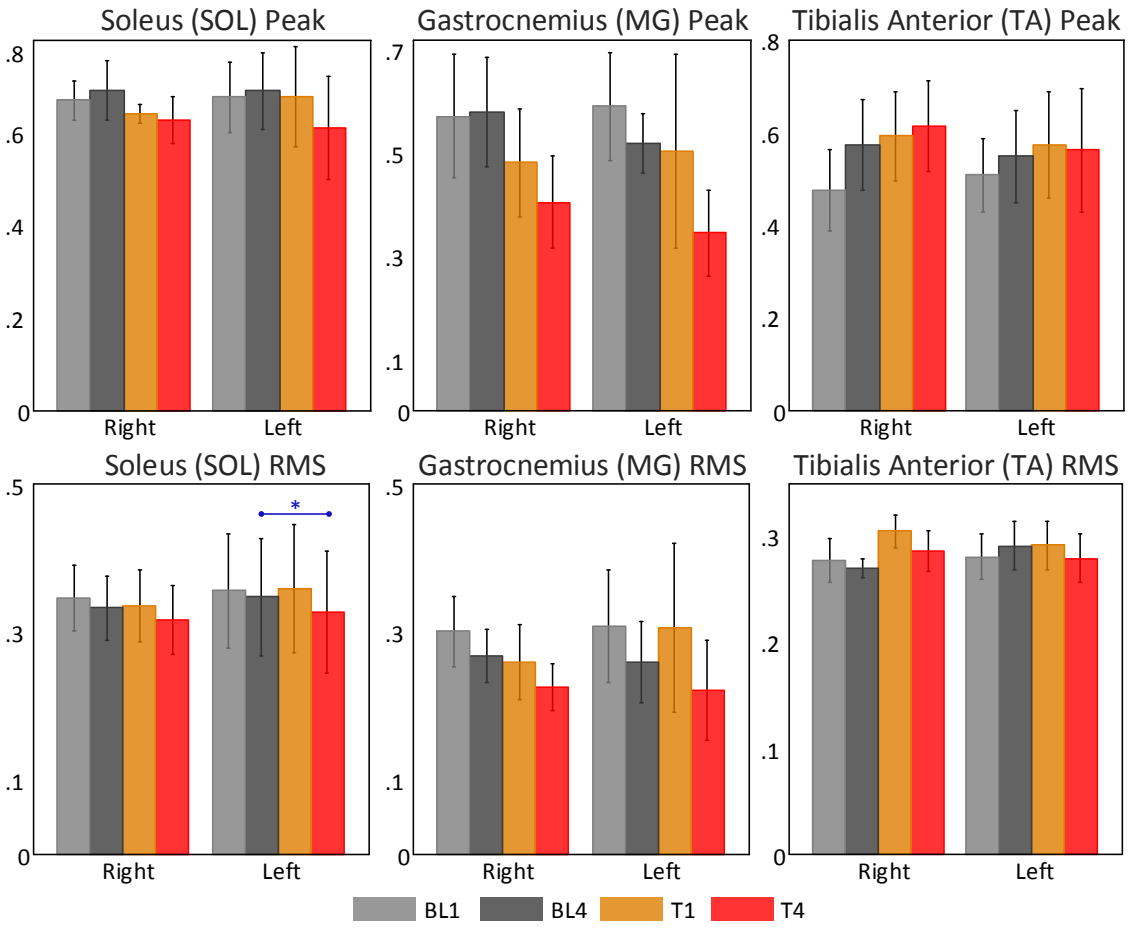

Figure 6.11: Left and right limb muscles peak and RMS values during the major burst over different trials of the experiment. Lower SOL and MG values were reported during the training trials. Statistical significance was observed between BL4 and T4 for left SOL RMS values. The peak and RMS values for TA were observed to be higher during the traininig session.

for left leg SOL RMS values and right leg MG peak values ($p < 0.05$). The post-hoc pairwise comparison reported significant difference only between BL4-T4 trials for left leg SOL RMS values. No statistical significance was reported for the changes in the TA peak and RMS values over the group.

6.5 Discussion and Conclusion

There is a great emphasis in the community to develop assistive devices for restoring the walking performances of individuals with lower limb impairments, such as lower limb amputees and elderly people. Recent technological advances have provided novel light weight passive and active force generating elements that can be used in parallel with human legs or to make up for a lost limb [94–104]. Despite these developments, very few of these efforts have shown improvement in metabolic cost of walking when compared to a condition of using a conventional device [94,96]. One potential reason for this is that humans adapt their walking pattern under different external conditions. The addition of external systems to apply forces at lower limbs modify the human walking dynamics, in particular due to the added mass on the leg and mismatch in timing when the external forces are applied [95,101,102].

Numerous efforts have been put in the community to understand the combined behavior of human-robot dynamics, such as inverted pendulum walking models, simulated prosthetic experiments with healthy individuals [91–93,95,102,105]. In the current work, we proposed a novel approach to understand the role of an external force intervention in altering human walking effort. A control methodology was developed to apply gait synchronized external forces at the pelvis. Due to the proximity of the pelvis segment to the body's COM during walking, the applied external forces assisted the trailing leg during the double support (DS) phase for forward propulsion and during the single support (SS) phase for vertical deceleration of the body's COM.

The current work has the advantage of using a cable-driven robot which does not add external mass and inertia on the user and does not add external mobility constraints. The force vector profile used during the experiment was selected to mimic the human biological effort during walking. The vertical component of the applied force vector in the current work was activated to assist the trailing leg during the weight transition on to the leading leg by decelerating the vertical fall of the

pelvis [93, 102]. Similarly, the anterior-posterior component of the applied force was used to propel the pelvis forward at push-off [93, 101, 105]. Thus, the vertical GRF values and the propulsive effort, calculated from the anterior-posterior GRF values during the late stance phase, of the trailing leg reduced. These changes in the GRF values were also reflected in the shank muscle activation levels, Gastrocnemius, MG, and Soleus, SOL, activities decreased in the presence of the applied force vector.

The changes in the metabolic cost of walking were not significant in the current study, and only three out of five subjects showed reduced volumetric oxygen consumption rate and heart rate values. This was because the applied force intervention was selected to reduce the trailing leg's walking effort. The applied forces did not assist the leading leg which performs negative work just after the heel strike [92, 93, 95, 105], denoted as the braking effort. In the current study, the braking effort, calculated from the anterior-posterior GRF values during the early stance phase, of the leading leg increased in presence of the applied force intervention.

The main goal of walking is to propel the COM forward while maintaining stability [32], therefore, an external intervention that directly alters the COM dynamics can provide better understanding for designing exoskeletons and prosthetic devices to reduce the overall walking effort. For example, in the current work, external forces were applied to assist the trailing leg during the step to step transition. This represents individuals having weaker ankle joints who demonstrate abnormal push-off effort from the trailing leg. As both the setup and methodology developed in this work are flexible to provide new force modalities, we can modify the current intervention to identify magnitude and actuation time of external forces that might be needed to assist these individuals. Similarly, for an individual needing assistance while braking the COM with the leading leg, current force intervention can be extended to include external forces that provide assistance to the leading leg.

Part IV

Conclusion

Chapter 7

Conclusion

7.1 Contributions of the Current Work

This dissertation presented the motivation, scientific and technical challenges, prototype design, algorithms, and simulations of a novel cable-driven pelvic robot. Experiments with healthy individuals and stroke patients using the cable-driven robot were also presented. The major contributions of this dissertation are summarized in the following sections.

7.1.1 Development of a Cable-Driven Pelvic Robot

The technological contribution of this work is the development of a novel cable-driven pelvic robot, the Active Tethered Pelvic Assist Device (A-TPAD). Unlike current use of cable systems as a body-weight support during gait rehabilitation, the A-TPAD can apply a controlled external wrench at the pelvic level in any direction and at any point during a gait cycle for a specified duration. The A-TPAD is a modular cable robot, and its design allows the flexibility to choose the number of motors and their placements to achieve different cable configurations to apply desired external wrench to the pelvis. Being a cable-driven system, the A-TPAD does not add undesirable mass/inertia on the user or does not undesirably constrain the human motion. In contrast, the robotic exoskeletons using rigid link members for actuation can affect human walking dynamics, as these do not actuate all lower limb degrees-of-freedom (DOFs) and also add external mass/inertia on the user. In addition, the A-TPAD can apply external interventions both during the swing phase and stance phase of a gait cycle as opposed to robotic exoskeletons, which typically apply the external forces

on the legs only during the swing phase.

During walking with the A-TPAD, the human motion is monitored in real-time using a motion capture system to calculate the desired external wrench values. An online optimization scheme is used to compute the desired cable tension values to be applied. This control methodology allows the A-TPAD to provide a subject's gait specific force intervention. Thus, the A-TPAD provides a technological platform to scientifically study human adaptation in gait due to externally applied forces and moments on the pelvis. These studies can help motivate new gait paradigms that can potentially be used to correct gait deficits in human walking.

7.1.2 Stance Phase Interventions

In this work, we developed motor adaptation approaches to gait rehabilitation through stance phase interventions. The applied force interventions modified the gait requirements while walking and drove the human CNS to make corrections to minimize the induced errors by modifying the motor commands. During these interventions, external forces were applied to the pelvis. The vertical force component provided an external downward force on the pelvis to provide increased weight bearing during walking. In addition, the anterior-posterior force component applied at the pelvis promoted longer stance periods along a leg. Sufficient weight bearing and limb support periods are very critical during walking, and are effectively accomplished during a healthy individuals walking. However, due to lack of muscle power and control, individuals with neural impairments, such as hemiparetic stroke patients, are unable to bear weight during the affected limb stance phase. This inability results in gait asymmetry, higher energetics, and risks of falls among other compensatory adaptations.

In Chapter 4, we presented experiments with healthy individuals. It was reported that healthy subjects adapt their gait kinematics and gait kinetics as a result of the applied force intervention. In addition, due to the anterior-posterior force component, the healthy subjects temporarily adapt an asymmetric gait with longer right stance duration compared to their baseline walking pattern after the removal of the force vector. In Chapter 5, a single-session study with hemiparetic stroke patients was reported. It was reported that hemipartic patients improved their gait performance in response to the applied stance phase intervention. We believe that stance phase interventions are critical for gait rehabilitation. During steady-state walking, the movement of lower limbs is

achieved through cyclic activation of leg muscles. These muscle activations generate joint torques which are in response to the net external forces on the body, gravitational and ground reaction forces (GRF). Therefore, an intervention that targets the asymmetry in kinetic variables, such as limited weight bearing, could have the potential to show overall gait improvements. In this regard, our presented force based training paradigms that target weight bearing during walking and promote longer stance duration of the targeted leg are novel contributions.

7.1.3 Gait Rehabilitation

In this work, we successfully conducted a single-session experiment with hemiparetic stroke patients. It was observed that the asymmetric weight bearing gait training used during the experiment resulted in improved ground reaction force symmetry, forward propulsion effort, and stance phase symmetry for these patients. This study provides sufficient evidence for extending the developed stance phase intervention to multi-session study to provide long-term gait improvements in hemiparetic stroke patients. We believe training with such interventions, where force magnitude can be regulated, when done in multiple sessions can show improvements in weight bearing capability with positive effects on gait symmetry and walking speed. In addition, the weight bearing stance phase gait interventions could also be useful for other neurologically impaired individuals. In particular, cerebral palsy children can benefit from this intervention.

7.1.4 Walking Effort Study

In this work, the A-TPAD was also used to develop an external gait synchronized force intervention to assist the trailing leg during the forward propulsion and vertical deceleration of the body. An adaptive frequency oscillator scheme was developed to adapt the timing of force actuation to the gait frequency during walking. In Chapter 6, an experiment with healthy subjects was reported. The results of the human experiment showed that in the presence of the applied force intervention the subjects reduced their walking effort during the late stance phase. We believe that studies conducted with the presented setup and control methodolgy can provide better understanding in designing assistive devices for individuals who spend higher than normal effort during walking.

7.2 Suggestions for the Future Work

The single-session study reported in Chapter 5 with the hemiparetic stroke patients provided sufficient evidence to further extend the paradigm to multiple sessions. Thus, the immediate future work would be to conduct a multi-session study with the hemiparetic stroke patients to investigate the long-term gait benefits of the asymmetric weight bearing during walking. In addition, visual feedback during gait training has been used in gait rehabilitation to promote active participation of the user in the training. Thus, we believe that there is a merit in conducting experiments to identify an appropriate gait measure to provide visual feedback while force training with the A-TPAD to further enhance the training effects.

In the gait rehabilitation literature, audio inputs have also been identified as a reliable measure to provide feedback to motivate users to synchronize the gait frequency. During the force training with the A-TPAD, similar interventions can be tested to promote symmetry between the affected and unaffected stance phase periods. In addition, to target the single support phase of the affected stance phase, a split-belt treadmill can be used to create a speed asymmetry between the legs. With the affected leg on the slower belt, subjects would spent more time in the affected single support phase. We believe the integration of split-belt treadmill and proposed stance phase intervention can provide improved gait adaptation in hemiparetic stroke patients.

In the various studies conducted as part of this work, the cables in the A-TPAD were attached to the human pelvis to provide the desired external force intervention. With the modular A-TPAD design, the cables can also be routed to control lower limb segments. Such cable configurations can be used to apply forces at lower limbs to assist the user in executing lower limb movements. In addition, the A-TPAD can be combined with other lower limb devices to further extend its usability. One appropriate choice would be to use the cable-driven active leg exoskeleton (C-ALEX) currently under study in the Robotics and Rehabilitation (ROAR) laboratory at the Columbia University.

In a separate study [110], the capability of the A-TPAD to apply controlled forces at the pelvis which are synchronized with the gait events was used to develop a perturbation experiment for healthy individuals. The goal of this experiment was to study the pro-active and reactive balancing strategies adapted by healthy individuals in response to the unexpected perturbations. This study provided unique application of the A-TPAD to provide balance training to elders with fall histories.

There is a need to conduct a long-term study with elderly people to explore the potential benefits of the perturbation based balance training. In future, the A-TPAD can also be combined with a virtual reality system to provide an immersive environment to the user. With this capability, the A-TPAD can be used to develop experimental paradigms mimicking real-life perturbations for training elderly people with fall histories.

Another application of the A-TPAD is to use it as a tool to understand the human walking dynamics. In the current work, we conducted various experiments with healthy individuals to explore the gait kinematics and kinetics adaptation when controlled external forces were applied at the pelvic level. In Chapter 6, we also reported an experiment to study changes in the walking effort when external forces were applied for a short duration during a section of the gait cycle. Similar studies can be conducted using the A-TPAD to study and identify the optimal force magnitudes and timings required to reduce the metabolic cost. Such knowledge can greatly benefit the design and control strategies to develop assitive devices to improve human performance during walking.

Part V

Bibliography

Bibliography

[1] Manual walker. http://www.medicaleshop.com/arjohuntleigh-hydraulic-lift-walker-manual.html.

[2] Body weight support system. https://www.youtube.com/watch?v=nGorMPmDaGQ.

[3] S.K. Banala, S.H. Kim, S.K. Agrawal, and J.P. Scholz. Robot assisted gait training with active leg exoskeleton (alex). *Neural Systems and Rehabilitation Engineering, IEEE Transactions on*, 17(1):2–8, 2009.

[4] Jan F Veneman, Rik Kruidhof, Edsko EG Hekman, Ralf Ekkelenkamp, Edwin HF Van Asseldonk, and Herman Van Der Kooij. Design and evaluation of the lopes exoskeleton robot for interactive gait rehabilitation. *Neural Systems and Rehabilitation Engineering, IEEE Transactions on*, 15(3):379–386, 2007.

[5] Sašo Jezernik, Gery Colombo, and Manfred Morari. Automatic gait-pattern adaptation algorithms for rehabilitation with a 4-dof robotic orthosis. *Robotics and Automation, IEEE Transactions on*, 20(3):574–582, 2004.

[6] Paul Stegall, Kyle Winfree, Damiano Zanotto, and Sunil Kumar Agrawal. Rehabilitation exoskeleton design: Exploring the effect of the anterior lunge degree of freedom. *Robotics, IEEE Transactions on*, 29(4):838–846, 2013.

[7] Damiano Zanotto, Paul Stegall, and Sunil Kumar Agrawal. Alex iii: A novel robotic platform with 12 dofs for human gait training. In *Robotics and Automation (ICRA), 2013 IEEE International Conference on*, pages 3914–3919. IEEE, 2013.

[8] D. Aoyagi, W.E. Ichinose, S.J. Harkema, D.J. Reinkensmeyer, and J.E. Bobrow. A robot and control algorithm that can synchronously assist in naturalistic motion during body-weight-supported gait training following neurologic injury. *Neural Systems and Rehabilitation Engineering, IEEE Transactions on*, 15(3):387–400, 2007.

[9] Yves Stauffer, Yves Allemand, Mohamed Bouri, Jacques Fournier, Reymond Clavel, Patrick Metrailler, Roland Brodard, and Fabienne Reynard. Pelvic motion measurement during over ground walking, analysis and implementation on the walktrainer reeducation device. In *Intelligent Robots and Systems, 2008. IROS 2008. IEEE/RSJ International Conference on*, pages 2362–2367. IEEE, 2008.

[10] M. Peshkin, D.A. Brown, J.J. Santos-Munné, A. Makhlin, E. Lewis, J.E. Colgate, J. Patton, and D. Schwandt. Kineassist: A robotic overground gait and balance training device. In *Rehabilitation Robotics, 2005. ICORR 2005. 9th International Conference on*, pages 241–246. IEEE, 2005.

[11] Trieu Phat Luu, Kin Huat Low, Xingda Qu, Hup Boon Lim, and Kay Hiang Hoon. Hardware development and locomotion control strategy for an over-ground gait trainer: Nature-gaits. *Translational Engineering in Health and Medicine, IEEE Journal of*, 2:1–9, 2014.

[12] James Albus, Roger Bostelman, and Nicholas Dagalakis. The nist robocrane. *Journal of Robotic Systems*, 10(5):709–724, 1993.

[13] Lawrence L Cone. Skycam-an aerial robotic camera system. *Byte*, 10(10):122, 1985.

[14] Xiaohua Zhao. *Statics and dynamics simulation of a multi-tethered aerostat system.* PhD thesis, University of Victoria, 2004.

[15] Tetsuya Morizono, Kazuhiro Kurahashi, and Sadao Kawamura. Analysis and control of a force display system driven by parallel wire mechanism. *Robotica*, 16(05):551–563, 1998.

[16] Giulio Rosati, Damiano Zanotto, Riccardo Secoli, and Aldo Rossi. Design and control of two planar cable-driven robots for upper-limb neurorehabilitation. In *Rehabilitation Robotics, 2009. ICORR 2009. IEEE International Conference on*, pages 560–565. IEEE, 2009.

[17] Ludovic Dovat, Olivier Lambercy, Roger Gassert, Thomas Maeder, Ted Milner, Teo Chee Leong, and Etienne Burdet. Handcare: a cable-actuated rehabilitation system to train hand function after stroke. *Neural Systems and Rehabilitation Engineering, IEEE Transactions on*, 16(6):582–591, 2008.

[18] Giulio Rosati, Paolo Gallina, and Stefano Masiero. Design, implementation and clinical tests of a wire-based robot for neurorehabilitation. *Neural Systems and Rehabilitation Engineering, IEEE Transactions on*, 15(4):560–569, 2007.

[19] Ying Mao and Sunil Kumar Agrawal. Design of a cable-driven arm exoskeleton (carex) for neural rehabilitation. *Robotics, IEEE Transactions on*, 28(4):922–931, 2012.

[20] Dragoljub Surdilovic, Jinyu Zhang, and Rolf Bernhardt. String-man: Wire-robot technology for safe, flexible and human-friendly gait rehabilitation. In *Rehabilitation Robotics, 2007. ICORR 2007. IEEE 10th International Conference on*, pages 446–453. IEEE, 2007.

[21] H Vallery, P Lutz, J Von Zitzewitz, G Rauter, M Fritschi, Christophe Everarts, Renaud Ronsse, A Curt, and M Bolliger. Multidirectional transparent support for overground gait training. In *Rehabilitation Robotics (ICORR), 2013 IEEE International Conference on*, pages 1–7. IEEE, 2013.

[22] S.C. Yen, B.D. Schmit, J.M. Landry, H. Roth, and M. Wu. Locomotor adaptation to resistance during treadmill training transfers to overground walking in human sci. *Experimental brain research*, pages 1–10, 2012.

[23] Vineet Vashista, Darcy S Reisman, and Sunil K Agrawal. Asymmetric adaptation in human walking using the tethered pelvic assist device (tpad). In *Rehabilitation Robotics (ICORR), 2013 IEEE International Conference on*, pages 1–5. IEEE, 2013.

[24] Vineet Vashista, Neelima Agrawal, S Shaharudin, DS Reisman, and Sunil K Agrawal. Force adaptation in human walking with symmetrically applied downward forces on the pelvis. In *Engineering in Medicine and Biology Society (EMBC), 2012 Annual International Conference of the IEEE*, pages 3312–3315. IEEE, 2012.

[25] Vineet Vashista, Neelima Agrawal, Shazlin Shaharudin, Darcy S Reisman, and Sunil K Agrawal. Force adaptation in human walking with symmetrically applied downward forces on the pelvis. *Neural Systems and Rehabilitation Engineering, IEEE Transactions on*, 21(6):969–978, 2013.

[26] Vineet Vashista, Xin Jin, and Sunil K Agrawal. Active tethered pelvic assist device (a-tpad) to study force adaptation in human walking. In *Robotics and Automation (ICRA), 2014 IEEE International Conference on*, pages 718–723. IEEE, 2014.

[27] Vineet Vashista and Sunil K Agrawal. A cable-driven pelvic robot to study human adaptation in gait due to externally applied forces. *Robotics, IEEE Transactions on*, -(-):–, -.

[28] Vineet Vashista, Dario Martelli, and Sunil K Agrawal. Locomotor adaptation to an asymmetric force on the human pelvis directed along the right leg. *Neural Systems and Rehabilitation Engineering, IEEE Transactions on*, -(-):–, 2015.

[29] Véronique L Roger, Alan S Go, Donald M Lloyd-Jones, Emelia J Benjamin, Jarett D Berry, William B Borden, Dawn M Bravata, Shifan Dai, Earl S Ford, Caroline S Fox, et al. Heart disease and stroke statistics2012 update a report from the american heart association. *Circulation*, 125(1):e2–e220, 2012.

[30] Michael Bernhard, André Gries, Paul Kremer, and Bernd W Böttiger. Spinal cord injury (sci)prehospital management. *Resuscitation*, 66(2):127–139, 2005.

[31] The united cerebral palsy 2011. http://ucp.org/.

[32] J. Perry, J.R. Davids, et al. Gait analysis: normal and pathological function. *Journal of Pediatric Orthopaedics*, 12(6):815, 1992.

[33] Christopher L Vaughan. Are joint torques the holy grail of human gait analysis? *Human Movement Science*, 15(3):423–443, 1996.

[34] Vivian Weerdesteyn, Mark de Niet, HJ Van Duijnhoven, A Cho, and MD Geurts. Falls in individuals with stroke. *differences*, 33:36, 2008.

[35] S.J. Olney and C. Richards. Hemiparetic gait following stroke. part i: Characteristics. *Gait & Posture*, 4(2):136–148, 1996.

[36] Jacquelin Perry. The mechanics of walking in hemiplegia. *Clinical orthopaedics and related research*, 63:23–31, 1969.

[37] Sandra J Olney, Patrick A Costigan, and Douglas M Hedden. Mechanical energy patterns in gait of cerebral palsied children with hemiplegia. *Physical therapy*, 67(9):1348–1354, 1987.

[38] Andrea L Behrman and Susan J Harkema. Locomotor training after human spinal cord injury: a series of case studies. *Physical Therapy*, 80(7):688–700, 2000.

[39] Kara K Patterson, Iwona Parafianowicz, Cynthia J Danells, Valerie Closson, Mary C Verrier, W Richard Staines, Sandra E Black, and William E McIlroy. Gait asymmetry in community-ambulating stroke survivors. *Archives of physical medicine and rehabilitation*, 89(2):304–310, 2008.

[40] C Maria Kim and Janice J Eng. Symmetry in vertical ground reaction force is accompanied by symmetry in temporal but not distance variables of gait in persons with stroke. *Gait & posture*, 18(1):23–28, 2003.

[41] P1 Zamparo, MP Francescato, G Luca, L Lovati, and PE Prampera. The energy cost of level walking in patients with hemiplegia. *Scandinavian journal of medicine & science in sports*, 5(6):348–352, 1995.

[42] Henning Stolze, Stephan Klebe, Christiane Zechlin, Christoph Baecker, Lars Friege, and Günther Deuschl. Falls in frequent neurological diseases. *Journal of neurology*, 251(1):79–84, 2004.

[43] Sarah J Mattes, Philip E Martin, and Todd D Royer. Walking symmetry and energy cost in persons with unilateral transtibial amputations: matching prosthetic and intact limb inertial properties. *Archives of physical medicine and rehabilitation*, 81(5):561–568, 2000.

[44] H Barbeau, M Wainberg, and L Finch. Description and application of a system for locomotor rehabilitation. *Medical and Biological Engineering and Computing*, 25(3):341–344, 1987.

[45] Alexander Duschau-Wicke, Joachim von Zitzewitz, Andrea Caprez, Lars Lunenburger, and Robert Riener. Path control: a method for patient-cooperative robot-aided gait rehabilitation. *Neural Systems and Rehabilitation Engineering, IEEE Transactions on*, 18(1):38–48, 2010.

[46] H Kazerooni and R Steger. The berkeley lower extremity exoskeleton. *Journal of dynamic systems, measurement, and control*, 128(1):14–25, 2006.

[47] Conor James Walsh, Ken Endo, and Hugh Herr. A quasi-passive leg exoskeleton for load-carrying augmentation. *International Journal of Humanoid Robotics*, 4(03):487–506, 2007.

[48] Hiroaki Kawamoto, Suwoong Lee, Shigehiro Kanbe, and Yoshihuki Sankai. Power assist method for hal-3 using emg-based feedback controller. In *Systems, Man and Cybernetics, 2003. IEEE International Conference on*, volume 2, pages 1648–1653. IEEE, 2003.

[49] T George Hornby, Donielle D Campbell, Jennifer H Kahn, Tobey Demott, Jennifer L Moore, and Heidi R Roth. Enhanced gait-related improvements after therapist-versus robotic-assisted locomotor training in subjects with chronic stroke a randomized controlled study. *Stroke*, 39(6):1786–1792, 2008.

[50] Ruth Dickstein. Rehabilitation of gait speed after stroke: a critical review of intervention approaches. *Neurorehabilitation and neural repair*, 2008.

[51] Joseph Hidler, Diane Nichols, Marlena Pelliccio, Kathy Brady, Donielle D Campbell, Jennifer H Kahn, and T George Hornby. Multicenter randomized clinical trial evaluating the effectiveness of the lokomat in subacute stroke. *Neurorehabilitation and Neural Repair*, 23(1):5–13, 2009.

[52] Chandramouli Krishnan, Rajiv Ranganathan, Yasin Y Dhaher, and William Z Rymer. A pilot study on the feasibility of robot-aided leg motor training to facilitate active participation. *PloS one*, 8(10):e77370, 2013.

[53] Jos H Meuleman, Edwin HF Van Asseldonk, and Herman Van der Kooij. The effect of directional inertias added to pelvis and ankle on gait. *Journal of neuroengineering and rehabilitation*, 10(40):1–12, 2013.

[54] C.J. Arellano, D.P. O'Connor, C. Layne, and M.J. Kurz. The independent effect of added mass on the stability of the sagittal plane leg kinematics during steady-state human walking. *Journal of Experimental Biology*, 212(12):1965–1970, 2009.

[55] Damiano Zanotto, Tommaso Lenzi, Paul Stegall, and Sunil K Agrawal. Improving transparency of powered exoskeletons using force/torque sensors on the supporting cuffs. In *Rehabilitation Robotics (ICORR), 2013 IEEE International Conference on*, pages 1–6. IEEE, 2013.

[56] W van Dijk, H Van Der Kooij, B Koopman, and EHF van Asseldonk. Improving the transparency of a rehabilitation robot by exploiting the cyclic behaviour of walking. In *Rehabilitation Robotics (ICORR), 2013 IEEE International Conference on*, pages 1–8. IEEE, 2013.

[57] Benefits Booklet, GI Bill, Life Insurance, Traumatic Injury Insurance, Refill Prescriptions, Crisis Prevention, Markers Headstones, Medallions Presidential Memorial Certificates, Nationwide Gravesite Locator, Burial Flags, et al. Zerog: Overground gait and balance training system. 2011.

[58] Devdas Shetty, Avital Fast, and Claudio Campana. Ambulatory suspension and rehabilitation apparatus, December 9 2008. US Patent 7,462,138.

[59] Takao Watanabe, Yo Kobayashi, and Masakatsu G Fujie. Pelvis motion analysis for gait phase estimation toward leg-dependent body weight support at different walking speed. In *Engineering in Medicine and Biology Society, EMBC, 2011 Annual International Conference of the IEEE*, pages 1590–1593. IEEE, 2011.

[60] Wiebren Zijlstra and At L Hof. Displacement of the pelvis during human walking: experimental data and model predictions. *Gait & posture*, 6(3):249–262, 1997.

[61] Peggy R Trueblood, Joan M Walker, Jacquelin Perry, and JoAnne K Gronley. Pelvic exercise and gait in hemiplegia. *Physical Therapy*, 69(1):18–26, 1989.

[62] R.R. Neptune, S.A. Kautz, and F.E. Zajac. Contributions of the individual ankle plantar flexors to support, forward progression and swing initiation during walking. *Journal of Biomechanics*, 34(11):1387 – 1398, 2001.

[63] A. Grabowski, C.T. Farley, and R. Kram. Independent metabolic costs of supporting body weight and accelerating body mass during walking. *Journal of Applied Physiology*, 98(2):579–583, 2005.

[64] C.P. McGowan, R.R. Neptune, and R. Kram. Independent effects of weight and mass on plantar flexor activity during walking: implications for their contributions to body support and forward propulsion. *Journal of applied physiology*, 105(2):486–494, 2008.

[65] Jan F Veneman, Jasper Menger, Edwin HF van Asseldonk, Frans CT van der Helm, and Herman van der Kooij. Fixating the pelvis in the horizontal plane affects gait characteristics. *Gait & posture*, 28(1):157–163, 2008.

[66] JA Zeni, JG Richards, and JS Higginson. Two simple methods for determining gait events during treadmill and overground walking using kinematic data. *Gait & posture*, 27(4):710–714, 2008.

[67] T. Lam, M. Anderschitz, and V. Dietz. Contribution of feedback and feedforward strategies to locomotor adaptations. *Journal of neurophysiology*, 95(2):766–773, 2006.

[68] D.S. Reisman, R. Wityk, K. Silver, and A.J. Bastian. Locomotor adaptation on a split-belt treadmill can improve walking symmetry post-stroke. *Brain*, 130(7):1861–1872, 2007.

[69] Aiguo Ming and Toshiro Higuchi. Study on multiple degree-of-freedom positioning mechanism using wires. i: Concept, design and control. *International Journal of the Japan Society for Precision Engineering*, 28(2):131–138, 1994.

[70] Shabbir Kurbanhusen Mustafa and Sunil Kumar Agrawal. On the force-closure analysis of n-dof cable-driven open chains based on reciprocal screw theory. *Robotics, IEEE Transactions on*, 28(1):22–31, 2012.

[71] So-Ryeok Oh and Sunil Kumar Agrawal. Cable suspended planar robots with redundant cables: controllers with positive tensions. *Robotics, IEEE Transactions on*, 21(3):457–465, 2005.

[72] Andreas Pott. An improved force distribution algorithm for over-constrained cable-driven parallel robots. In *Computational Kinematics*, pages 139–146. Springer, 2014.

[73] Johann Lamaury and Marc Gouttefarde. A tension distribution method with improved computational efficiency. In *Cable-driven parallel robots*, pages 71–85. Springer, 2013.

[74] Tobias Bruckmann, Andreas Pott, and Manfred Hiller. Calculating force distributions for redundantly actuated tendon-based stewart platforms. In *Advances in Robot Kinematics*, pages 403–412. Springer, 2006.

[75] Clément Gosselin and Martin Grenier. On the determination of the force distribution in overconstrained cable-driven parallel mechanisms. *Meccanica*, 46(1):3–15, 2011.

[76] Douglas N Savin, Shih-Chiao Tseng, Jill Whitall, and Susanne M Morton. Poststroke hemiparesis impairs the rate but not magnitude of adaptation of spatial and temporal locomotor features. *Neurorehabilitation and neural repair*, 27(1):24–34, 2013.

[77] Darcy S Reisman, Heather McLean, Jennifer Keller, Kelly A Danks, and Amy J Bastian. Repeated split-belt treadmill training improves poststroke step length asymmetry. *Neurorehabilitation and neural repair*, 27(5):460–468, 2013.

[78] JP Regnaux, D Pradon, N Roche, J Robertson, B Bussel, and B Dobkin. Effects of loading the unaffected limb for one session of locomotor training on laboratory measures of gait in stroke. *Clinical Biomechanics*, 23(6):762–768, 2008.

[79] Gianna M Rodriguez and Alexander S Aruin. The effect of shoe wedges and lifts on symmetry of stance and weight bearing in hemiparetic individuals. *Archives of physical medicine and rehabilitation*, 83(4):478–482, 2002.

[80] Panagiotis V Tsaklis, Wilhelmus JA Grooten, and Erika Franzén. Effects of weight-shift training on balance control and weight distribution in chronic stroke: a pilot study. *Topics in stroke rehabilitation*, 19(1):23–31, 2012.

[81] A Gabell and USL Nayak. The effect of age on variability in gait. *Journal of Gerontology*, 39(6):662–666, 1984.

[82] TA Martin, JG Keating, HP Goodkin, AJ Bastian, and WT Thach. Throwing while looking through prisms ii. specificity and storage of multiple gazethrow calibrations. *Brain*, 119(4):1199–1211, 1996.

[83] A.J. Bastian. Understanding sensorimotor adaptation and learning for rehabilitation. *Current opinion in neurology*, 21(6):628, 2008.

[84] Chris A McGibbon. Toward a better understanding of gait changes with age and disablement: neuromuscular adaptation. *Exercise and sport sciences reviews*, 31(2):102–108, 2003.

[85] A. Houldin, K. Luttin, and T. Lam. Locomotor adaptations and aftereffects to resistance during walking in individuals with spinal cord injury. *Journal of Neurophysiology*, 106(1):247–258, 2011.

[86] National stroke association. http://www.stroke.org/we-can-help/survivors/stroke-recovery/post-stroke-conditions/physical/hemiparesis.

[87] Lindsey J Turns, Richard R Neptune, and Steven A Kautz. Relationships between muscle activity and anteroposterior ground reaction forces in hemiparetic walking. *Archives of physical medicine and rehabilitation*, 88(9):1127–1135, 2007.

[88] Mark G Bowden, Chitralakshmi K Balasubramanian, Richard R Neptune, and Steven A Kautz. Anterior-posterior ground reaction forces as a measure of paretic leg contribution in hemiparetic walking. *Stroke*, 37(3):872–876, 2006.

[89] Reza Shadmehr and Ferdinando A Mussa-Ivaldi. Adaptive representation of dynamics during learning of a motor task. *The Journal of Neuroscience*, 14(5):3208–3224, 1994.

[90] J.W. Noble and S.D. Prentice. Adaptation to unilateral change in lower limb mechanical properties during human walking. *Experimental brain research*, 169(4):482–495, 2006.

[91] Tad McGeer. Passive dynamic walking. *the international journal of robotics research*, 9(2):62–82, 1990.

[92] Arthur D Kuo. Energetics of actively powered locomotion using the simplest walking model. *Journal of biomechanical engineering*, 124(1):113–120, 2002.

[93] Arthur D Kuo, J Maxwell Donelan, and Andy Ruina. Energetic consequences of walking like an inverted pendulum: step-to-step transitions. *Exercise and sport sciences reviews*, 33(2):88–97, 2005.

[94] Steven H Collins, M Bruce Wiggin, and Gregory S Sawicki. Reducing the energy cost of human walking using an unpowered exoskeleton. *Nature*, 2015.

[95] Gregory S Sawicki, Cara L Lewis, and Daniel P Ferris. It pays to have a spring in your step. *Exercise and sport sciences reviews*, 37(3):130, 2009.

[96] Hugh M Herr and Alena M Grabowski. Bionic ankle–foot prosthesis normalizes walking gait for persons with leg amputation. *Proceedings of the Royal Society of London B: Biological Sciences*, 279(1728):457–464, 2012.

[97] Steven H Collins, Myunghee Kim, Tianjian Chen, and Tianyao Chen. An ankle-foot prosthesis emulator with control of plantarflexion and inversion-eversion torque. In *Proc. Int. Conf. Rob. Autom*, 2015.

[98] Michael Goldfarb, Brian E Lawson, and Amanda H Shultz. Realizing the promise of robotic leg prostheses. *Science translational medicine*, 5(210):210ps15–210ps15, 2013.

[99] Tommaso Lenzi, L Hargrove, and J Sensinger. Speed-adaptation mechanism: Robotic prostheses can actively regulate joint torque. *Robotics & Automation Magazine, IEEE*, 21(4):94–107, 2014.

[100] Michael Wehner, Brendan Quinlivan, Patrick M Aubin, Ernesto Martinez-Villalpando, Martin Baumann, Leia Stirling, Kenneth Holt, Roger Wood, and Conor Walsh. A lightweight soft exosuit for gait assistance. In *Robotics and Automation (ICRA), 2013 IEEE International Conference on*, pages 3362–3369. IEEE, 2013.

[101] Philippe Malcolm, Wim Derave, Samuel Galle, and Dirk De Clercq. A simple exoskeleton that assists plantarflexion can reduce the metabolic cost of human walking. *PloS one*, 8(2):e56137, 2013.

[102] Joshua M Caputo and Steven H Collins. Prosthetic ankle push-off work reduces metabolic rate but not collision work in non-amputee walking. *Scientific reports*, 4, 2014.

[103] Tommaso Lenzi, Maria Carrozza, and Sunil K Agrawal. Powered hip exoskeletons can reduce the user's hip and ankle muscle activations during walking. *Neural Systems and Rehabilitation Engineering, IEEE Transactions on*, 21(6):938–948, 2013.

[104] Thomas G Sugar, Andrew Bates, Matthew Holgate, Jason Kerestes, Marc Mignolet, Philip New, Ragesh K Ramachandran, Sangram Redkar, and Chase Wheeler. Limit cycles to enhance human performance based on phase oscillators. *Journal of Mechanisms and Robotics*, 7(1):011001, 2015.

[105] Andy Ruina, John EA Bertram, and Manoj Srinivasan. A collisional model of the energetic cost of support work qualitatively explains leg sequencing in walking and galloping, pseudo-elastic leg behavior in running and the walk-to-run transition. *Journal of theoretical biology*, 237(2):170–192, 2005.

[106] Ludovic Righetti, Jonas Buchli, and Auke Jan Ijspeert. Dynamic hebbian learning in adaptive frequency oscillators. *Physica D: Nonlinear Phenomena*, 216(2):269–281, 2006.

[107] Damiano Zanotto, Paul Stegall, and Sunil K Agrawal. Adaptive assist-as-needed controller to improve gait symmetry in robot-assisted gait training. In *Robotics and Automation (ICRA), 2014 IEEE International Conference on*, pages 724–729. IEEE, 2014.

[108] Robert A Robergs, Dan Dwyer, and Todd Astorino. Recommendations for improved data processing from expired gas analysis indirect calorimetry. *Sports Medicine*, 40(2):95–111, 2010.

[109] D.A. Winter. *Biomechanics and motor control of human gait: normal, elderly and pathological*. 1991.

[110] Dario Martelli, Vineet Vashista, Silvestro Micera, and Sunil K Agrawal. Direction-dependent adaptation of dynamic gait stability following waist-pull perturbations. *Neural Systems and Rehabilitation Engineering, IEEE Transactions on*, -(-):–, -.

[111] A.L. Bell, R.A. Brand, and D.R. Pedersen. Prediction of hip joint centre location from external landmarks. *Human Movement Science*, 8(1):3–16, 1989.

[112] Joshua T Weinhandl and Kristian M OConnor. Assessment of a greater trochanter-based method of locating the hip joint center. *Journal of biomechanics*, 43(13):2633–2636, 2010.

[113] Hermie J Hermens, Bart Freriks, Roberto Merletti, Dick Stegeman, Joleen Blok, Günter Rau, Cathy Disselhorst-Klug, and Göran Hägg. European recommendations for surface electromyography. *Roessingh Research and Development*, 8(2):13–54, 1999.

Part VI

Appendix

Appendix A

Gait Cycle and Events

A gait cycle is defined as the time interval between two subsequent foot contacts of one leg. In Fig. A.1, a gait cycle is shown from a right heel strike event (RHS) to subsequent right heel strike. There are two phases of the gait cycle. Stance phase is the part of the cycle when the foot is in contact with the ground. It comprises 62% of the cycle, beginning with initial foot strike and ending with toe-off, RHS to RTO or LHS to LTO. Swing phase occurs when the foot is in the air and comprises 38% of the cycle, beginning with toe-off and ending with second (ipsilateral) foot strike, RTO to RHS or LTO to LHS.

Each stance phase further includes two double support (DS) and one single support (SS) phases, as shown in Fig. A.1. Thus, a gait cycle can further be divided into four periods.

- Initial Double Support (iDS - 0-12% of gait cycle): This phase begins with the first foot strike

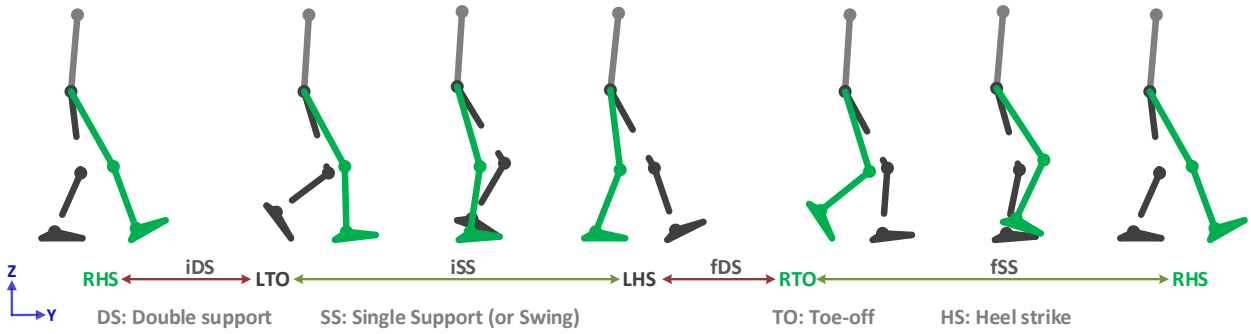

Figure A.1: A gait cycle is shown from a right leg heel strike event, RHS, to subsequent right leg heel strike. The left leg gait events as well as the double and single support gait phases are indicated.

and ends with the opposite foot's toe-off.

- Initial Single Support (iSS - 12-50% of gait cycle): This phase begins with the opposite toe-off and ends with opposite foot strike.
- Final Double Support (fDS - 50-62% of gait cycle): This phase begins with opposite foot strike and ends with first leg's toe-off.
- Final Single Support (fSS - 62-100% of gait cycle): This phase begins with first leg's toe-off and ends with the subsequent first leg's foot strike.

A stance phase therefore comprises iDS, iSS, and fDS, and a swing phase comprises fSS. In Fig. A.1, these phases are defined in terms of a right leg gait cycle. Notably, these phases can similarly be defined in terms of a left leg gait cycle.

Appendix B

Lower Limb Frame Assignments

Human anatomy is defined using three anatomical planes as described in Fig. B.1.

- Sagittal plane: The sagittal plane divides the body into right and left sides.
- Transverse plane: The transverse plane divides the body horizontally into upper and lower portions. Transverse plane is also called as a horizontal plane.
- Coronal plane: The coronal plane divides the body into an anterior (front) portion and a posterior (rear) portion. The coronal plane is also called as a frontal plane.

Along these body anatomical planes, body segments are further referred using three anatomical axes, as shown in Fig. B.1.

- Anterior-posterior: it lies in the sagittal plane and describes segments at the front (anterior) and back (posterior) of the body. For example, the ankle is anterior to the pelvis at foot strike event during walking.
- Superior-inferior: it lies in the coronal plane and describes a position above (superior) or below (inferior) another part of the body. For example, the pelvis is superior to the foots but inferior to the abdomen.
- Medial-lateral: it lies in the transverse plane and describes a position that is closer to (medial) or further from (lateral) the body's mid-line.

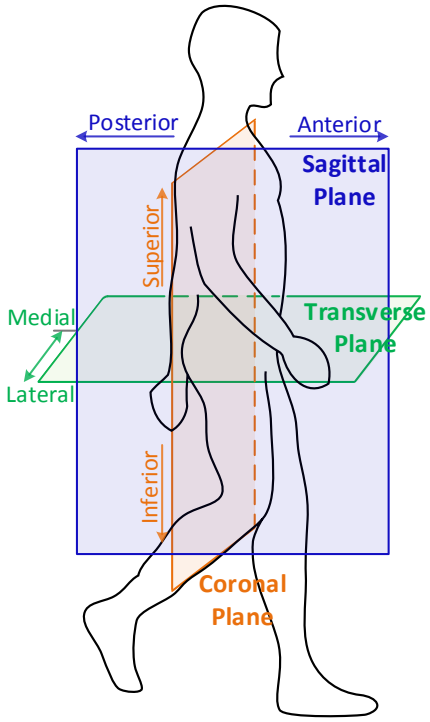

Figure B.1: The three anatomical planes of human body includes the sagittal, transverse, and coronal. The anterior-posterior, medial-lateral, and inferior-superior body axes are also shown.

B.1 Body Frames

To track the subject's performance in terms of the joint range-of motion and global position of pelvis, the first step requires the attachment of reflective tracking markers on the subject to setup the local moving frames at the lower limb segments. Figure B.2 presents the location of the reflective markers, and how these markers are utilized to form the local coordinate frames at each segment.

Pelvic Coordinate Frame: The pelvic frame origin, {P}, is chosen to be at the center of RASI and LASI markers. The positive x-axis is from {P} to LASI, while the positive y-axis is from the SACR, to {P}.

Hip Coordinate Frame: The hip frame origin is chosen at the virtual hip joint center (HJC). This is based on the pelvis anatomical landmark (AL) method [111]. As the name suggests, AL is based on the anterior-superior iliac spine (ASIS) landmarks. Expressed as a percentage of the distance between the right and left ASISs, the HJC is located 30% distal, 40% medial and 22% posterior to the ASIS, with 95% certainty [111]. There is another more accurate approach known as the greater trochanter (GT) method [112]. As the name suggests, this method is based on the

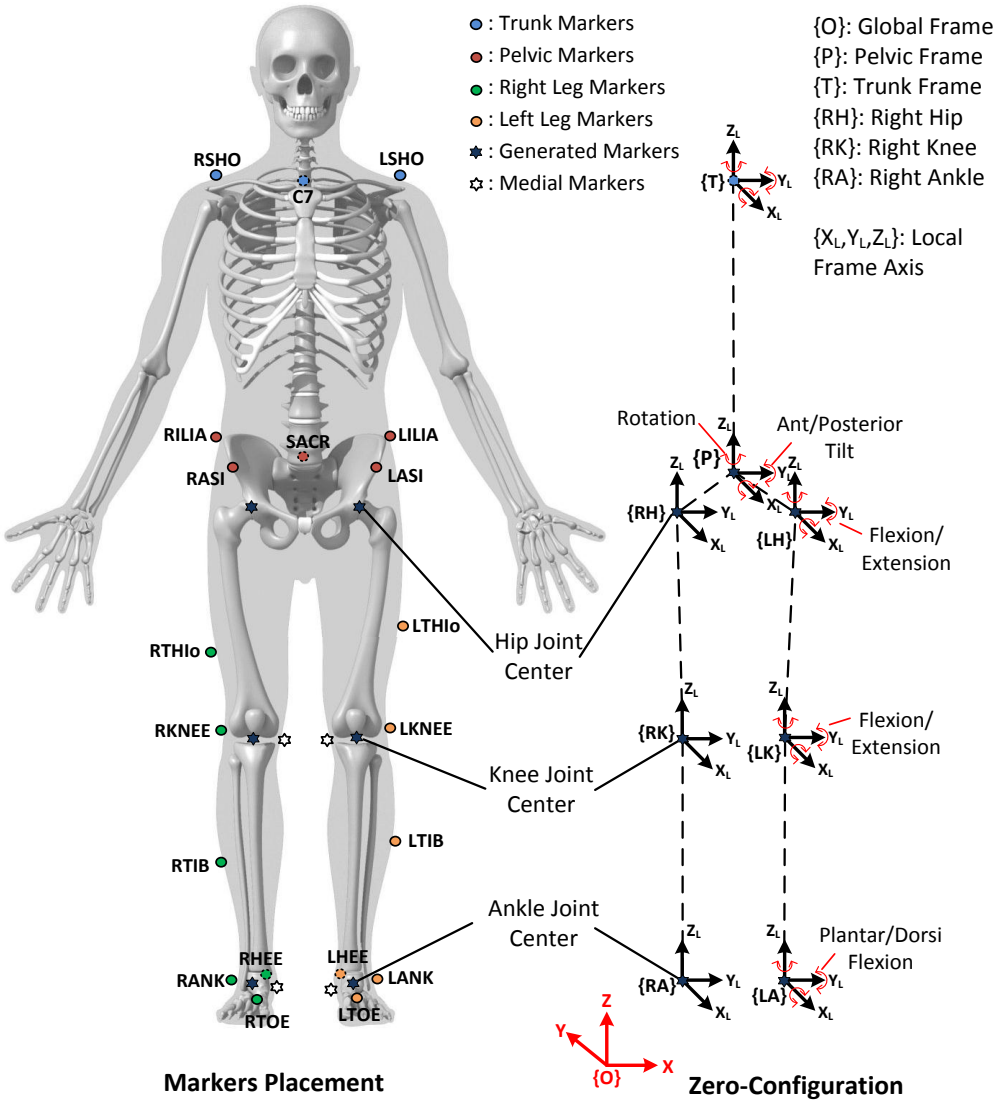

Figure B.2: Frame assignments based on the marker location. Zero-Configuration refers to upright standing posture and {O}:XYZ denotes the global coordinate frame.

greater trochanter landmarks. For this method, HJC is located at one-quarter of the distance from the ipsolateral to the contralateral greater trochanter. The AL method was adopted as the hip brace prevents attaching any marker to the greater trochanter. The positive z-axis is along the line connecting from the knee joint centre to HJC. The y-axis is chosen to lie parallel to the knee joint flexion axis, and positive direction being from the right side to the left side. This assignment is adopted to both hips.

Knee Coordinate Frame: The knee frame origin is chosen at the knee joint center (KJC). The positive z-axis is along the line connecting from the ankle joint center to KJC. The y-axis is

chosen to lie along its flexion axis, and positive direction being from the right side to the left side. This assignment is adopted to both knees.

Ankle Coordinate Frame: The ankle frame origin is chosen at the ankle joint center (AJC). The y-axis is chosen to lie along its flexion axis, and positive direction being from the right side to the left side. The positive x-axis is chosen to lie parallel to the line connecting from the heel to the toe markers. This assignment is adopted to both ankles.

Appendix C

Surface Electromyography Activity

Surface Electromyography (EMG) activity from the lower limb muscles were measured bilaterally, namely Gastrocnemius Medialis (MG), Soleus (SOL), Tibialis Anterior (TA), Vastus Lateralis (VL), Rectus Femoris (RF) and Biceps Femoris (BF) of each leg. Each electrode site was shaved and cleaned with alcohol. Surface electrodes with inter-electrode distance of 20 mm were placed on the muscles as per SENIAM guidelines [113]. Electrodes were kept in place during the complete experiment. Single-differential signals were high-pass filtered with a first order analog filter (cut off frequency equal to 10 Hz), digitalized and received by a wireless desktop unit (DTS Desktop Receiver, Noraxon Inc., Arizona). This unit was connected to the Vicon motion capture system.

C.1 Muscle locations

C.1.1 Soleus (SOL)

Location - The electrodes need to be placed at 2/3 of the line between the medial condylis of the femur to the medial malleolus.

Orientation - In the direction of the line between the medial condylis to the medial malleolus.

Clinical test - Put a hand on the knee and keep/push the knee downward while asking the subject/patient to lift the heel from the floor.

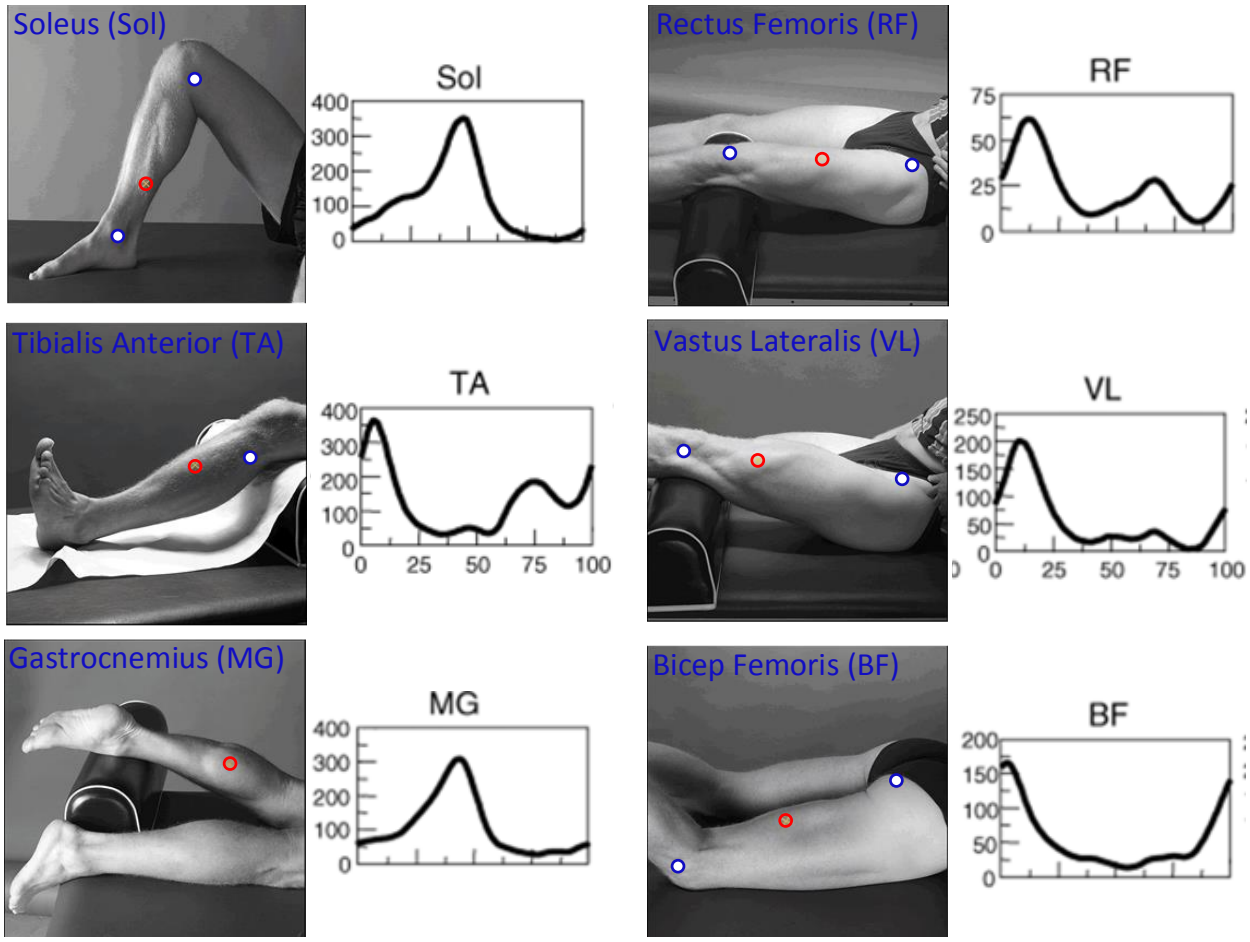

Figure C.1: EMG electrodes locations on human lower limbs.

C.1.2 Tibialis Anterior (TA)

Location - The electrodes need to be placed at 1/3 on the line between the tip of the fibula and the tip of the medial malleolus.

Orientation - In the direction of the line between the tip of the fibula and the tip of the medial malleolus.

Clinical test - Support the leg just above the ankle joint with the ankle joint in dorsiflexion and the foot in inversion without extension of the great toe. Apply pressure against the medial side, dorsal surface of the foot in the direction of plantar flexion of the ankle joint and eversion of the foot.

C.1.3 Gastrocnemius (MG)

Location - Electrodes need to be placed on the most prominent bulge of the muscle.

Orientation - In the direction of the leg (see picture).

Clinical test - Plantar flexion of the foot with emphasis on pulling the heel upward more than pushing the forefoot downward. For maximum pressure in this position it is necessary to apply pressure against the forefoot as well as against the calcaneus.

C.1.4 Rectus Femoris (RF)

Location - The electrodes need to be placed at 50% on the line from the anterior spina iliaca superior to the superior part of the patella.

Orientation - In the direction of the line from the anterior spina iliaca superior to the superior part of the patella.

Clinical test - Extend the knee without rotating the thigh while applying pressure against the leg above the ankle in the direction of flexion.

C.1.5 Vastus Lateralis (VL)

Location - Electrodes need to be placed at 2/3 on the line from the anterior spina iliaca superior to the lateral side of the patella.

Orientation - In the direction of the muscle fibers.

Clinical test - Extend the knee without rotating the thigh while applying pressure against the leg above the ankle in the direction of flexion.

C.1.6 Bicep Femoris (BF)

Location - The electrodes need to be placed at 50% on the line between the ischial tuberosity and the lateral epicondyle of the tibia.

Orientation - In the direction of the line between the ischial tuberosity and the lateral epicondyle of the tibia.

Clinical test - Press against the leg proximal to the ankle in the direction of knee extension.